ASSESSMENT OF MODELING SENSITIVITY FOR NONLINEAR SEISMIC ANALYSIS OF HIGHWAY BRIDGES IN ILLINOIS

BY

CARLOS ANDRES PAEZ VARGAS

THESIS

Submitted in partial fulfillment of the requirements
for the degree of Master of Science in Civil Engineering
in the Graduate College of the
University of Illinois at Urbana-Champaign, 2018

Urbana, Illinois

Advisers:

Professor James M. LaFave
Associate Professor Larry A. Fahnestock

ABSTRACT

The American Association of State Highway and Transportation Officials (AASHTO) seismic provisions were updated in 2008. These provisions increased the design earthquake return period from 500 to 1000 years, eventually demanding special structural systems to counteract seismic forces and therefore increasing construction costs. The updates were based on the seismic practices in the western United States, which focus on bridge configurations that dissipate energy either by plastic deformation of the piers or by specially designed isolation devices placed between the superstructure and substructure.

The Illinois Department of Transportation (IDOT) has focused on this second isolation approach, however considering only conventional bearings, in order to formulate a cost-effective "quasi-isolation" concept targeted to the seismic hazard and typical bridge configurations in Illinois. An Earthquake Resisting System (ERS) based on quasi-isolation uses elastomeric bearings and is different from conventional seismic design by permitting bearing anchorages to fracture during a design earthquake. The ERS also depends on subsequent bearing deformation and sliding to accommodate seismic demands.

IDOT has organized two research phases to analyze and develop the concept of an ERS based on quasi-isolation. Phase I performed an experimental investigation of the seismic response of bridge bearings and formulated structural models of typical bridges based on information obtained after testing these structural components. The structural models of this phase only considered regular bridges and a simplified abutment model. The structural performance of these models was assessed for various hazard levels by using a suite of synthetic ground motions based on representative seismic records of the New Madrid Seismic Zone (NMSZ), a geographical region that encompasses several locations with high seismicity, including southern Illinois. Phase II continued the assessment process of the proposed ERS by formulating structural models that considered additional features such as skew angles and a detailed abutment model that included elements such as approach slabs and wingwalls. In this phase, a suite of synthetic ground motions specifically formulated for Cairo, Illinois, the geographical location with the highest seismic hazard of the state, was developed to analyze the structural performance of these models for design hazard levels.

The principal objective of the present work is to evaluate modeling sensitivity between Phase I and Phase II models in order to determine to what extent the additional elements included in Phase II models affect overall structural response. In order to perform a consistent comparison, bridge configurations that can be found in both Phase I and Phase II parametric studies were selected. The comparison encompassed static pushover analyses and nonlinear dynamic analyses. Static pushover analyses were considered to determine similarities and/or differences of bridge response characteristics such as force distribution among substructures, sequence of limit state occurrences, fusing of sacrificial connections, and vulnerability of critical bridge components. Nonlinear dynamic analyses were considered to assess the seismic performance of Phase I and Phase II models based on a comparison of the number of occurrences of various limit states. The synthetic ground motions developed during Phase II were used for this comparison.

This study found that additional Phase II elements, such as approach slabs, increased structural stiffness at abutments in the longitudinal direction of analysis, which allowed a redistribution of forces at this location. This redistribution precluded the concentration of forces in sacrificial connections and reduced superstructure displacements. In general, these conditions diminished the occurrence of fusing limit states at abutments and damaging limit states at intermediate substructures in comparison to Phase I models.

Likewise, in the transverse direction of analysis, it was observed that additional elements, especially wingwalls, increased abutment stiffness that allowed a redistribution of forces that essentially reduced the concentration of demands on sacrificial connections at that location. Generally, the stiffness increase observed in the transverse direction was lower compared to the longitudinal direction.

Finally, according to the results of nonlinear static analyses and nonlinear dynamic analyses, it was not possible to identify a marked difference in the occurrence of limit states between Phase I and Phase II models, especially regarding damaging limit states. Even though the formulation of Phase II models resemble more closely the real structural configuration of seat-type abutment bridges, the Phase I models require less computational resources to be analyzed. For this reason, it is possible to employ the more simplified Phase I models as a preliminary assessment tool, before using more complex formulations (as needed) for definitive structural analysis of seat-type abutment bridges.

To God, Our Lady of Sorrows, my parents, and my sister for their help, support, and encouragement throughout my entire life.

ACKNOWLEDGEMENTS

I would like to express my gratitude to my research advisers Dr. James M. LaFave and Dr. Larry A. Fahnestock for giving me the opportunity to be part of this research group and work in this project. I really appreciate the guidance and support they have given me throughout the development of this thesis.

I will never be able to fully acknowledge the support, encouragement and sacrifices of my parents. I learned from them the determination and the necessary skills to endure difficult times, face challenges, and persist in my convictions and objectives.

I would like to thank Dr. Derek L. Kozak for his support, advice, and recommendations that were essential in to be familiarized with the required tools and resources to complete this thesis project.

I would like to thank Dr. Jie Luo for providing documents and materials developed during the second phase of the research project that were necessary to obtain the required information for the completion of this thesis project.

I would like to acknowledge the excellent work of former graduate research assistants Dr. Joshua Steelman, Dr. Evgueni Filipov, and Jessica Revell who developed the first phase of the research project, which is a foundation of the current study.

I would like to acknowledge the Extreme Science and Engineering Discovery Environment (XSEDE) as well as the Texas Advanced Computing Center (TACC) at The University of Texas at Austin that provided the computational resources required for the parametric study developed in this thesis project

This thesis is based on the research projects ICT-R27-070, “Seismic Performance of Quasi-Isolated Highway Bridges in Illinois: Phase I” and ICT-R27-133, “Calibration and Refinement of Illinois’ Earthquake Resisting System Bridge Design Methodology: Phase II”. These projects were conducted in cooperation with the Illinois Center for Transportation (ICT), the Illinois Department of Transportation (IDOT), and the U.S Department of Transportation, Federal Highway Administration (FHWA). The contents of the present study do not necessarily reflect the official views or policies of the ICT, IDOT or FHWA.

TABLE OF CONTENTS

1. INTRODUCTION 1
2. LITERATURE REVIEW 11
3. MODELING OF PROTOTYPE QUASI-ISOLATED HIGHWAY BRIDGES 35
4. ABUTMENT MODELS FOR QUASI-ISOLATED HIGHWAY BRIDGES 63
5. STATIC PUSHOVER ANALYSES OF PROTOTYPE BRIDGE MODELS 79
6. DYNAMIC ANALYSES OF PROTOTYPE HIGHWAY BRIDGES 98
7. SUMMARY AND CONCLUSIONS 130
REFERENCES 140

1. INTRODUCTION

1.1. Quasi-Isolation Strategy for Highway Bridges in Illinois

The American Association of State Highway and Transportation Officials (AASHTO) updated the standards related to seismic provisions for the design of highway bridges in early 2008. These standards were AASHTO Load and Resistance Factor Design (LRFD) Bridge Design Specifications (AASHTO, 2008a) and AASHTO Guide Specifications for LRFD Seismic Bridge Design (AASHTO, 2008b). These standards increased the return period of the design earthquake from 500 to 1000 years. This increment entails significantly greater design accelerations for highway bridges on the West Coast, which is prone to high seismicity, and several regions in the Midwest and on the East Coast, such as the southern region of Illinois, where high-magnitude and low-probability seismic hazards represent a primary concern for transportation networks.

Classical bridge isolation systems are based on seismically designed isolators, restrainers, or dampers. Regarding seismically designed isolators, there are two primary types: elastomeric bearings (e.g., laminated rubber bearings and lead-rubber bearings) and sliding isolation devices (e.g., resilient base isolation system and friction pendulum system) (Kunde & Jangid, 2003). Figures 1.1 and 1.2 illustrate these types of isolators.

Considering the increased demands of seismic design established by the new AASHTO standards and the higher cost of classical bridge isolation systems, the Illinois Department of Transportation (IDOT) has developed an innovative Earthquake Resisting System (ERS) concept for design, construction, and retrofit of highway bridges in the state of Illinois (Tobias et al. 2008). This quasi-isolated bridge system features a simplified design and construction process which is focused to economically protect highway bridges in regions with moderate to high seismic activity, such as southern Illinois.

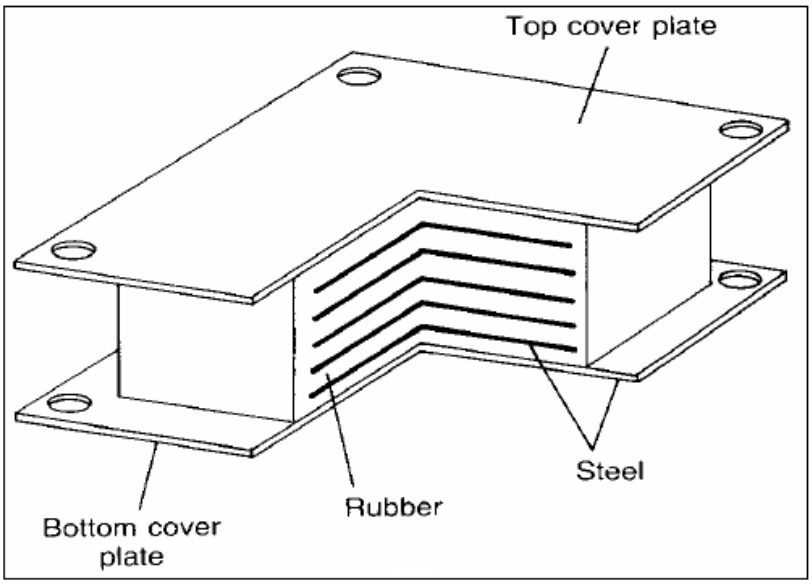

a) Laminated rubber bearing

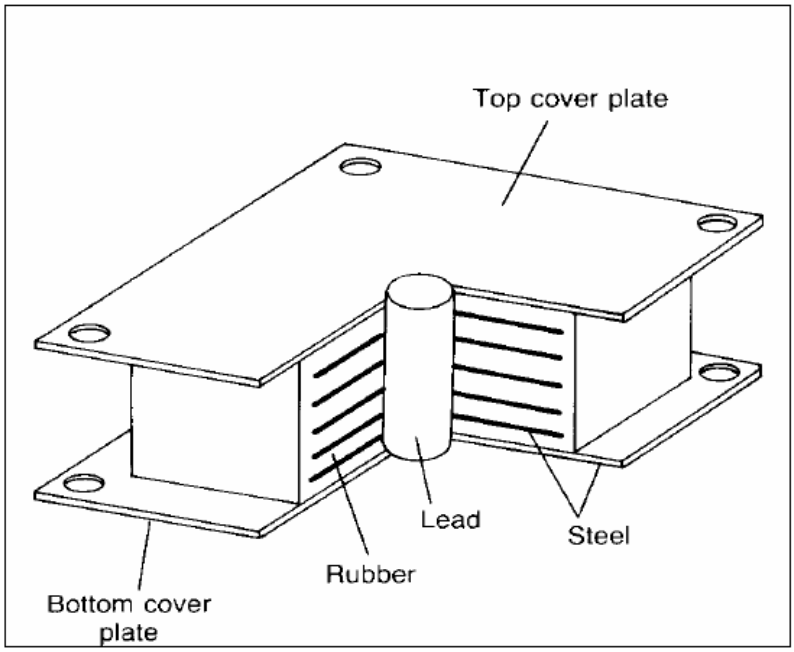

b) Lead-rubber bearing

Figure 1.1: Elastomeric isolation bearings per Kunde & Jangid (2003)

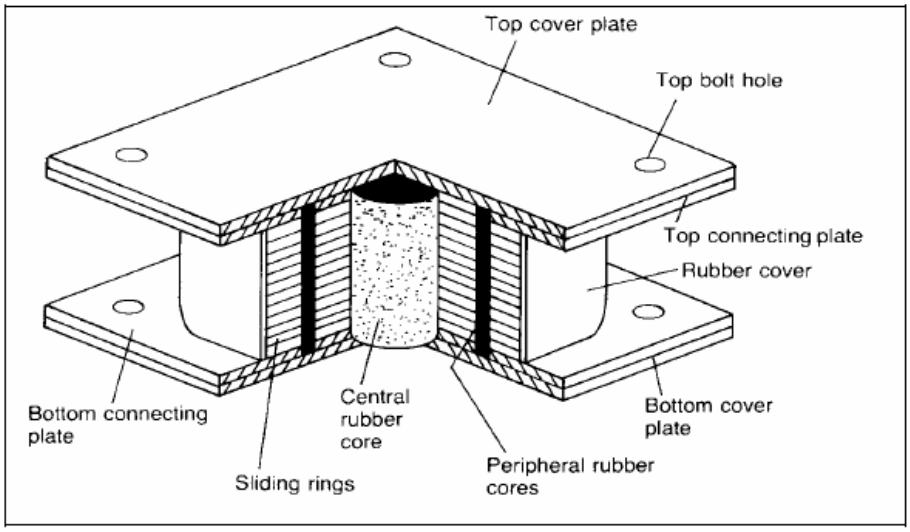

a) Resilient base isolation system

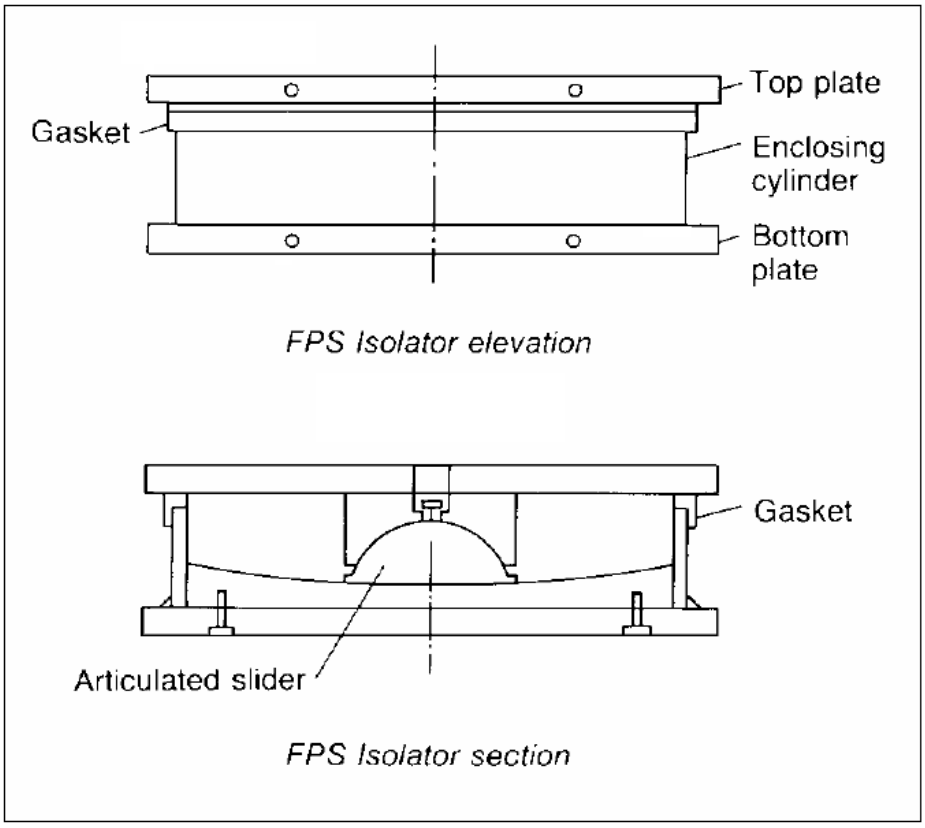

b) Friction Pendulum System

Figure 1.2: Sliding isolation systems per Kunde & Jangid (2003)

The concept of quasi-isolation uses non-seismically designed sacrificial connections between the superstructure and substructure of a bridge, along with conservatively designed bearing seat widths at superstructures (especially at pile caps of abutments and piers). If a seismic event occurs, damage and failure of these sacrificial connections are expected to limit superstructure inertial forces that are transmitted to the substructure and foundations, to dissipate seismic energy, and to elongate the natural period of the structure. This failure mechanism protects bridge substructures and foundations from severe seismic damage (Luo, 2016).

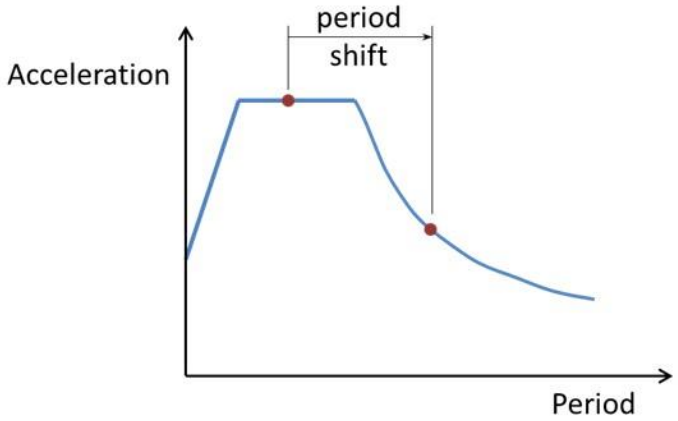

Figure 1.3: Effect of period shift on acceleration per LaFave et al. (2013)

Once sacrificial connections are fused after the beginning of a seismic excitation, the friction at bearing-substructure interfaces is the only restriction to sliding and displacement of the bridge superstructure. The displacements of the superstructure and bearings can be accommodated by designing appropriate bearing seat widths at the substructure. This feature is one of the key parts of the IDOT ERS bridge design philosophy because a conservative seat width is necessary in order to prevent loss of bridge span, which can be the main cause of disruption of transportation lifelines during seismic events (IDOT, 2012).

The quasi-isolation bridge design strategy proposed by IDOT comprises three levels of seismic structural redundancy that are strategically implemented in order to avoid excessive seismic damage and span loss during major seismic events (Tobias et al., 2008).

The first level of seismic structural redundancy consists of sacrificial superstructure-substructure connections, such as elastomeric expansion bearings, bearing retainers, low-profile steel fixed bearings, and steel dowel connections. An IDOT Type I elastomeric expansion bearing and low-profile steel fixed bearing are illustrated in Figures 1.4a and 1.4b. Type I bearings consist of a block of steel-reinforced, laminated elastomer vulcanized to a steel plate on its top. The steel plate is connected to the bottom flange of a bridge girder by using welded studs. The bottom of the elastomer is directly placed against the surface of the concrete substructure. If the bearing is subjected to horizontal forces, the elastomer experiences shear deformation. Additionally, the bottom of the elastomer can be subjected to initial static or kinetic sliding friction at the elastomer-concrete interface. Besides the main structure of the bearing, in the transverse direction, two L-shaped steel retainer brackets are anchored to the surface of the concrete substructure on both sides of the elastomeric bearing. The low-profile steel fixed bearing consists of a curved top steel plate and a flat bottom steel plate anchored to the surface of the concrete substructure. The top and bottom steel plates are joined by using two steel pintles. An elastomeric leveling pad is placed between the bottom steel plate and the concrete surface of the substructure. The second level of seismic structural redundancy consists of the conservatively designed bearing seat widths at substructures. This provision is intended to avoid bridge span loss by accommodating large superstructure and bearing displacements after the first level of seismic structural redundancy has been reached. Finally, the third level of seismic structural redundancy, related to limited yielding and damage of the substructure and foundation components, such as RC columns, foundation piles and backfill soil, is allowed to occur. In order to ensure an appropriate structural response, the capacity of these components should be larger than that of the sacrificial superstructure-substructure connection in the first level.

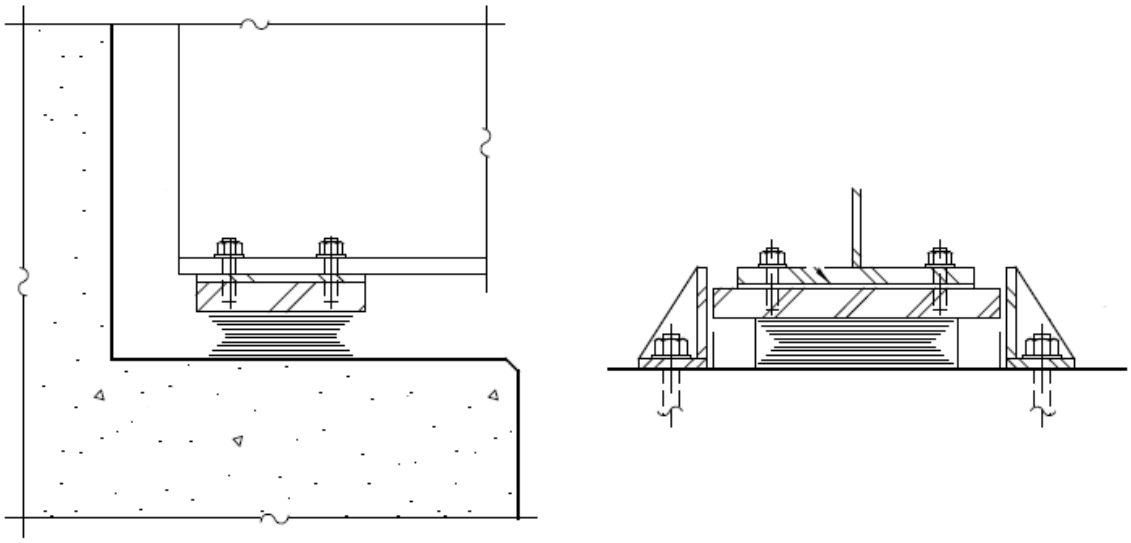

a) Type I elastomeric bearings

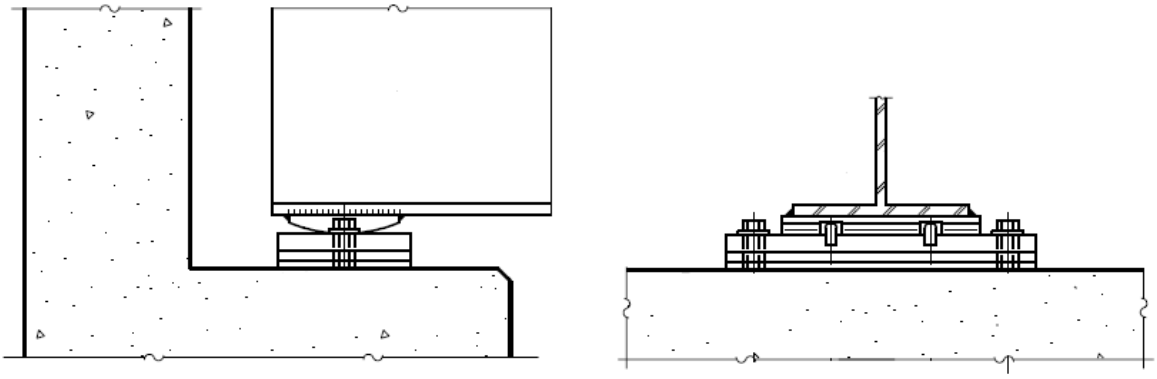

b) Low-profile fixed bearings

Figure 1.4: Type I bearings and low-profile fixed bearings per (IDOT, 2012)

1.2. Objectives and Scope of Research

1.2.1. Objectives

- Review the formulation of structural models of bridges of the research projects "Seismic Performance of Quasi-Isolated Highway Bridges in Illinois: Phase I" (Report ICT-R27-070) (LaFave et al., 2013b) and "Calibration and Refinement of Illinois' Earthquake Resisting System Bridge Design Methodology: Phase II) (Report ICT-R27-133) (LaFave et al., 2018), especially regarding the abutment model configuration employed for each project.

- Compare static pushover analyses of Phase I and Phase II models to determine differences or similarities of bridge response characteristics such as force distribution among substructures, sequence of limit states occurrences, fusing of sacrificial connections, and vulnerability of critical bridge components.

- Compare nonlinear dynamic analyses to assess the sensitivity of seismic performance to differences in Phase I and Phase II models based on the comparison of the number of occurrences of fusing limit states and damaging limit states, by considering design level ground motions.

- Perform an Incremental Dynamic Analysis (IDA) in order to further study the seismic response of bridge models against the synthetic ground motions developed in Phase II for different hazard levels (i.e., scale factors).

1.2.2. Scope of research

This study is based on a comparison of the structural response of models of a selection of bridges that can be found both in "Seismic Performance of Quasi-Isolated Highway Bridges in Illinois: Phase I" (Report ICT-R27-070) (LaFave et al., 2013a) and in "Calibration and Refinement of Illinois' Earthquake Resisting System Bridge Design Methodology: Phase II) (Report ICT-R27-133) (LaFave et al., 2018), which focuses on the analysis of differences and similarities of the structural response.

This selection consists of three-span bridges with steel-plate girders that have sequential span lengths of 24.4, 36.6, and 24.4 m (80, 120 and 80 ft). These bridges are supported by non-skew seat-type abutments and RC multi-column intermediate piers. Superstructure girders are supported by IDOT Type I bearings at the abutments and at Pier 1, and by low-profile fixed bearings at Pier 2. The RC multi-column intermediate piers are 4.57 or 12.19 m high (15 or 40 ft). These substructures are supported by steel H pile foundations. Soft or hard foundation soil conditions are considered. The combination of these parameters results in 4 bridge variants in total. An example of the bridges studied in this thesis can be found in Figure 1.5. Additional details about these bridge variants will be discussed in the following chapters.

Regarding static pushover analyses, only Phase II performed this type of analysis. For this reason, the pushover analysis is going to be executed using the structural models of Phase I in order to have all the required information to make a comprehensive comparison between the models of Phase I and Phase II.

Originally, the nonlinear dynamic analyses of the structural models of Phase I were performed by using a set of 20 synthetic ground motions based on the seismic hazard of Paducah, KY, and Cape Girardeau, MO (Fernandez & Rix, 2008). In order to perform a consistent comparison between the structural models of Phase I and Phase II, the nonlinear dynamic analyses of the structural models of Phase I will be performed again by using the suite of 20 synthetic ground motions used in Phase II (Kozak et al., 2017).

An Incremental Dynamic Analysis (IDA) will be performed using the synthetic ground motions of Phase II and considering scale factors of 0.50, 0.75, 1.00, 1.25, 1.50, and 1.75. These analyses will be performed using Phase I models in order to further evaluate the seismic response of the selected bridge variants.

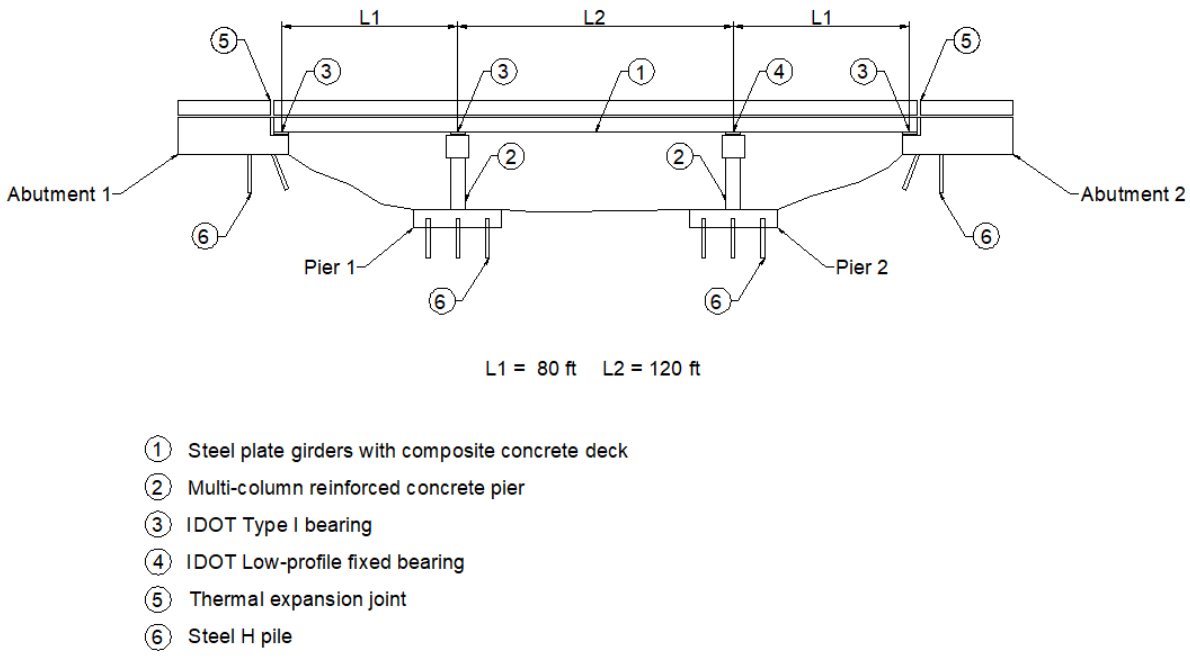

Figure 1.5: Prototype quasi-isolated seat-type abutment highway bridge

1.3. Organization of Thesis

The chapters of this thesis are organized in the following order:

- Chapter 1: Defines the Earthquake Resisting System (ERS) concept based on quasi-isolation for highway bridge design, as proposed by the Illinois Department of Transportation (IDOT), and establishes the objectives and scope of research.
- Chapter 2: Provides information about prior research related to quasi-isolated highway bridges, which includes results of experimental testing of bearings as well as previous parametric analyses.
- Chapter 3: Presents a description of the general elements of the structural models of prototype quasi-isolated bridges, such as their superstructure, substructure, and foundations.
- Chapter 4: Shows the formulation of Phase I and Phase II numerical models for bridge abutments.

- Chapter 5: Presents a comparison between results of the static pushover analyses of models for Phase I and Phase II.
- Chapter 6: Presents a description of the concepts employed to develop the synthetic ground motions used in Phase I and Phase II as well as a comparison between the nonlinear dynamic analyses of the structural models for Phase I and Phase II. An IDA is included to further assess the seismic response of the selected bridge variants.
- Chapter 7: Summarizes the similarities and differences found in the response of the structural models for Phase I and Phase II. This chapter includes suggestions about the use of Phase I and Phase II models as well as recommendations for future research.

2. LITERATURE REVIEW

This chapter presents a brief introduction to the methodology and findings of previous research projects related to quasi-isolated highway bridges in Illinois. A discussion focused on the structural modeling techniques of these research projects is presented. Finally, a summary is also included of research related to the comparison of structural modeling techniques for bridges, especially regarding their abutments.

2.1. Prior Research Related To Quasi-Isolated Highway Bridges in Illinois

The Illinois Department of Transportation (IDOT) and the Illinois Center for Transportation (ICT) sponsored a research project with the University of Illinois at Urbana-Champaign in order to calibrate and refine the earthquake resisting system (ERS) bridge design methodology. Experimental and computational investigations were performed during Phase I of this research project (Project No. ICT-R27-070) (LaFave et al., 2013a and 2013b) regarding the following aspects:

1. Tests on full-scale specimens of typical bridge bearings.
2. Computational modeling of bridge bearings.
3. Computational modeling of complete bridge systems.
4. Parametric studies that involved complete bridge models and synthetic ground motions.
5. Design and construction recommendations to improve the seismic performance of quasi-isolated ERS bridges.

2.1.1. Experimental tests on full-scale specimens of typical bearing components

In order to determine the mechanical properties of typical bearing components, an experimental and analytical program was performed in the Newmark Civil Engineering Laboratory at the University of Illinois at Urbana-Champaign from 2009 to 2012 (LaFave et al., 2013a; Steelman, 2013). A customized setup was designed to simulate real seismic loading conditions for the bearing components installed in bridges.

These tests were performed by installing full-scale specimens of bearings on a concrete pad with broom-finished surface. A pair of actuators with 445 kN (100 kip) capacity was employed to apply an approximately constant vertical load in order to simulate the gravity loads imposed on a bearing due to the self-weight of the bridge superstructure. In addition, another actuator with a 980 kN (220 kip) force capacity and 762 mm (30 in) stroke was used to induce horizontal forces and displacements on the bearings, in order to simulate seismic forces. The customized setup used for these tests is shown in Figure 2.1.

Three types of non-seismically designed bridge bearings were tested: IDOT Type I elastomeric bearings, IDOT Type II elastomeric bearings and low-profile steel fixed bearings. IDOT Type I elastomeric bearings consist of a rectangular steel-reinforced laminated elastomer restrained on two sides by steel retainers. IDOT Type II elastomeric bearings comprise a rectangular steel-reinforced laminated elastomer and a stainless steel-on-Teflon sliding surface. This type of bearing is also restrained on two sides by steel retainers. Low-profile steel fixed bearings consist of two steel plates connected by pintles. The base steel plate is attached to the concrete surface using anchor bolts. A detail of each one of these bearings is shown in Figure 2.2.

Testing of Type I elastomeric bearings showed that bearing specimens had an approximately linear elastic response before the onset of sliding. The initial coefficient of friction is in the range of 0.25 to 0.50 at a shear strain between 125% and 250%. This coefficient of friction varies according to conditions related to contact surface roughness, loading velocity, and axial load on the bearing. The AASHTO specification (AASHTO, 2010) recommends a coefficient of friction for elastomer to concrete of 0.20, which is a lower bound compared to the observed coefficient of friction during the tests under different vertical loads (Steelman et. al., 2013).

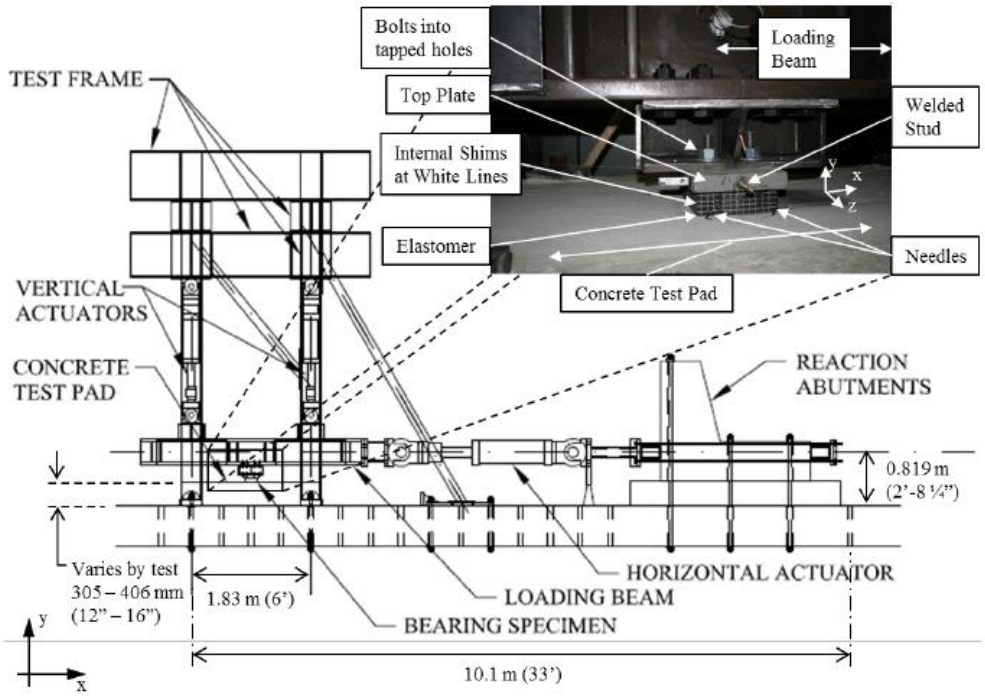

Figure 2.1: Customized setup for full-scale bearing tests (LaFave et al., 2013a; Steelman, 2013)

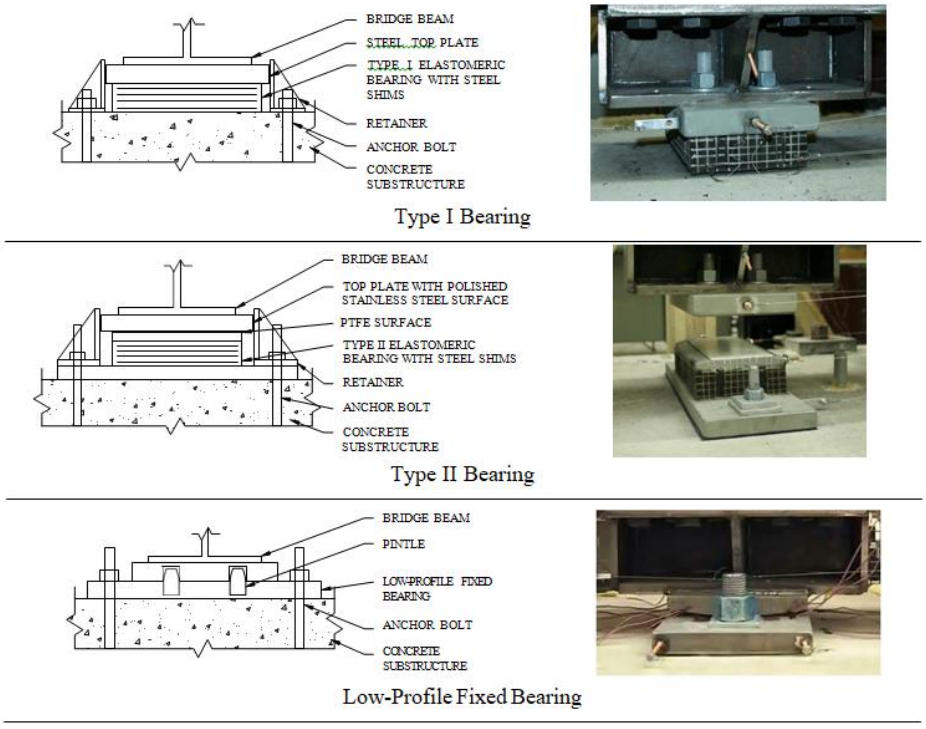

Figure 2.2: Type I, Type II, and low-profile fixed bearings per LaFave et al. (2013a)

Testing of Type II bearings showed that large bearing sliding displacements are likely to cause delamination and progressive removal of the PTFE (Teflon) material from the bearing middle plate. Although delamination processes occurred, it was possible to notice that this type of bearings slid even when 20% of the Teflon was exposed. The coefficient of friction at the PTFE to stainless steel interface varied with vertical loads and sliding rates. It was found that this coefficient ranged from about 0.12 to 0.18 (Steelman et. al., 2016).

Regarding low-profile fixed bearings, two competing failure mechanisms were identified: weak anchors fastening the bottom steel plate to the concrete substructure vs. weak pintles connecting the top and bottom steel plates. These failure mechanisms lead to two design options. The weak anchor design option is preferred to the weak pintle option because the former exhibits a clear shear failure of the anchor bolts with limited damage to the surrounding concrete (Steelman et al., 2014).

The fusing capacity of one anchor bolt can be predicted from the following expression:

$$R_u = \varphi(0.6)(0.8)F_u A_g \qquad (2.1)$$

Where, φ is the strength reduction factor (φ = 1.0 for nominal capacity), F_u is the ultimate tensile strength of the anchor bolt material, and A_g is the gross cross-sectional area of the anchor bolt. The coefficient of friction for the post-fusing sliding of the fixed bearing elastomeric leveling pad on concrete substructures is around 0.30.

The width of the bearing side retainer in the transverse bridge direction has a significant influence on the interaction with the concrete to which it is anchored. The IDOT Bridge Manual (IDOT, 2012) specifies that the anchorage of the bearing retainer has to be designed to resist a lateral load equivalent to 20% of the superstructure dead load on the bearing. However, retainer test specimens had a much higher fusing capacity in experiments. The failure process of this component starts with plastic deformation of the retainer anchor bolt followed by crushing of the surrounding concrete near the anchor and retainer toe. This process ended with a shear-tension rupture of the anchor bolt. The fusing capacity of one retainer anchor bolt can be predicted using the following expression:

$$R_u = \varphi(0.8)F_u A_g \qquad (2.2)$$

Where, φ is the strength reduction factor (φ = 1.0 for nominal capacity), F_u is the ultimate tensile strength of the anchor bolt material, and A_g is the gross cross-sectional area of the anchor bolt.

2.1.2. Computational models of typical bearing components

A coupled bi-directional nonlinear element was developed by Filipov et. al (2013a) to capture shear and sliding behavior of Type I and Type II elastomeric bearings from experimentally tested bearing response data. This model simulates different phases of bearing shear and sliding behavior by using several coefficients of friction. These coefficients of friction are the initial static coefficient of friction μ_{SI}, the kinetic coefficient of friction μ_K, and a stick-slip coefficient of friction μ_{SP}. A schematic representation of the definition of these coefficients is shown in Figure 2.3.

This model has been validated and calibrated using results of tests on full-scale bearing specimens. The numerical simulations performed on complete bridge models determined values of 0.60, 0.45, and 0.50 for the coefficients, μ_{SI}, μ_K, and μ_{SP} of Type I bearings, respectively; whereas, values of 0.16, 0.15 and 0.15 were determined for Type II bearings, respectively; 85 psi was used as the shear modulus for the elastomer.

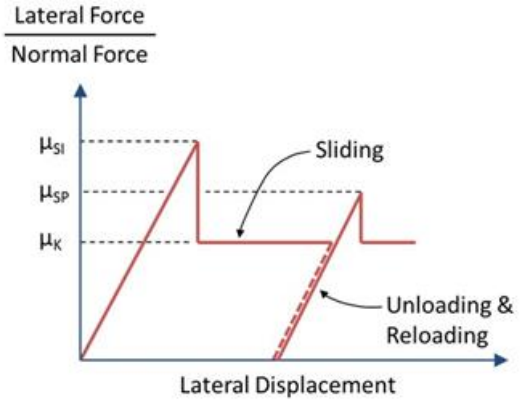

Figure 2.3: Schematic representation for the stick-slip shear and friction behavior of elastomeric bearings (LaFave et al., 2013a; Filipov et al., 2013a)

In the case of Type I and Type II elastomeric bearings, yielding and rupture of the retainer anchor bolts under lateral forces was modeled using a uni-directional elasto-plastic

computational model (LaFave et al., 2013b; Filipov et al., 2013b). The force-displacement relation of this model is illustrated in Figure 2.4.

In the case of low-profile steel fixed bearings, a coupled bi-directional nonlinear element was developed to capture the elasto-plastic behavior of steel anchor bolts that fasten these components to concrete when subjected to horizontal shear demands (LaFave et al., 2013b; Filipov et al., 2013b). The force-displacement relation of this model is schematically represented in Figure 2.5. In addition, the model for sliding behavior of elastomer on concrete is superimposed with the steel anchor model to simulate the post-fusing sliding at the elastomeric pad-concrete interface. The combination of these two different types of model was also validated against experimental results.

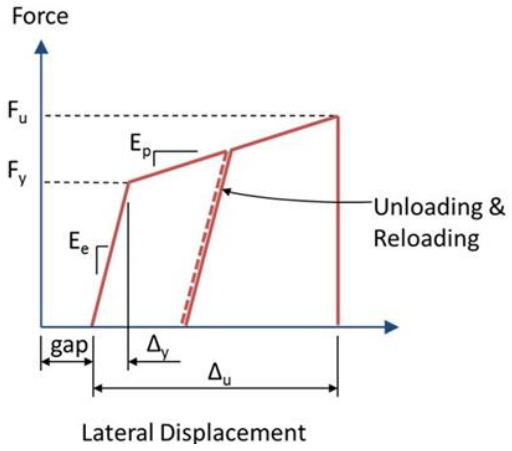

Figure 2.4: Schematic representation of the elasto-plastic shear behavior of bearing retainer anchors (LaFave et al., 2013b; Filipov et al., 2013b)

2.1.3. Previous parametric studies: "Phase I" (Report ICT-R27-070)

The parametric study of the first phase of this research project was based on the current bridge stock in Illinois as defined in prior research conducted by Bignell et al. (2005). In the current bridge stock, elastomeric bearings are the preferred type of expansion bearing. At the time of the study 75% of the bridges had three spans, with lengths ranging from 33.53 m (110 ft) to 82.30 m (270 ft), consisting of 86% steel girders and 14% concrete girders (all with composite decks). Of these bridges, 67% had multi-column piers, and 33% had wall piers. Pier heights ranged from 2.74 m (9 ft) to 14.02 m (46 ft).

Regarding soil related parameters, site conditions ranged from Class B to E, which are soil conditions commonly found in southern Illinois. Foundations consisted primarily of piles (86%).

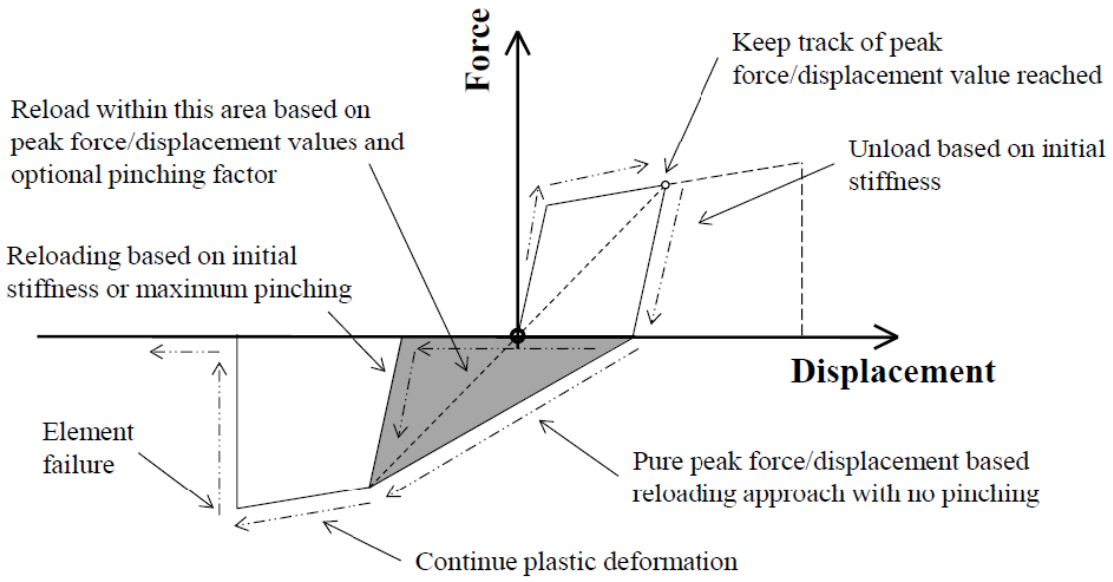

Figure 2.5: Schematic representation of the elasto-plastic shear behavior of steel fixed bearing anchors per LaFave et al. (2013b) and Filipov et al. (2013b)

The findings of that study were then used to develop a suite of 48 quasi-isolated highway bridges with three-span continuous superstructures, non-seismically designed bearing components, and non-skew seat type abutments (LaFave et al., 2013b; Filipov et al., 2013b). These parametric variations are summarized in Table 2.1.

Besides the models used to simulate the behavior of elastomeric bearings and low-profile fixed bearings, a simplified model was also developed to simulate the interaction between the superstructure and abutments. This model consists of elements that represent abutment components such as the backwall, superstructure, and pile cap, as well as the links between these elements such as the gap between the top of backwall and superstructure, and the connection between the bottom of the backwall and pile cap. This model does not consider elements such as approach slabs or wingwalls. A detail of this model is shown in Figure 2.6.

Nonlinear finite element models were developed for these 48 bridges. A suite of 20 synthetic ground motions developed by Fernandez & Rix (2008) was employed to perform nonlinear dynamic analyses. These ground motions were formulated based on the uniform hazard spectra (UHS). These ground motions considered a 1,000-year return period and were based on seismic records of Paducah, KY and Cape Girardeau, MO, which are locations close to southern Illinois within the New Madrid Seismic Zone (NMSZ).

Table 2.1: Phase I parametric variations (LaFave et al., 2013b; Filipov et al., 2013b)

		Bridge Type 1 Steel - Short				Bridge Type 2 Steel - Long				Bridge Type 3 Concrete - Short			
Parameter	**Alternatives**	1	2	3	4	5	6	7	8	9	10	11	12
Span Length	50' - 50' - 50'	*	*	*	*								
	60' - 60' - 60'									*	*	*	*
	80' - 120' - 80'					*	*	*	*				
Pier Type	Continuous Wall	*	*			*	*			*	*		
	Multi Column Pier			*	*			*	*			*	*
Pier Height	Short - 15'	*		*		*		*		*		*	
	Tall - 40'		*		*		*		*		*		*
Movement Bearings	Type I Elastomeric	All (12) of the above bridges are modeled with Elastomeric Type I and Type II Bearings											
	Type II Elastomeric												
Foundations	Fixed Foundation	All (24) of the above bridges are modeled with Fixed and Flexible Foundations											
	Flexible Foundation												

Important observations were obtained from the nonlinear dynamic analysis of Phase I parametric variations:

- Only a few bridge models experienced bearing unseating for design-level earthquakes. Consequently, most bridge structures in Illinois would not experience severe damage during their typical design life.

- Bridge models with Type II elastomeric bearings were more likely to experience unseating because the area of the bearing surface was often insufficient given the magnitude of the displacement demand.

- Bridge models with Type I bearings showed superior performance in preventing unacceptable system behavior. No bearing unseating was observed when these bridges were subjected to longitudinal excitations. Transverse unseating was only noted at the Maximum Considered Earthquake (MCE) hazard level.

- Bridge displacement response was noted to be significantly larger for systems with tall pier substructures (40 ft) and Type II bearings.

- Displacements in the longitudinal direction are generally much lower compared the transverse direction because of the influence of the backwall elements. For design level earthquakes, transverse bearing displacements were about 36% higher than longitudinal displacements.

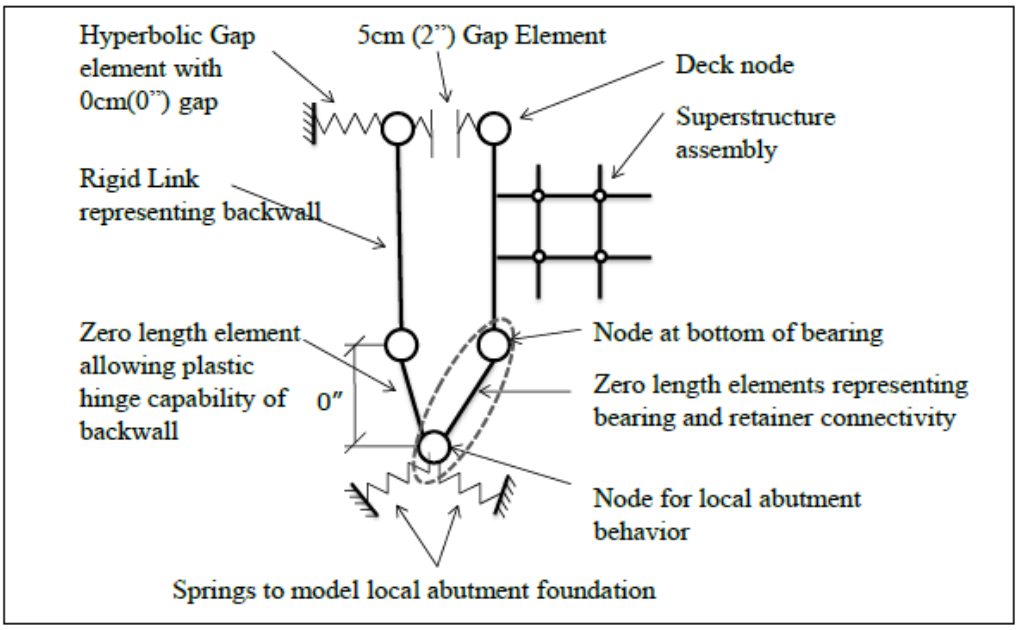

Figure 2.6: Phase I abutment model (LaFave et al., 2013b; Filipov et al. 2013b)

Based on the nonlinear dynamic analyses, the following recommendations were made in order to improve the quasi-isolation strategy for earthquake resisting systems (ERS) bridges in Illinois:

- Consider limiting the use of Type II bearings to regions of low or moderate seismicity where bearing unseating is less likely to occur.

- Type I bearings are generally appropriate for use with all seismic hazard levels and most soil types in Illinois (excluding special geotechnical conditions).

- Fixed bearings and retainers were often found to have higher fuse capacities than predicted by IDOT provisions; therefore, it is suggested to reduce the strength of these elements.

- The abutment-backwall had significant capacity to limit longitudinal displacements; hence, it is feasible to consider the contribution of this element for seismic design.

2.1.4. Previous parametric studies: "Phase II" (Report ICT-R27-133)

The overall parametric study for the second phase of the research project was focused on the analysis of seat-type abutment bridges and integral abutment bridges. Seat-type abutment bridge models selected for analysis as part of this second phase included additional features such as skew and continuous superstructures with four spans (Luo, 2016). These models only considered Type I elastomeric bearings and low-profile fixed bearings. A list of the features for the parametric variations analyzed in this study is shown in Table 2.2.

In addition to these features, a more complex model was developed to simulate the interaction between the superstructure and abutments. Apart from the elements that simulate the interaction between the superstructure and the backwall, additional elements were included to model approach slabs, wingwalls, and pile foundations in order to increase the accuracy of the structural models (Luo, 2016). A detail of this abutment model is shown in Figure 2.7.

Table 2.2: Phase II parametric variations per Luo (2016)

Component	Alternatives	3-span steel (3S)				4-span steel (4S)				3-span concrete (3C)				4-span concrete (4C)				Variants
		1	2	3	4	5	6	7	8	9	10	11	12	13	14	15	16	
Span length [m (ft)]	24.4-36.6-24.4 (80-120-80)	✓	✓	✓	✓					◊	◊	◊	◊					4
	44.2-48.8-48.8-44.2 (145-160-160-145)					○	○	○	○					□	□	□	□	
Pier column height [m (ft)]	4.57 (15)	✓		✓		○		○		□		□		◊		◊		2
	12.19 (40)		✓		✓		○		○		□		□		◊		◊	
Foundation soil condition	Hard	✓	✓			○	○			□	□			◊	◊			2
	Soft			✓	✓			○	○			□	□			◊	◊	
Skew angle	0°, 15°, 30°, 45°, 60°	5 skew angles are considered for each of the above 16 combinations.																5
Total number of bridge variants		**80**																

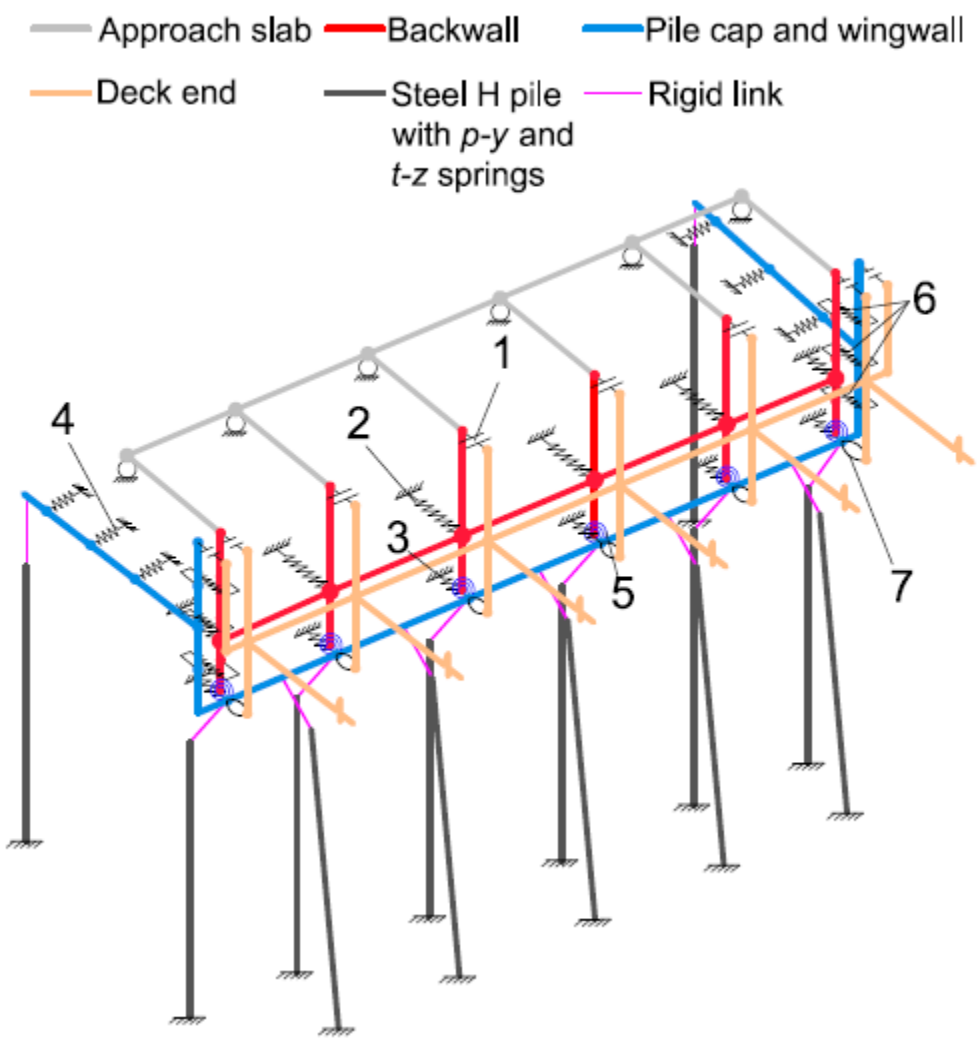

Figure 2.7: Phase II seat-type bridge abutment model per Luo (2016)

Nonlinear finite element models were developed for these bridge models. Instead of employing the suite of 20 synthetic ground motions developed by Fernandez & Rix (2008), a new suite of 20 synthetic ground motions was developed by Kozak et al. (2017) for this purpose. These new ground motions were formulated by using the concept of conditional mean spectra (CMS). The ground motions considered a 1,000-year return period and were based on a seismic deaggregation analysis for the city of Cairo, one of the locations with the highest seismicity in far southern Illinois.

Important observations were obtained from the nonlinear dynamic analysis of Phase II parametric variations:

Longitudinal analysis

- Once the expansion joint closed, the abutment was pushed by the superstructure, providing larger resisting forces than the intermediate piers.
- Fusing of sacrificial connections at the fixed pier was not observed in longitudinal analyses; this undesired fusing performance resulted in global yielding of short fixed-pier columns.
- The total longitudinal stiffness of the four-span bridges is much larger than that of the three-span bridges.

Transverse analysis

- Fusing of bearing retainers at the abutments was commonly observed.
- Intermediate piers usually resist larger forces than the abutments, in contrast to the force distribution observed in longitudinal analyses.
- Soft foundation soil precluded the fusing action of sacrificial superstructure-substructure connections at piers and abutments
- Similar to the observation from longitudinal analysis, the overall stiffness of the four-span bridge models is much larger than that of the three-span bridge models.

Based on the Phase II nonlinear dynamic analyses, the following recommendations were made in order to improve the quasi-isolation strategy of earthquake resisting systems (ERS):

- Bearing retainers are usually employed at the substructures to prevent bearing unseating, whereas concrete shear keys are not used as motion-limiting devices for bearings and girders; since tall pier bridges are prone to bearing unseating at their abutments, so concrete shear keys could be used as a second line of defense against bearing sliding and unseating.

- A detailed full bridge model was developed in order to perform a rigorous assessment of bridge seismic response; nevertheless, less complex bridge models can be used for design work when computational resources are limited.

- Unlike conventionally isolated bridges that employ specially designed bearings and damper devices, quasi-isolated bridges use economical and non-seismically designed bearing components; a detailed comparison between the isolation performance and construction cost of quasi-isolated and conventionally isolated bridges could provide further insight into the efficiency of quasi-isolated bridges.

2.2. Available Information Related to Comparison of Bridge Structural Models

Phase I and Phase II proposed structural models of different complexity levels in order to simulate the response of seat-type bridge abutments. Although high-fidelity models that capture structural behavior in great detail are in one respect more desirable, modeling complexity must be balanced with computational efficiency and the effort required to develop the models. Thus, judiciously simplified models are a common necessity in academic research and professional design practice. However, simplified models must also be validated and their sensitivities understood to ensure that the results are meaningful and not overly conservative on one hand or supportive of unsafe designs on the other. As background to the present sensitivity study of bridge model with varying levels of complexity, prior studies that compare the response of simplified and detailed bridge abutment models are presented in this section.

2.2.1. "Seismic analysis incorporating detailed structure-abutment-foundation interaction for quasi-isolated highway bridges"

Luo et al. (2017) discuss in their paper about the differences between the detailed abutment model developed for "Phase II" (Report ICT-R27-133) and a conventional simplified abutment model that is commonly used to perform seismic analyses of highway bridges.

The simplified model used in this study only includes elements to represent backfill passive resistance, elastomeric bearings and side retainers, expansion joints, and the pile foundation. Elements such as the RC backwall, wingwall, and approach slab are excluded. Contact and friction between the backwalls and deck ends at the expansion joints are also not modeled. A detail of this model is shown in Figure 2.8.

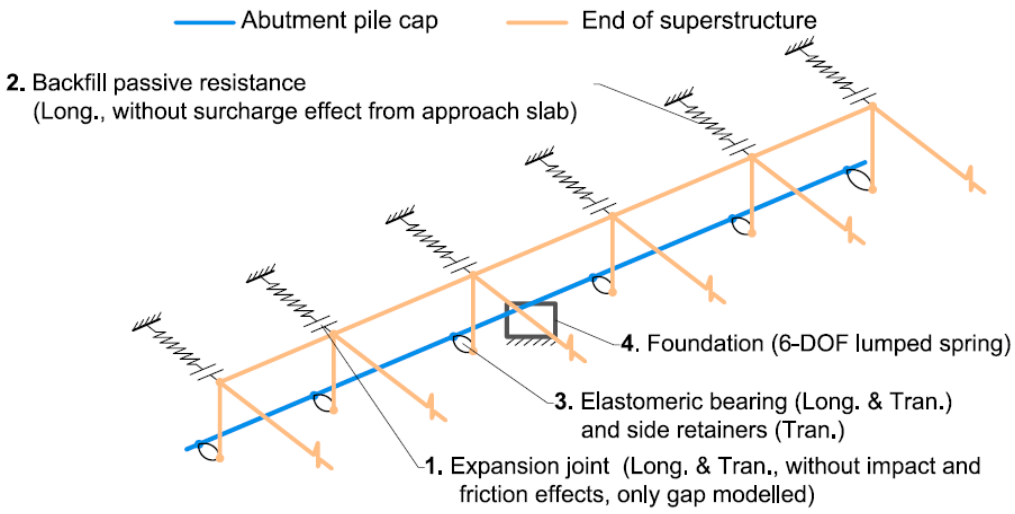

Figure 2.8: Simplified abutment model per Luo et al. (2017)

Static pushover analyses were performed in the longitudinal and transverse directions in order to assess the response of a prototype bridge (proportioned according to the IDOT (2012) Bridge Manual) with the previously mentioned simplified and detailed abutment models.

According to these analyses, in the longitudinal direction, the forces obtained from the simplified model are much lower than those obtained from the detailed model. One of

the reasons for this difference was that, in the simplified model, the abutment resistance relies only on the backfill passive pressure (the backwall is omitted by assuming a post-fusing state from the beginning of the analysis). Under this modeling assumption, the abutment foundation barely provides longitudinal resistance to the displaced structure. In addition, omission of the approach slab friction and surcharge effects also reduce the abutment resistance. A plot that illustrates the differences between the longitudinal pushover analyses of these models is shown in Figure 2.9.

In the transverse direction, it was observed that both models provide similar total abutment force; nevertheless, the foundation force of the simplified model is considerably higher than that of the detailed model. This observation is consistent with the simplified modeling strategy that is based on only the foundation to provide transverse resistance forces. A plot that illustrates the differences between the transverse pushover analyses of these models is shown in Figure 2.10.

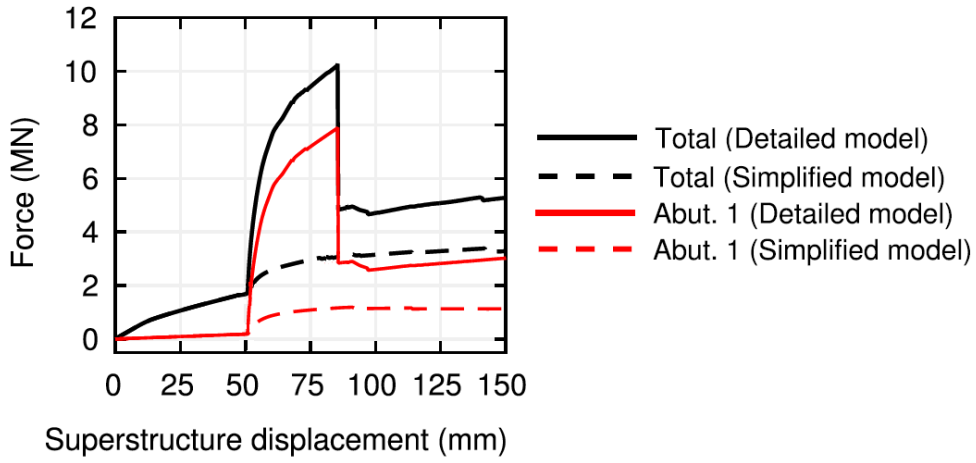

Figure 2.9: Longitudinal pushover analysis of bridges with simplified and detailed abutment models per Luo et al. (2017)

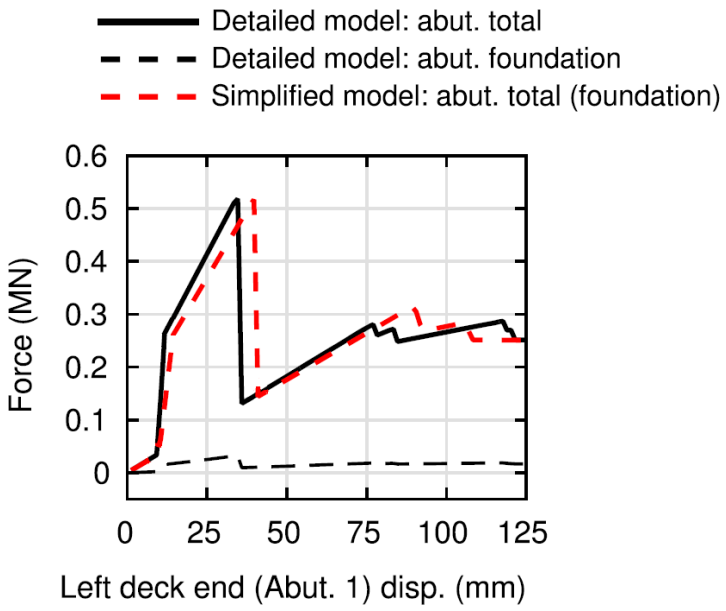

Figure 2.10: Transverse pushover analysis of bridges with simplified and detailed abutment models per Luo et al. (2017)

Likewise, nonlinear dynamic analyses were performed in the longitudinal and transverse directions. A suite of 10 synthetic ground motions that modeled the regional seismic hazard for a 1000-year return period at Paducah, Kentucky was utilized. This suite of ground motions was considered during Phase I (Report ICT-R27-070).

In order to summarize the results of nonlinear dynamic analyses, an indicator that quantifies the influence of abutment model sophistication on key components of the bridge was utilized. This indicator is the percentage change (PC) and is defined as follows:

$$PC = \frac{\max_t |u_{SM}(t)| - \max_t |u_{DM}(t)|}{\max_t |u_{DM}(t)|} \times 100 \qquad (2.3)$$

In this expression, $u_{DM}(t)$ is the time history of a specific structural response obtained from the detailed abutment model, whereas $u_{SM}(t)$ is obtained from the simplified abutment model. A plot that contains values of this indicator for the response of different structural elements is shown in Figure 2.11.

In the longitudinal direction, the simplified abutment model results in significantly overestimated displacements of the superstructure, piers, and foundations. In the transverse

direction, the two models had similar structural response except for the case of abutment foundation displacement in soft soil. These results are consistent with the observations of the pushover analysis.

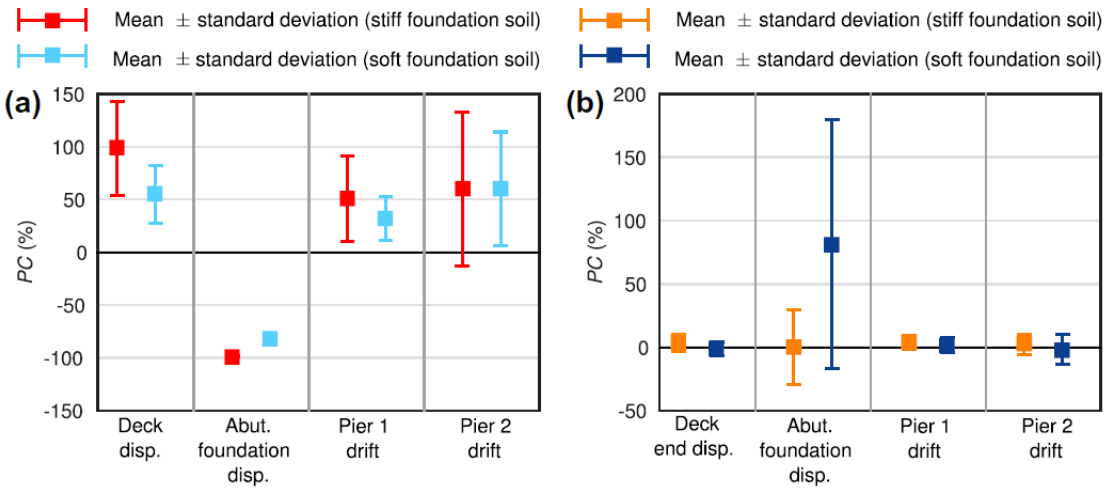

Figure 2.11: Comparison of bridge seismic response for simplified and detailed abutment models per Luo et al. (2017): a) longitudinal direction b) transverse direction

2.2.2. "Seismic design of bridges with seat-type abutments considering the participation of the abutments during earthquake excitation"

Mitoulis (2012) performed a parametric study in order to analyze the influence of abutment-backfill interaction on the overall structural behavior of a set of bridges. This set comprises three seat-type abutment bridges with different kinds of superstructures, substructures, number of spans, and soil types. These bridges are examples of infrastructure of the Greek highway system. A detail of these bridges is shown in Figure 2.12.

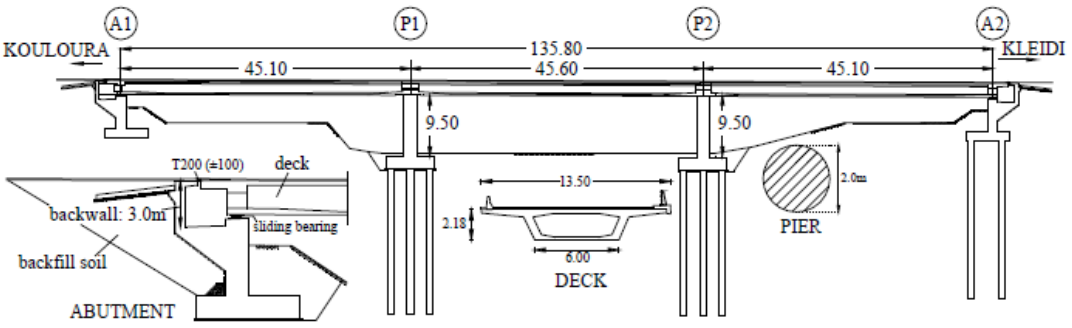

Figure 1. Longitudinal section of Kleidi-Kouloura bridge and the cross sections of the abutment, the deck at the mid-span and the pier.

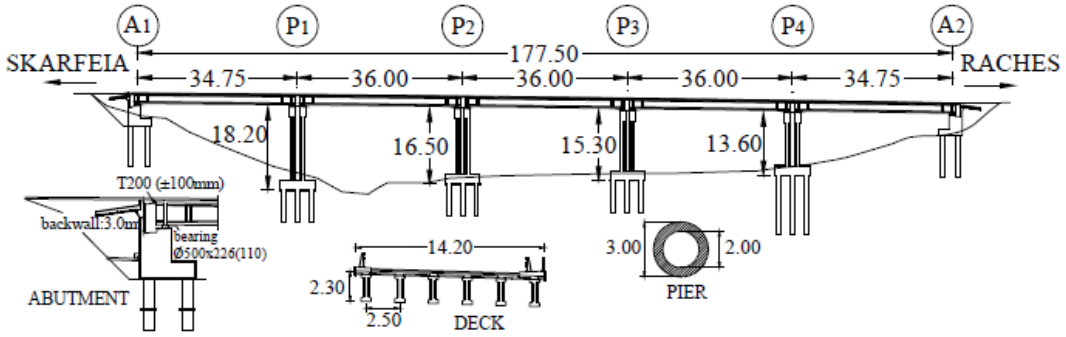

Figure 2. Longitudinal section of Scarfeia-Raches bridge and the cross sections of the abutment, the deck at the mid-span and the pier.

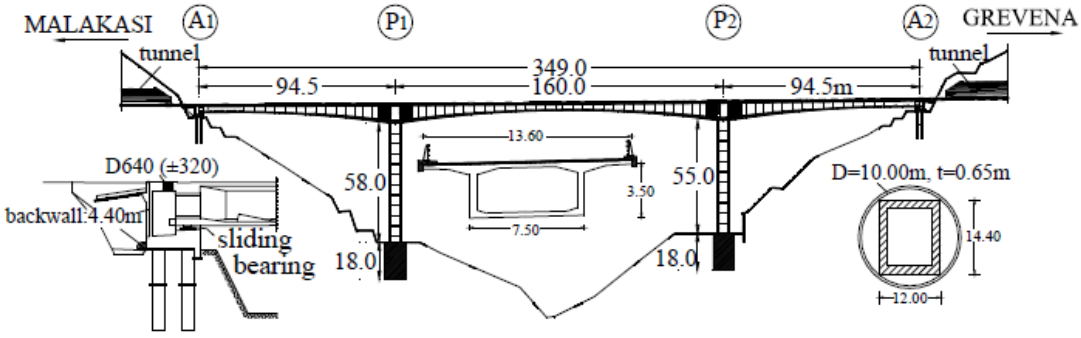

Figure 3. Longitudinal section of Malakasi-Grevena bridge and the cross sections of the abutment, the deck at the mid-span and the pier.

Figure 2.12: Bridge models analyzed by Mitoulis (2012)

These bridges were modeled by either neglecting or considering abutment-backfill participation, as follows:

- The models that neglected backfill participation were formulated by using frame elements and discrete springs. In these models, the deck was seated on slide

supports at the abutments. The deck was connected to the piers by using stiff zones and rigid connections. Pier foundations were connected in series with nonlinear rotational spring elements to model possible plastic hinges. Soil springs were used to model the flexibility of the foundation. A detail of these models is shown in Fig. 2.13.

- The models that considered backfill participation were formulated by using three-dimensional elements that accounted for the abutment's stiffness, backfill soil resistance and mass, the friction between backfill and wingwalls, the friction between backfill and approach slab, and the masses of wingwalls. The resistance of the backwall was taken into account by considering the Caltrans (2006) model or the formulation based on the mobilized logarithmic spiral failure coupled with modified hyperbolic abutment-backfill stress-strain behavior (the so-called LSH model per Shamsabadi et al. (2007) . A detail of these models is shown in Fig. 2.14.

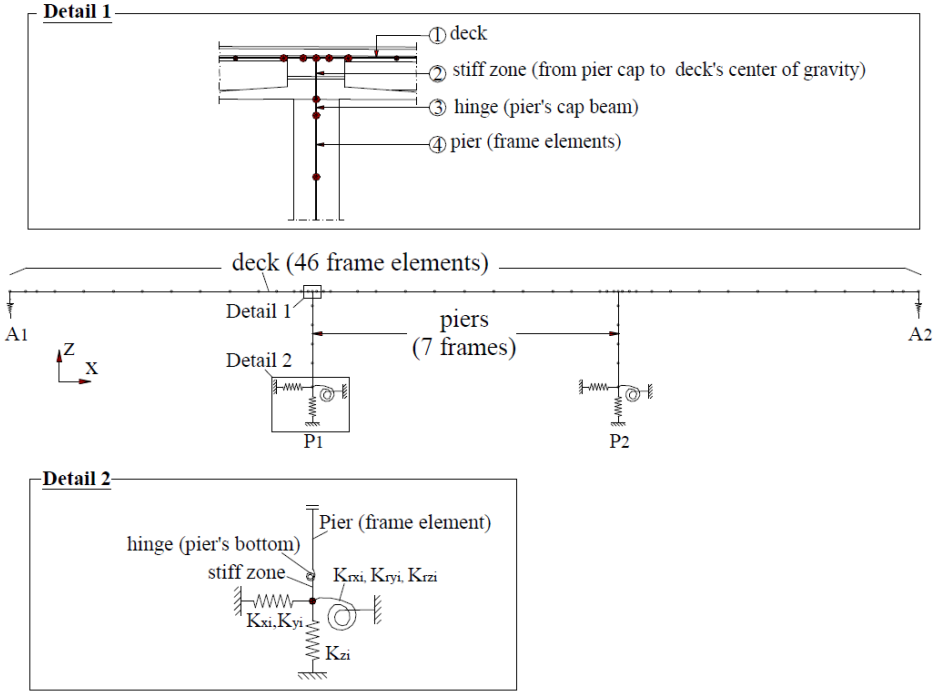

Figure 2.13: Bridge model without abutment-backfill participation per Mitoulis (2012)

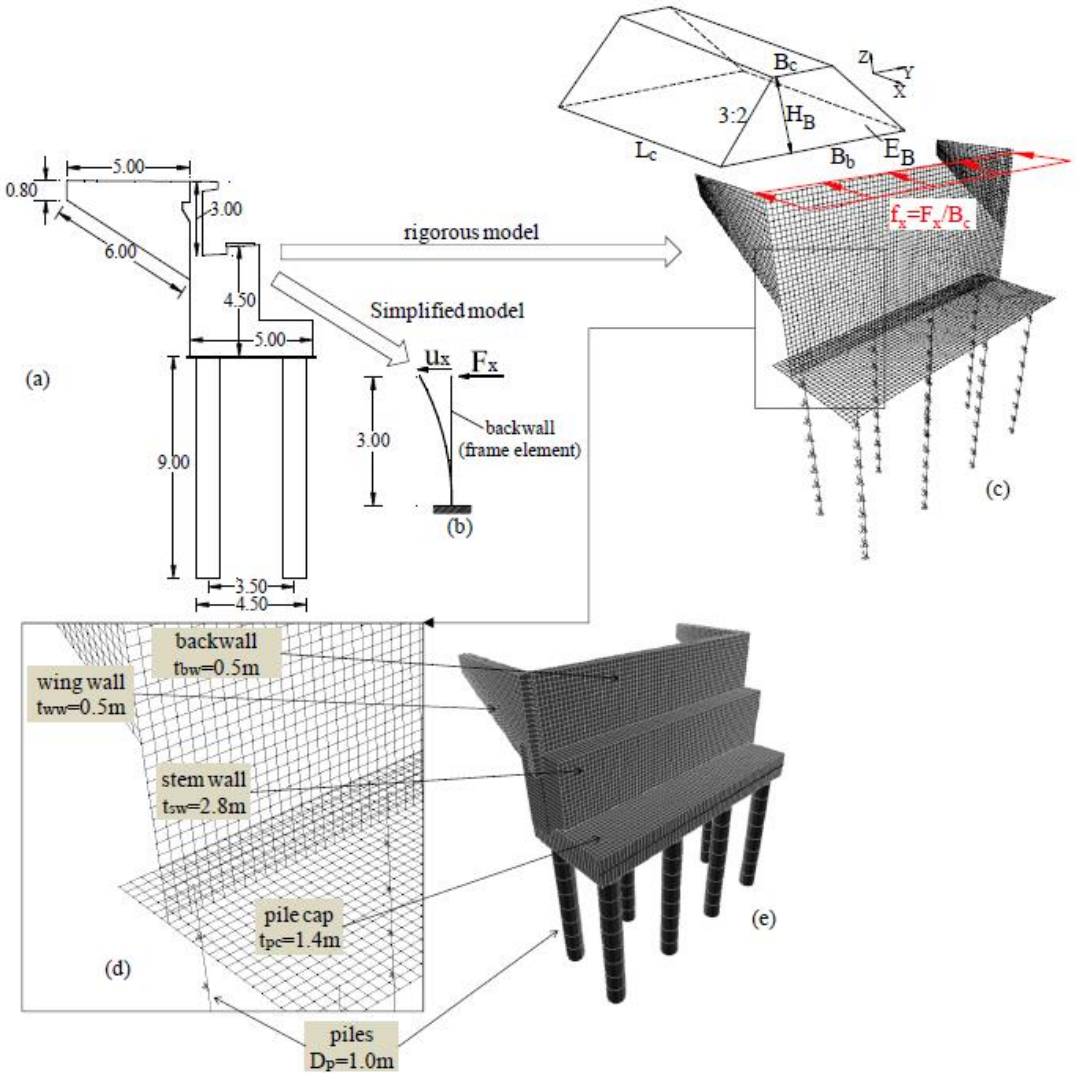

Figure 2.14: Bridge model with abutment-backfill participation per Mitoulis (2012)

After completing the dynamic analyses of the proposed parametric variations, Mitoulis (2012) made the following observations:

- The bridge model became stiffer when abutment-backfill participation was considered. Due to this stiffness modification, the first longitudinal modal period of the bridge models was found to be reduced by approximately 28%.

- Likewise, it was possible to notice a reduction in the deck movements. Considering the Caltrans model for the resistance of backwalls, these reductions were approximately 25%, 13%, and 11% for the cases of soil types A, B, and C, respectively.
- Considering the LSH model for the resistance of backwalls, these reductions were approximately 22%, 25%, and 18% for the cases of soil types A, B, and C respectively.
- When considering abutment-backfill interaction, the dynamic stiffness and mobilized mass of the abutment and the backfill soil become less significant in comparison to the total stiffness and mass of the bridge.

2.2.3. "Seismic response of bridge abutments on surface foundation subjected to collision forces"

Argyroudis et al. (2013) performed a comparison between abutment models developed with 2D nonlinear finite elements using the program Plaxis and abutment models developed with frame elements and discrete springs using the program SAP2000. This comparison focused only on abutment models (without developing comprehensive bridge models). A step-by-step analysis-comparison procedure was followed, starting from simple static to complex nonlinear dynamic models.

The Plaxis model consisted of a 2D finite element model. In order to define this model, a set of analysis was first performed to simulate initial geostatic stresses, as well as the construction of the wall and backfill. Elasto-plastic soil behavior was used, and proper interface elements were included to model friction conditions between the backfill and foundation soil with the wall. A detail of this model is shown in Figure 2.15.

Among the different models developed in SAP2000, a model was to resemble the response of the Plaxis model against dynamic excitations. This model was developed by placing springs along the entire height of the wall. These springs follow a linear behavior. For the abutment foundation, linear springs were also placed all along this element. A detail of this model is shown in Figure 2.16. The stiffnesses of the springs for the wall and foundation were determined based on an iterative analysis that attempts to match the

response of the Plaxis model. A plot that shows both the response of the final SAP2000 model and the Plaxis model is shown in Figure 2.17.

In order to compare this SAP2000 model and the model developed with Plaxis, four different simplified input motions were chosen. The following periods (T) and durations (t) were used: a) T=0.10 s, t=0.35 s; b) T=0.25 s, t=0.875; s c) T=0.50 s, t=1.75; s; d) T=1.00 s, t=3.50 s. A maximum input force of 1000 kN was applied.

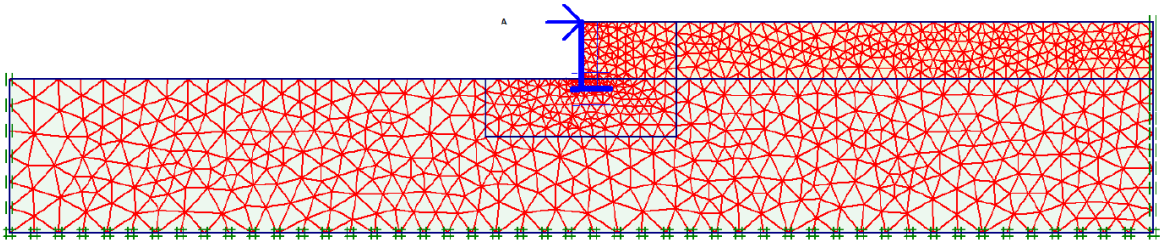

Figure 2.15: Plaxis 2D finite element model per Argyroudis et al. (2013)

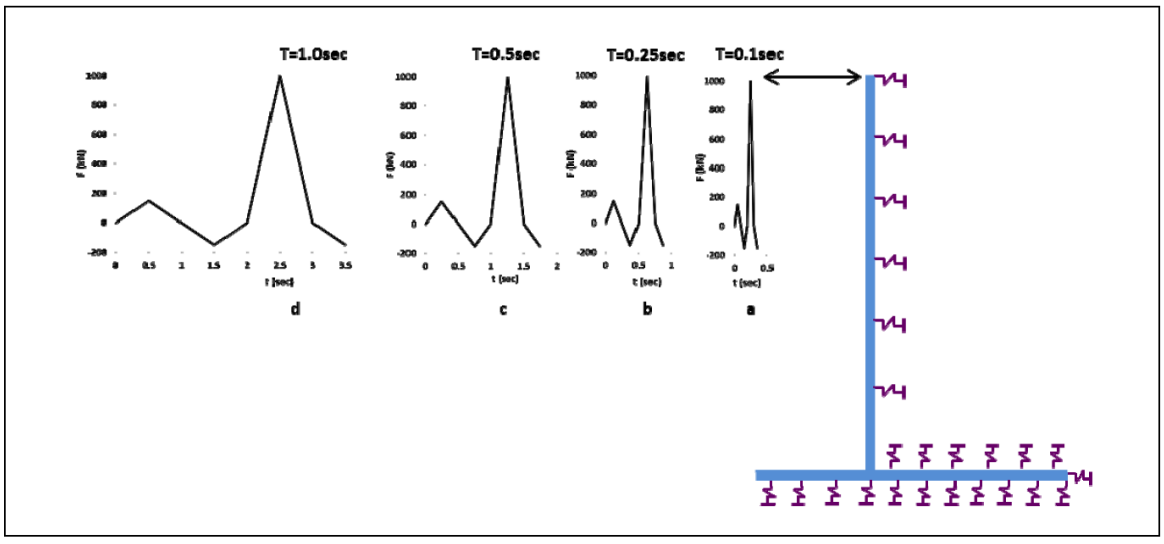

Figure 2.16: SAP2000 model for dynamic excitations per Argyroudis et al. (2013)

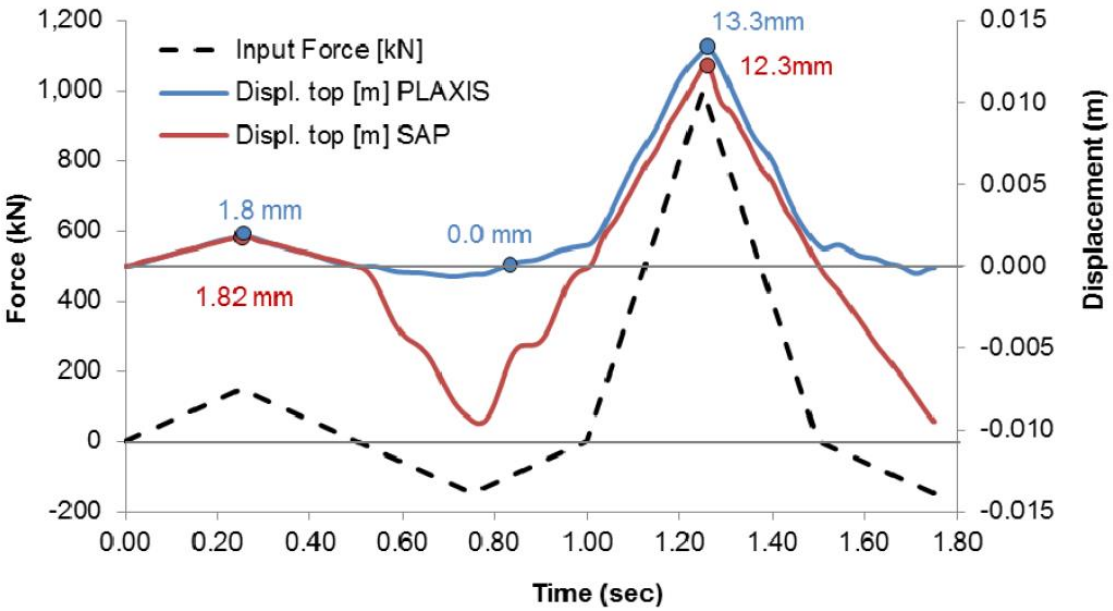

Figure 2.17: Comparison of abutment response between Plaxis and SAP2000 models per Argyroudis et al. (2013)

Once the iterative process determined the appropriate values of stiffness for the linear springs placed at the wall and foundation, a good agreement for the peak values of the positive displacements, which correspond to the maximum applied forces towards the backfill.

The difference between the two models at t=0.7 s, t=1.0 s, and t=1.45s is due to the resistance of the backfill at the lower part of the abutment in the Plaxis model, when the force towards the deck is applied.

3. MODELING OF PROTOTYPE QUASI-ISOLATED HIGHWAY BRIDGES

This chapter presents the detailed features for the superstructures, substructures, foundations, and superstructure-substructure connections of the bridge models that were generally specified back in Chapter 1. As indicated in that chapter, these four bridge model variants can be found in both of "Seismic Performance of Quasi-Isolated Highway Bridges in Illinois: Phase I" (Report ICT-R27-070) (LaFave et al., 2013a) and "Calibration and Refinement of Illinois' Earthquake Resisting System Bridge Design Methodology: Phase II) (Report ICT-R27-133) (LaFave et al., 2018). These bridge models were selected in order to otherwise perform a consistent comparison of the structural response for bridge prototypes that present different levels of modeling sophistication.

The nonlinear finite element program Open System for Earthquake Engineering Simulation (OpenSees) (McKenna et al., 2011) was utilized to formulate the computational models of these bridges. Detailed three-dimensional finite element models were developed for each of the four bridge variants.

3.1. Selected Prototypes of Quasi-Isolated Highway Bridges

The selection of bridges for the current study consists of three-span bridges with steel-plate girders that have sequential span lengths of 24.4, 36,6 and 24.4 m (80, 120 and 80 ft). These bridges are supported by non-skew seat-type abutments and RC multi-column intermediate piers. Superstructure girders are supported by IDOT Type I bearings at the abutments and Pier 1, and by low-profile fixed bearings at Pier 2. The RC multi-column intermediate piers are 4.57 or 12.19 m high (15 or 40 ft). Soft and hard foundation soil conditions are considered. The combination of these parameters results in 4 bridge variants. The design parameters for these variants are specified in Table 3.1 and Table 3.2. An example of these bridges is shown in Figure 3.1.

In this study, the deck width was kept constant for all the selected bridge models. The out-to-out deck width of 43 ft – 2in (13.2 m), is a typical width for two-lane highway bridges with roadways and shoulders (Luo, 2016). A detail of the deck cross-section is shown in Figure 3.2.

Table 3.1: Design parameters of structural components of three-span steel bridges

Bridge type	3-span steel-girder (3S) Bridge
Span length [m (ft)]	24.4-36.6-24.4 (80-120-80)
Superstructure	
No. of girders	6
Girder depth [mm (in.)]	1067 (42)
Girder spacing [m (ft)]	2.29 (7.5)
Deck width [m (ft)]	13.15 (43.2)
Deck thickness [mm (in.)]	210 (8.25)
Bearing components	
Bearings at abutments	Type I, 11-d
Elastomer planar dimensions [mm (in.)]	280 x 406 (11 x 16)
Elastomer thickness [mm (in.)]	89 (3.50)
No. of anchors per retainer	1
Retainer anchor dia. [mm (in.)]	25.4 (1.0)
Retainer anchor steel	A36
Bearings at expansion piers	Type I, 18-a
Elastomer planar dimensions [mm (in.)]	457 x 610 (18 x 24)
Elastomer thickness [mm (in.)]	76 (3.0)
No. of anchors per retainer	1
Retainer anchor dia. [mm (in.)]	38.1 (1.5)
Retainer anchor steel	A36
Sacrificial connections at fixed pier	Steel fixed bearing
Anchor diameter [mm (in.)]	38.1 (1.5)
No. of anchor per girder line	2
Anchor steel grade	A36
Multi-column pier	
Column clear height [m (ft)]	4.57 (15) / 12.19 (40)
Column diameter [m (ft)] 4.57 (15) / 12.19 (40)	1.07 (3.5) / 1.22 (4.0)
No. of columns	4
Concrete nominal strength [MPa (ksi)]	24 (3.5)
Reinforcement ratio	2%
Reinforcement yield strength [MPa (ksi)]	414 (60)
Pier cap cross-sectional width and height [m (ft)]	1.52 x 1.22 (5 x 4)
Pile cap cross-sectional width and height [m (ft)]	3.66 x 1.07 (12 x 3.5)

Table 3.1 continued

Bridge type	3-span steel-girder (3S) Bridge
Seat-type abutment	
Expansion joint width [mm (in.)]	50.8 (2)
Backwall cross section [m (in.)]	1.14 x 0.61 (45 x 24)
Pile cap cross section [m (in.)]	1.98 x 1.07 (78 x 42)

Table 3.2: Bridge variants

Component	Alternatives
Span Length [m (ft)]	24.4-36.6-24.4 (80-120-80)
Pier column height [m (ft)]	4.57 (15) 12.19 (40)
Foundation soil condition	Hard Soft
Total number of bridge variants	**4**

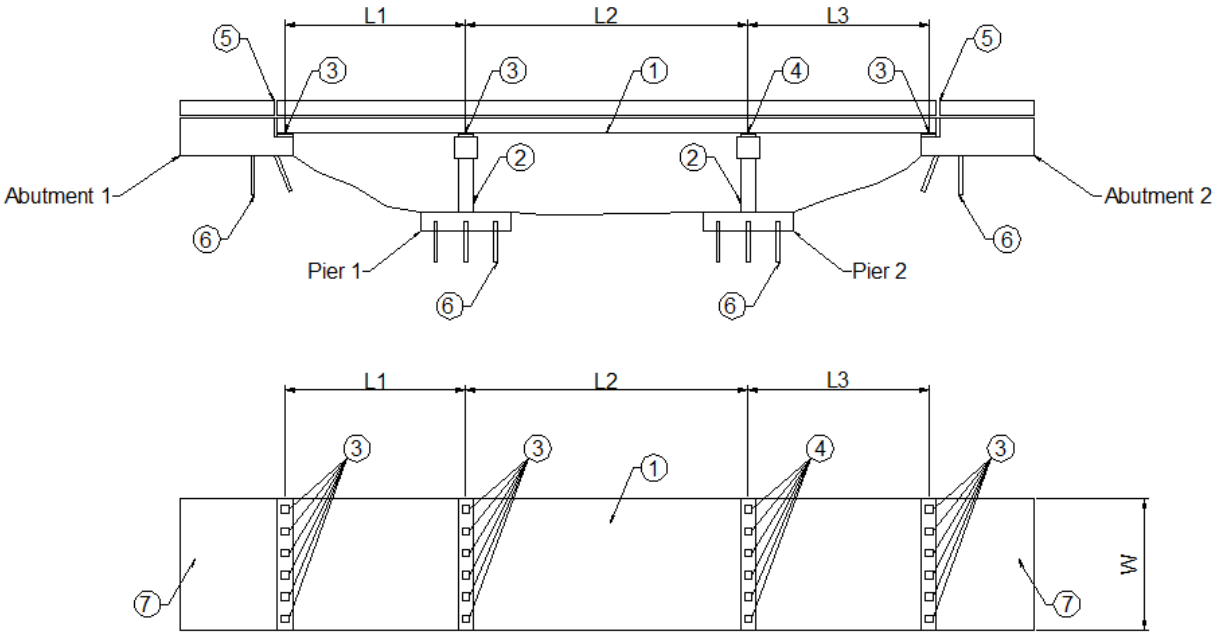

① Steel plate girders with composite concrete deck
② Multi-column reinforced concrete pier
③ IDOT Type I bearing
④ IDOT Low-profile fixed bearing
⑤ Thermal expansion joint
⑥ Steel H pile
⑦ Concrete approach slab

W = 13.16 m (43' - 2")
L1 = 24.38 m (80')
L2 = 36.58 m (120')
L3 = 24.38 m (80')

Figure 3.1: Prototype three-span steel-plate-girder (3S) quasi isolated seat-type abutment bridge

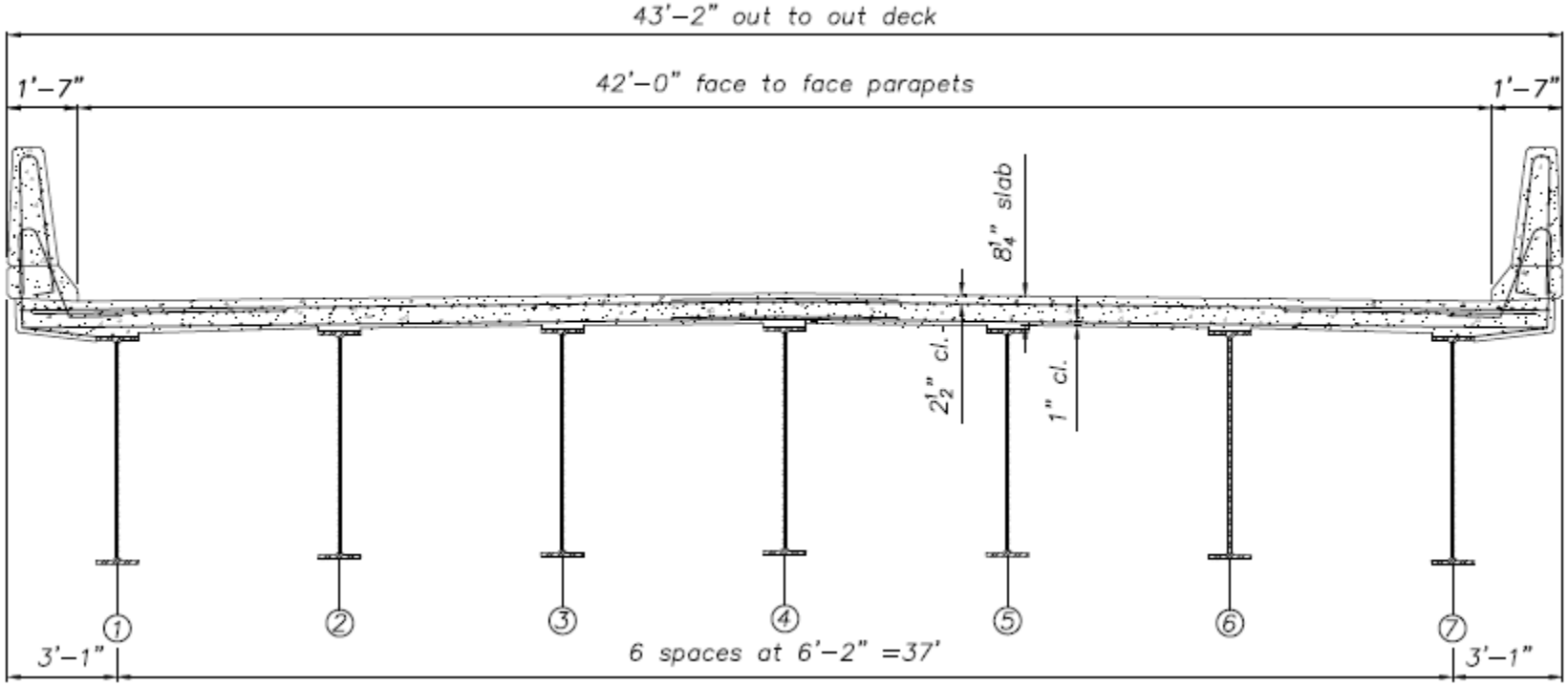

Figure 3.2: Cross section of the three-span steel-plate-girder (3S) bridge superstructure per Luo (2016)

Phase I and Phase II structural models of seat-type abutment bridges are referred to by using a different nomenclature string.

Phase I nomenclature strings are composed of 8 characters. For instance, "**SlC15T1F**" indicates a three-span steel-plate girder bridge ("**Sl"**), pier columns with a clear height of 15-ft (4.57 m) ("**C15"**), IDOT Type I bearings at abutments and expansion pier ("**T1"**) and hard (fixed) soil foundation ("**F"**).

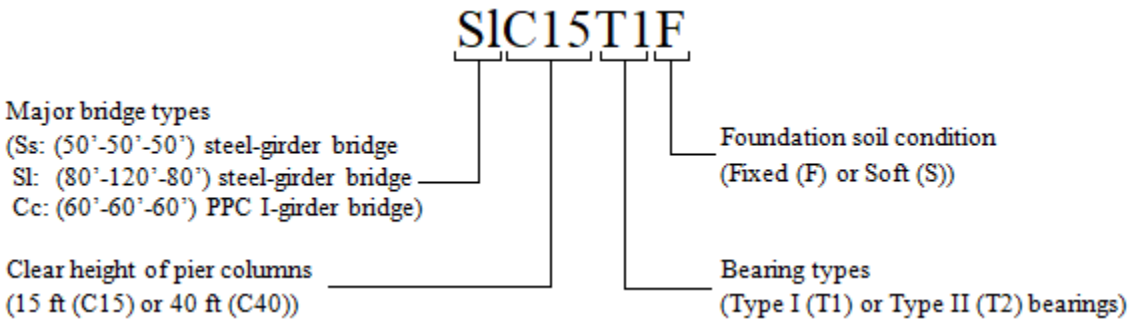

Figure 3.3: Nomenclature for prototype bridge variants of Phase I

Phase II nomenclature strings are also composed of 8 characters. For example, the same bridge variant mentioned before is named as "**3S00P15H**". Likewise, this nomenclature indicates a three-span steel-plate girder bridge ("**3S**"), with a skew angle of 0° ("**00**"), pier columns with a clear height of 15-ft (4.57 m) ("**P15**"), and hard foundation soil ("**H**").

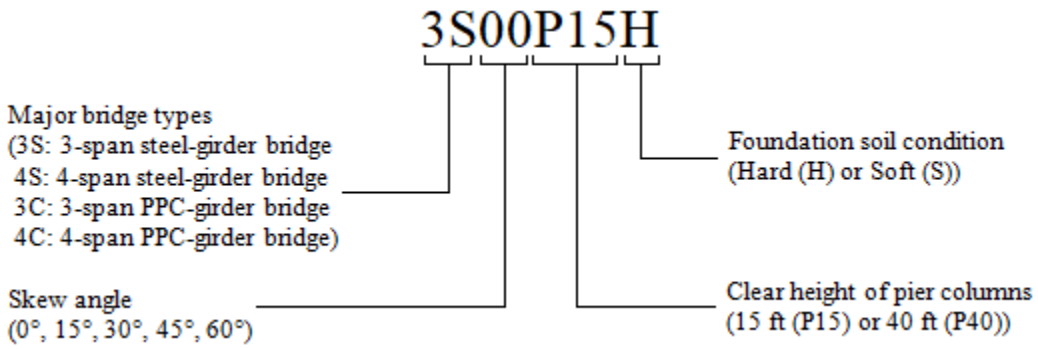

Figure 3.4: Nomenclature for prototype bridge variants of Phase II

For this study, the Phase I nomenclature will be used to identify the selected bridge variants.

Table 3.3 shows the component and total mass of the bridge variants selected ("Sl" bridges) for the case of pier columns with a clear height of 4.57 m (15-ft). For these structural models, superstructure mass is directly related to the seismic force demand on the bridge.

Table 3.3: Component and total mass of prototype bridges (units: 10^3 kg)

Bridge	**"Sl" Bridges**
Superstructure	1197
Abutments	
Backwall	48
Pile cap	128
Wingwall	54
Piers	
Pier cap	117
Pier column	79
Pile cap	240
Total mass	1863

Figures 3.5 and 3.6 illustrate examples of three-dimensional finite element models of three-span steel-plate girder bridges and pier columns with a clear height of 15-ft and 40-ft respectively.

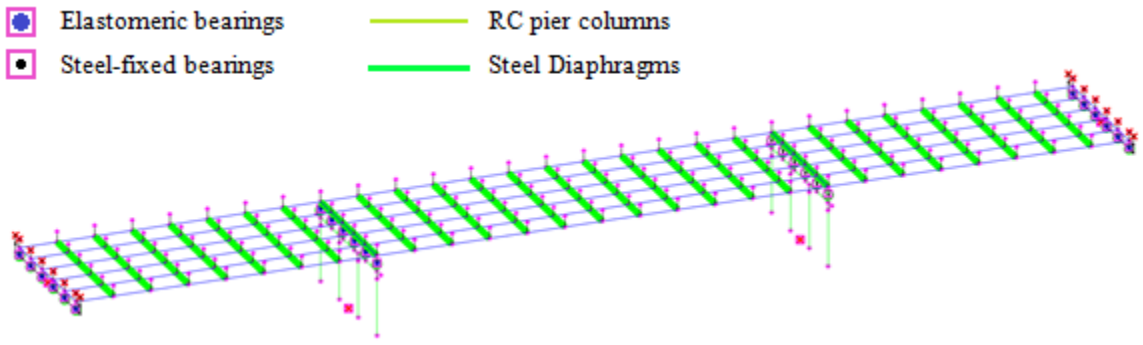

Figure 3.5: Three-dimensional finite element model of SlC15T1F bridge

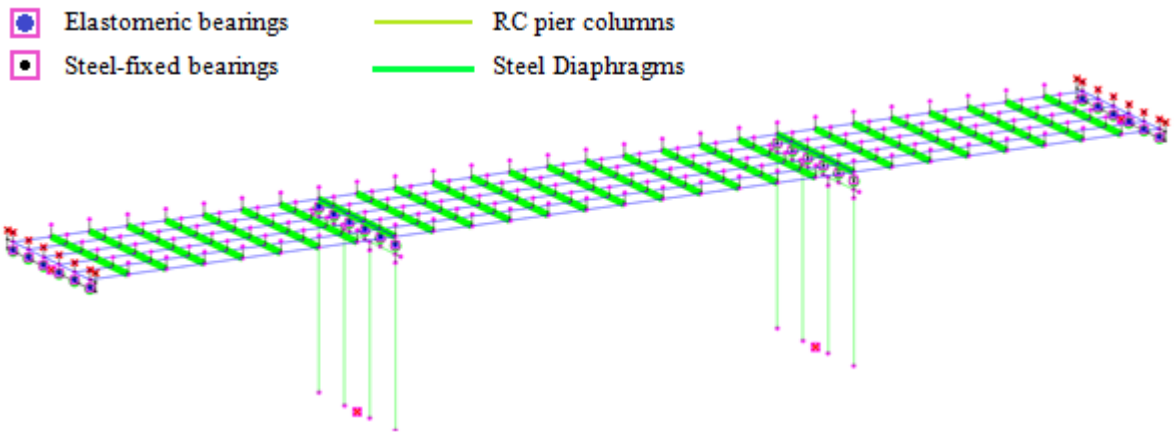

Figure 3.6: Three-dimensional finite element model of SlC40T1F bridge

3.2. Bridge Superstructure Model

The bridge superstructure was modeled using a grid model as proposed by Chang & White (2008) and Barth & H. Wu (2006). This model is illustrated in Figure 3.7. The grid model distributes mass in the plane of the deck and captures superstructure stiffness in three dimensions. Six longitudinal elements represented the composite stiffness of the steel girders and concrete deck. Transverse elements were added to represent the deck stiffness in that direction, linking the girders for torsional stiffness and out-of-plane deformation. Transverse elements were also added to represent diaphragms. Parapet stiffness was neglected, and the gross moments of inertia about the "x" and "y" axes were multiplied by 0.75 and 0.35, respectively, to account for cracking (LaFave et al., 2013b).

The properties of the longitudinal beam elements were determined using composite sectional properties of the girders and concrete slab. According to Article 4.6.2.6 of the AASHTO LRFD Bridge Design Specification (AASHTO, 2010), the slab effective flange width, b_{eff}, of the interior girders is taken as the tributary width perpendicular to the axis of the girder. For exterior girders with deck overhang and concrete parapets, b_{eff}, includes half of the girder spacing and the full overhang width that is further extended to take into account the concrete parapet After determining b_{eff}, the concrete slab within b_{eff} was transformed into an extended portion of the girder section, based on the elastic modular ration between girder steel and slab concrete materials $\left(n_E = \frac{E_{S,\,girder}}{E_{c,slab}}\right)$ (Luo, 2016).

Figure 3.8 shows the transformed section of a steel-plate girder with concrete slab. Table 3.4 includes a summary of the elastic properties of the materials used for steel girders and slab.

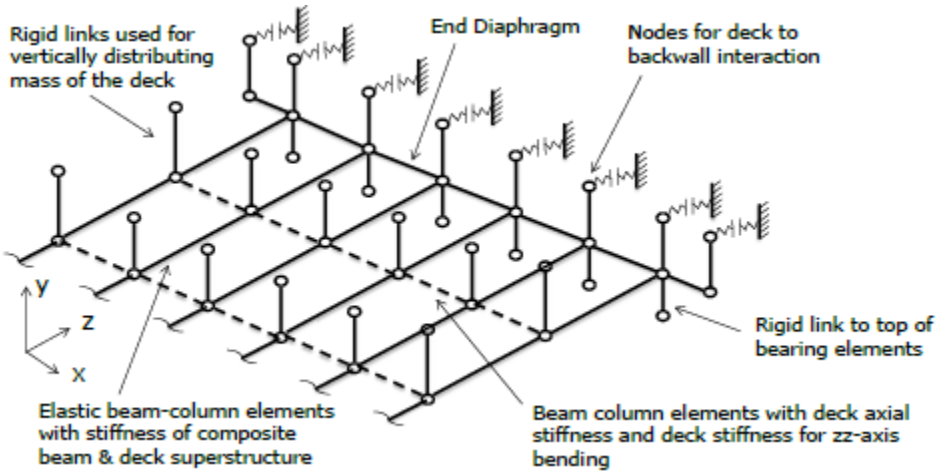

Figure 3.7: Grid model used to represent superstructure per LaFave et al. (2013b)

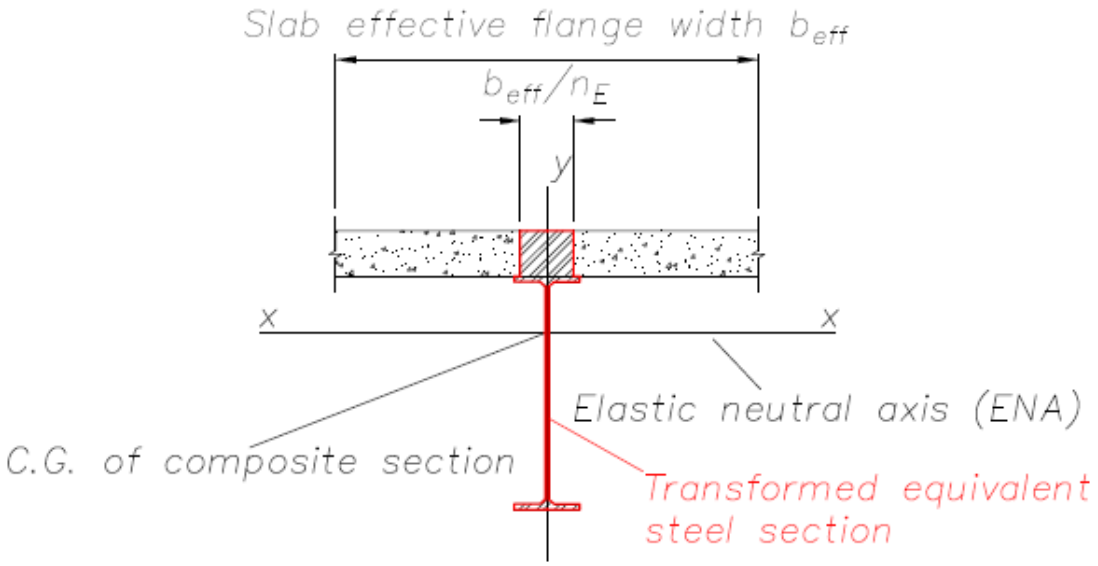

Figure 3.8: Transformed section of a steel-plate girder with concrete slab per Luo (2016)

Table 3.4: Superstructure material properties

Material	Strength	Modulus of elasticity
Concrete slab	$f'_{c,\ slab}$ = 27.6 MPa (4 ksi)	$E_{c,slab}$ = 24.9 GPa (3605 ksi)
Steel of plate girder	$f_{y,\ girder}$ = 345 MPa (50 ksi)	$E_{s,girder}$ = 200 GPa (29000 ksi)

The properties of the transformed sections were calculated and included in Table 3.5. These properties were assigned to the longitudinal beam elements in the grid model.

Table 3.5: Sectional properties of longitudinal beam elements in superstructure models

Bridge Type		"Sl" Bridges
Girder type		Steel plate girder
Girder depth [cm (in.)]		116.8 (46.8)
Flange width [cm (in.)]		30.5 (12)
Flange thickness [cm (in.)]		5.1 (2)
Web depth [cm (in.)]		106.7 (42)
Web thickness [cm (in.)]		1.1 (0.44)
Concrete slab thickness [cm (in.)]		21.0 (8.25)
Properties of transformed interior girder section	Area [cm^2 ($in.^2$)]	1024 (158.7)
	Moment of inertia about x-x axis [cm^4 ($in.^4$)]	$2.27x10^6$ ($5.43x10^4$)
	Moment of inertia about y-y axis [cm^4 ($in.^4$)]	$2.58x10^6$ ($6.18x10^4$)
	Torsional constant [cm^4 ($in.^4$)]	$8.57x10^4$ (2059)
Properties of transformed exterior girder section	Area [cm^2 ($in.^2$)]	1138 (176)
	Moment of inertia about x-x axis [cm^4 ($in.^4$)]	$2.37x10^6$ ($5.70x10^4$)
	Moment of inertia about y-y axis [cm^4 ($in.^4$)]	$4.96x10^6$ ($1.19x10^5$)
	Torsional constant [cm^4 ($in.^4$)]	$1.03x10^5$ (2467)

The member size, longitudinal spacing, and configuration of the diaphragm (cross-frame) members are indicated in Table 3.6 and Figure 3.9. In the selected bridges, a single C shaped structural member is used to connect the webs of adjacent girders at bracing locations along the span (IDOT, 2012).

Table 3.6: Configuration of diaphragms (cross-frames) between girders

Bridge type	"Sl" Bridges
Member size	C15x50
Longitudinal spacing [m (ft)]	6.10 (20)

The diaphragms, which consist of a C-shaped structural member, were modeled using transverse beam elements whose elastic stiffness was determined based on the sectional properties of the corresponding steel shape. The diaphragms link the girders for torsional stiffness and out-of-plane deformation.

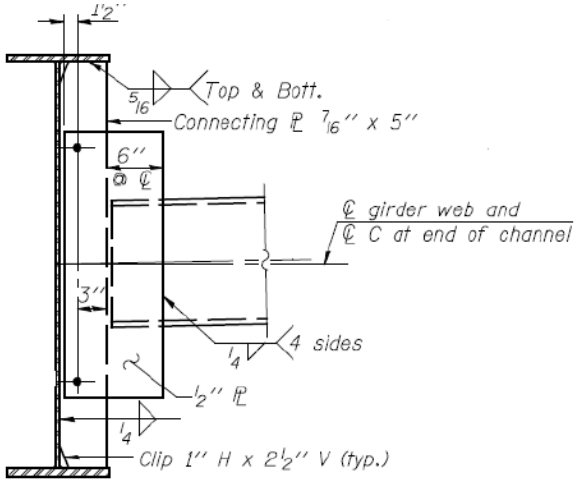

Figure 3.9: Diaphragm of "Sl" bridges (C15x50 structural shape) per IDOT (2012)

3.3. Bridge Substructure Model

The bridge superstructure is supported by RC multi-column intermediate piers along with seat-type abutments. Each pier consists of four circular columns, a pier cap, and a pile cap. The two piers of any of the four bridge variants have the same column height; i.e., either 4.57 m (15 ft) or 12.19 m (40 ft). Figure 3.10 shows the pier and the elements employed to formulate a computational model based on finite elements. Parameters such as number, diameter, and spacing of pier columns are indicated in Table 3.7.

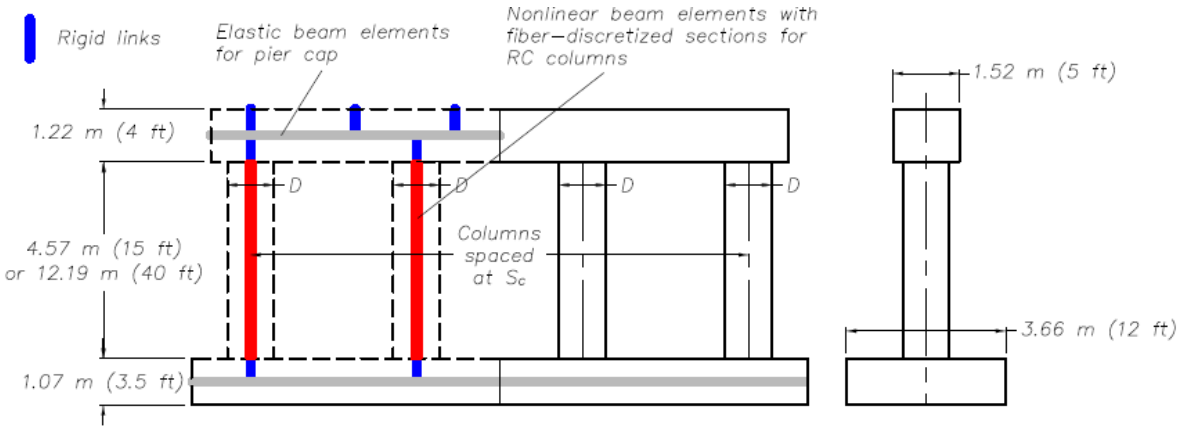

Figure 3.10: Multi-column intermediate pier substructure per Luo (2016)

Table 3.7: Parameters of columns at intermediate piers

Bridge	"Sl" Bridges
Column number per pier	4
Diameter of 4.57-m-tall columns [m (ft)]	1.07 (3.5)
Diameter of 12.19-m-tall columns [m (ft)]	1.22 (4.0)
Center-to-center column spacing [m (ft)]	3.81 (12.5)
Spacing normalized to diameter (4.57-m-tall columns)	3.56
Spacing normalized to diameter (12.9-m-tall columns)	3.12

The finite element model shown in Figure 3.10 was formulated with linear elastic beam elements to represent the pier cap and pile cap. The pier columns were modeled using nonlinear beam elements with distributed plasticity (Neuenhofer & Filippou, 1997). Each pier column was discretized into ten nonlinear beam elements of equal length, and each element had three integration points for Legendre-Gauss quadrature. At each integration point, a fiber discretized reinforced concrete section was employed to determine the element stiffness matrix, considering the nonlinear constitutive relation of concrete and steel materials under combined axial and flexural loads. Figure 3.11 shows the fiber mesh of the column cross section. Fibers of three types of materials were included in the section in order to model the unconfined concrete cover, confined concrete core, and the vertical reinforcing steel (Luo, 2016). Table 3.8 indicates the properties of the concrete and reinforcing steel.

Constitutive properties of the confined concrete core were defined using the model proposed by Mander et al. (1988), per Article 8.8.4 of the AASHTO Guide Specifications for LRFD Seismic Bridge Design (AASHTO, 2010). The material properties were assigned as the Concrete02 (Mohd Yassin, 1994) and Steel02 (Menegotto & Pinto, 1973) materials in OpenSees. Figure 3.12 shows the constitutive models of these two materials in OpenSees. The axial and flexural stiffnesses of the column were captured by the fiber-discretized sections, whereas shear stiffness of the column section was defined as $0.8\ G_c A_g$, where G_c is the shear modulus of concrete and A_g is the gross cross-sectional area of the column, per article 8.6.2 of the AASHTO Guide Specifications for LRFD Seismic Bridge Design (AASHTO, 2010). According to article 5.6.5 of this specification, the effective torsional moment of inertia of the column cross-section was defined as $0.2\ J_g$, where J_g is the gross torsional moment of inertia of the column cross section (Luo, 2016).

The pier columns, pier cap, and pile cap indicated in Figure 3.10 were modeled at their axis locations, which resulted in offsets between the column ends and the pier and pile caps. For this reason, rigid links were used to consider these offsets and connect the column ends to the pier and pile caps. Likewise, rigid links were also used to connect the pier cap to the bearings (Luo, 2016).

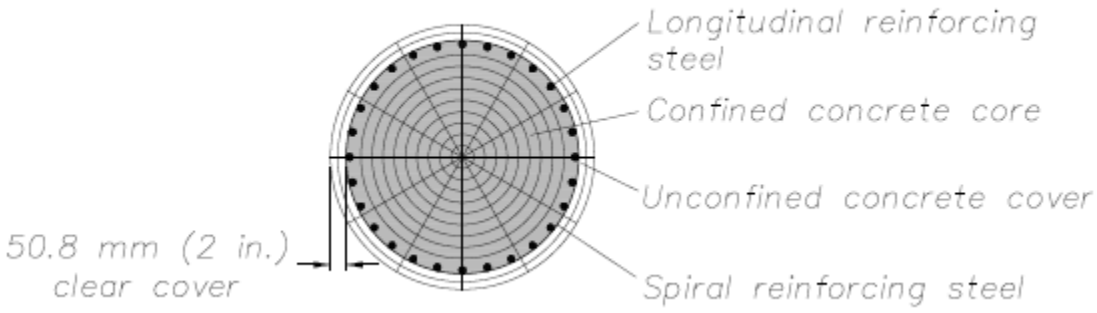

Figure 3.11: Fiber discretized section of RC pier columns per Luo (2016)

Table 3.8: Material properties of pier column

Element	Component	4.57 m (15 ft) Pier columns	12.19 m (40 ft) Pier columns
Concrete	Clear cover thickness [mm (in.)]	50.8 (2.0)	50.8 (2.0)
	Compressive strength [MPa (ksi)]	24.1 (3.5)	24.1 (3.5)
Vertical reinforcement	Bar diameter [mm (in.)]	28.7 (1.128)	28.7 (1.128)
	No. of bars	28	36
	Yield strength [MPa (ksi)]	414 (60)	414 (60)
	Reinforcement ratio	2%	2%
Transverse reinforcement	Spiral diameter [mm (in.)]	12.7 (0.5)	12.7 (0.5)
	Spiral hoop spacing [mm (in.)]	76.2 (3.0)	76.2 (3.0)
	Yield strength [MPa (ksi)]	414 (60)	414 (60)

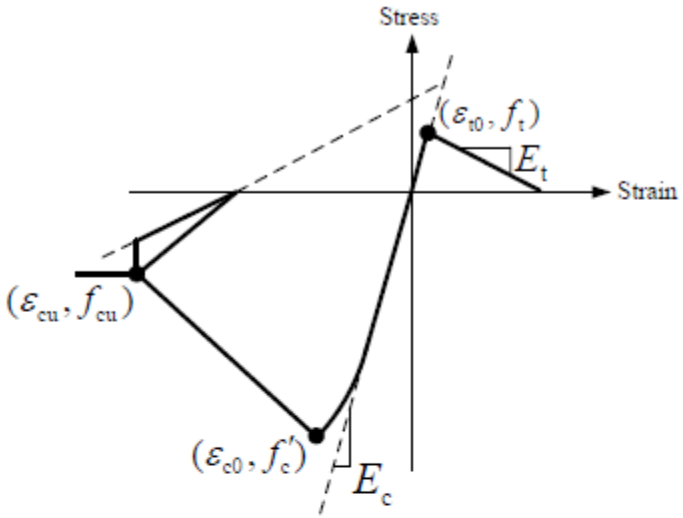

(a) Concrete02

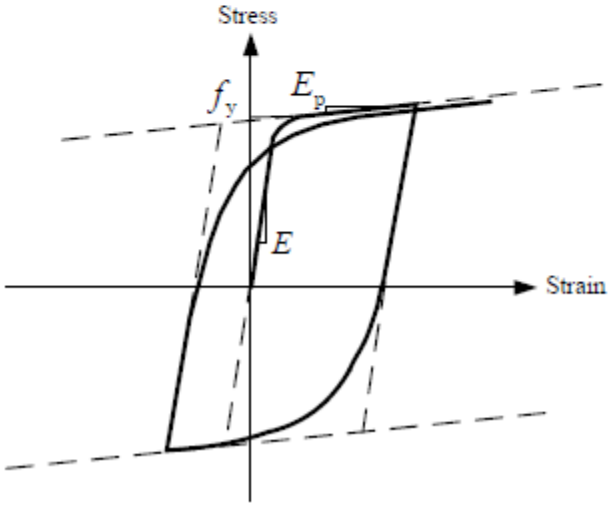

(b) Steel02

Figure 3.12: Nonlinear constitutive models of Concrete02 (Mohd Yassin, 1994) and Steel02 (Menegotto & Pinto, 1973) materials in OpenSees.

3.4. Bridge Foundation Model

Phase I foundation models were developed by using uniaxial and rotational springs calibrated according to nonlinear models based on the geotechnical features of a single type of soil for each foundation condition. On the other hand, Phase II foundation models were developed by directly modeling steel piles using fiber discretized sections and placing springs at specific locations. These springs were defined using a constitutive model whose parameters were based on an analysis of the geotechnical properties of soils found in two sets of boring logs of Southern Illinois. This section briefly reviews the features of the foundation models used in Phase I and Phase II.

3.4.1. Phase I foundation model

Filipov (2012) defined a foundation model based on a study of common representative bridge foundations and soils. The study was developed with the geotechnical pile group analysis program, GROUP 7.0, which was provided by Ensoft Inc. The pile group response was verified using the single pile analysis software LPILE 5.0. The proposed abutment foundation model was defined with (11) HP12x63 piles at a depth of 13.7 m (45 ft), with a 1.2 m x 1.8 m x 12.8 m (4 ft x 6 ft x 42 ft) concrete pile cap. The abutment had a row of four piles battered toward the superstructure at a 1 to 3 slope, a row of five piles placed straight, and two piles placed in the wingwalls as shown in Figure 3.13. The foundation for the pier column substructures has three rows of four HP12x63 straight piles driven to a depth of 13.7 m (45 ft). The pile group is covered with a 0.76 m x 3.7 m x 10.7 m (2.5 ft x 12 ft x 35 ft) cap as shown in Figure 3.14.

The foundations were modeled considering the following soil types:

i. Soft clay or loamy soil, modeled with a 0.014 – 0.024 MPa (300 – 500 psf) shear strength (Flexible foundation condition).
ii. Stiff rock, modeled as a fixed base (Hard foundation condition).

The soil-foundation interaction behavior was calculated for the flexible foundation condition as a curvilinear force-displacement relation. Figure 3.15 shows the modeling scheme for this condition. The flexible foundation condition was simulated in OpenSees as a zero-length element that restrains the bottom node of each substructure using springs for

lateral and rotational stiffnesses. Figure 3.16 shows the flexible foundation condition where the nonlinear force-displacement and moment-rotation behaviors for the abutment and intermediate substructures are modeled based on soft soil.

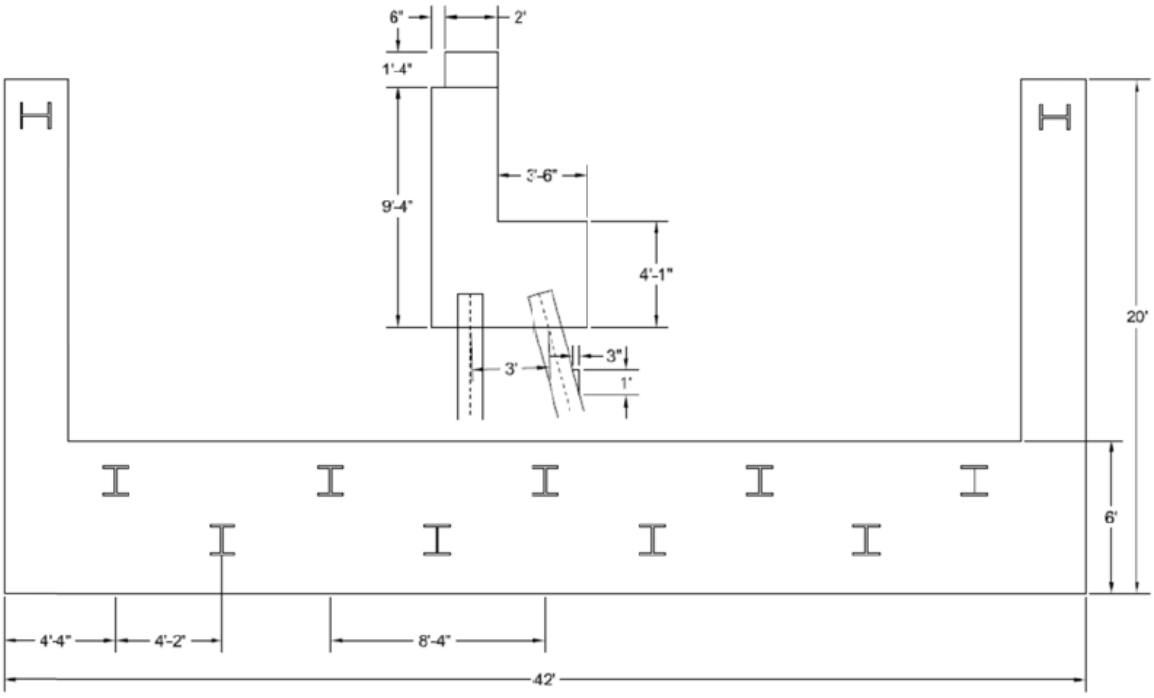

Figure 3.13: Abutment foundation model per Filipov (2012)

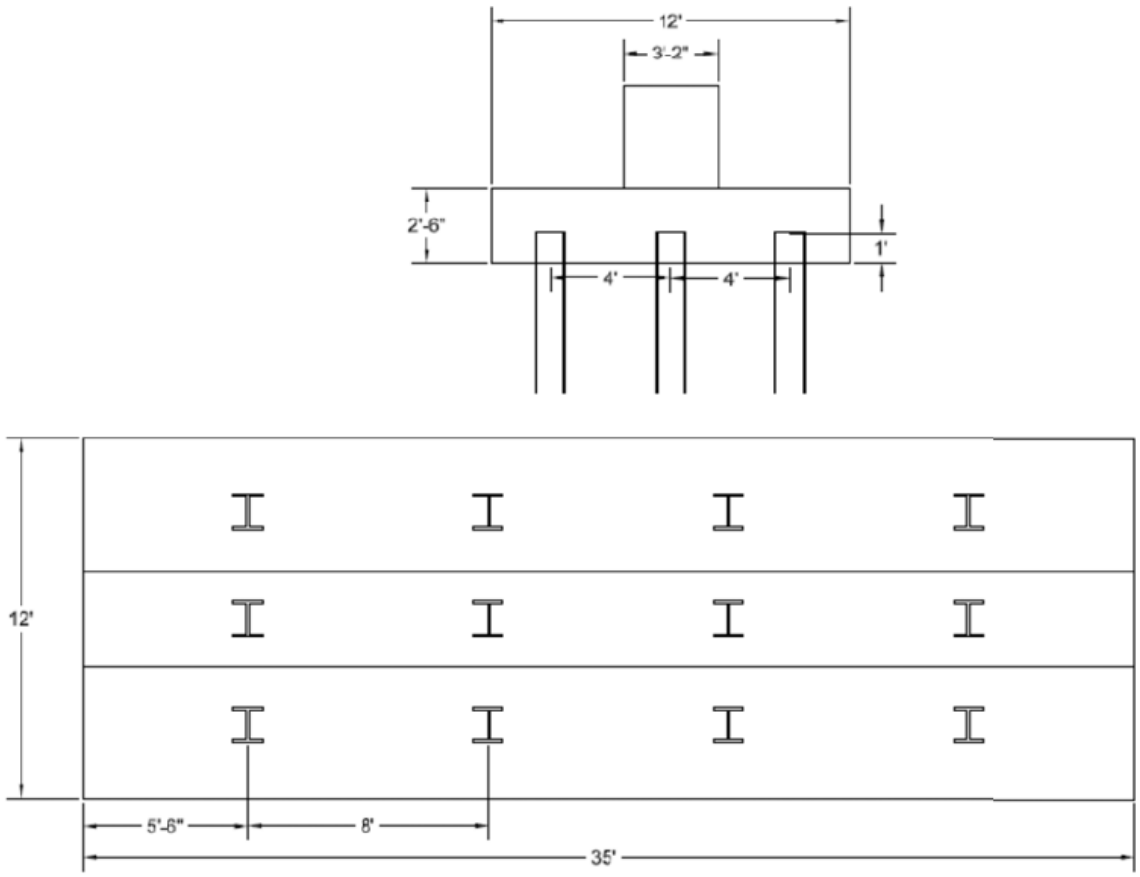

Figure 3.14: Pier foundation model per Filipov (2012)

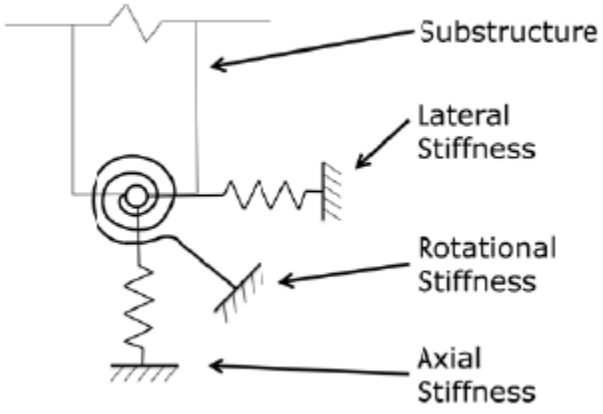

Figure 3.15: Formulation for foundation modeling per Filipov (2012)

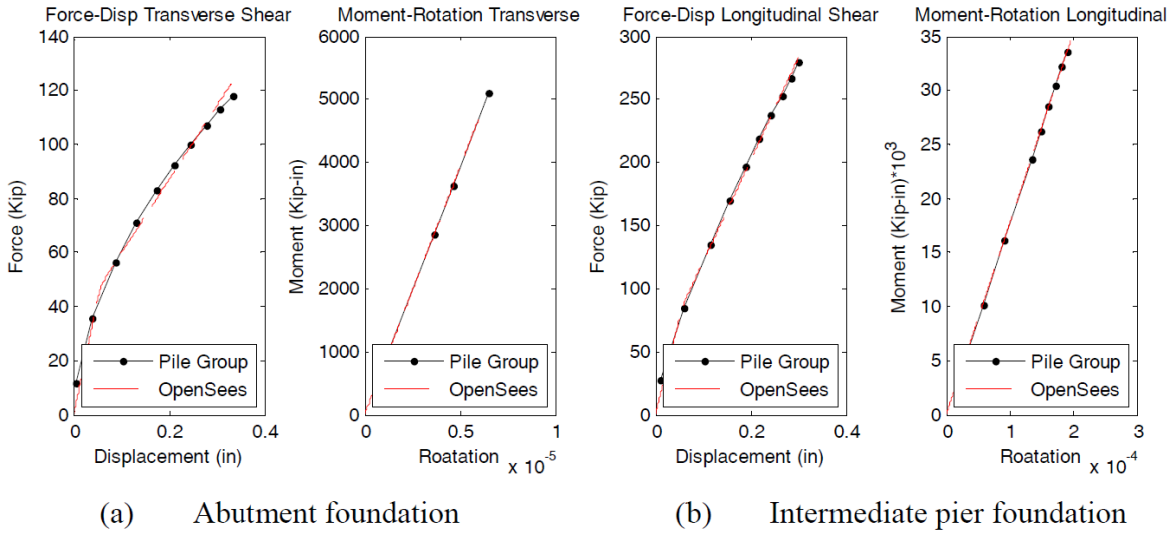

(a) Abutment foundation (b) Intermediate pier foundation

Figure 3.16: Flexible foundation condition based on soft soil per Filipov (2012)

3.4.2. Phase II foundation model

In order to represent soft and hard foundation soil conditions, two real soil profiles were selected from 20 sets of geotechnical boring logs for bridge construction projects in the 10 southernmost counties in Illinois. These counties possess the highest seismicity of the state (Luo, 2016). In the two selected soil profiles, the portion between the ground surface and a depth of 14.6 m (48 ft) was considered because it was assumed that the steel H piles of the prototype bridges were driven to the bedrock at this depth. Driving bridge foundation piles into the bedrock is a common practice in Illinois (Luo, 2016). The soft and hard soil profiles are indicated in Figure 3.17. Figure 3.18 shows the layout of piles at an intermediate pier foundation. For each of the bridge variants, two rows of HP12x84 steel piles were used to support an intermediate pier. Table 3.9 lists the number of piles (N_P) and the center-to-center pile spacing (S_P) in one row for the selected bridge variants ("Sl" bridges).

Using a similar procedure to the RC pier column model, the steel H-piles supporting the intermediate piers and abutments were modeled by using nonlinear elements with distributed plasticity (Neuenhofer & Filippou, 1997). These elements were selected to consider the nonlinear material behavior of steel. Each pile was divided into a number of

elements. The number and size of the elements were defined to have at least five elements for the top pile portion of ten diameters and at least five elements for the rest of the pile, according to the recommendation of Kornkasem et al. (2001). The pile meshes in the soft and hard profiles are indicated in Figure 3.17. The short red lines in the figure represent the nodes between pile elements. Each element of the pile had three integration points for Legendre-Gauss quadrature (Luo, 2016). Figure 3.19 indicates the fiber discretized pile section at each integration point of the nonlinear element.

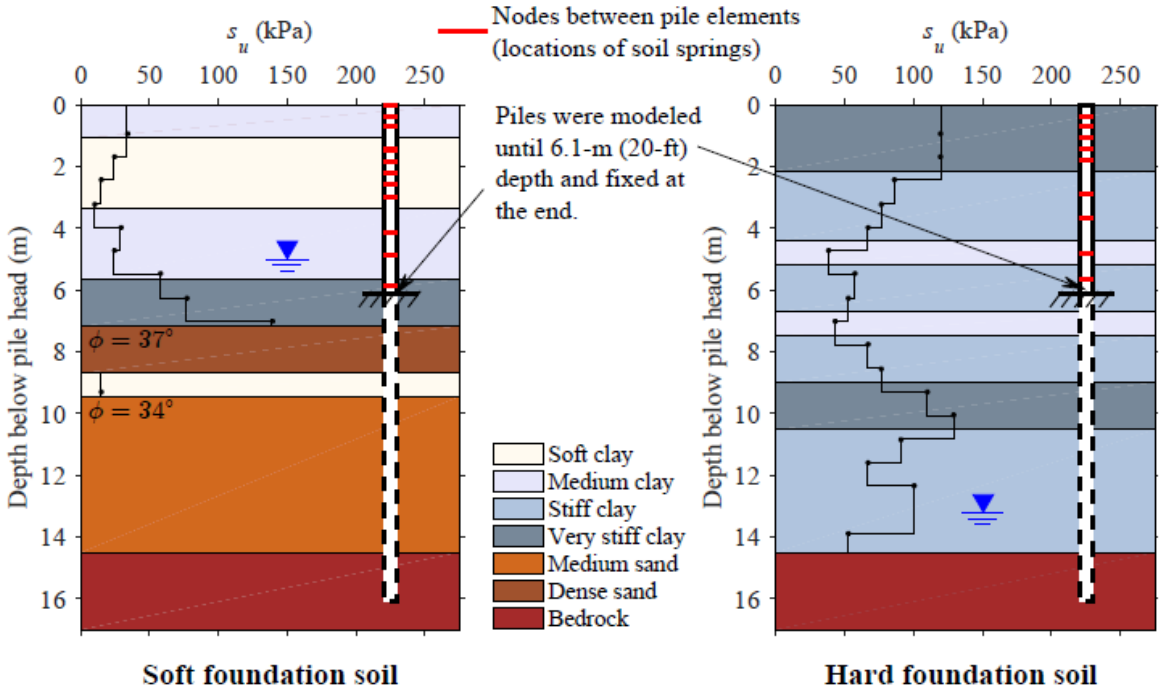

Figure 3.17: Soft and hard foundation soil profiles for modeling bridge pile foundations per Luo (2016)

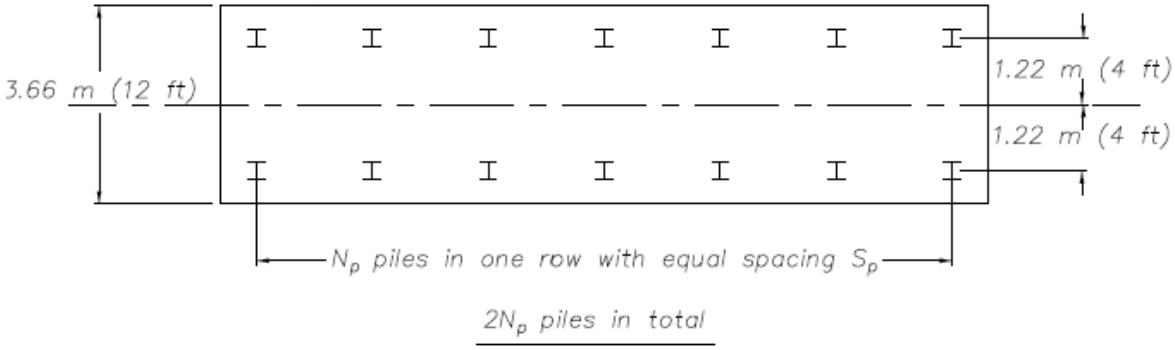

Figure 3.18: Piles at intermediate pier foundations per Luo (2016)

Table 3.9: Pile number and spacing at an intermediate pier per Luo (2016)

Bridge Type	Pile member size	Pile number in one row N_P	Center-to-center Pile spacing S_P [m (ft)]	Spacing normalized to pile width S_P / b_P
"Sl"	HP 12x84	7	2.13 (7)	6.8

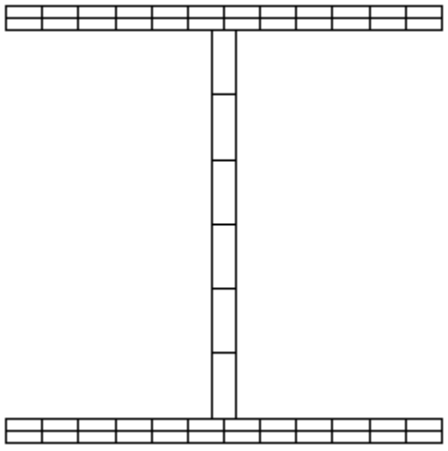

Figure 3.19: Fiber discretized section of foundation piles per Luo (2016)

The interaction between the pile body and surrounding soil was modeled using the nonlinear Winkler foundation method which is widely used for modeling pile foundations under axial and laterals loads (Matlock et al., 1978; Novak & Sheta, 1980; Nogami et al., 1992). At each node between two pile elements, a nonlinear p – y spring and nonlinear t –

z spring model developed by Boulanger et al., 1999 for use in OpenSees, was used to simulate the lateral soil resistance to the pile and the vertical friction between the pile and surrounding soil, respectively (Luo, 2016). A schematic representation of the pile model with nonlinear springs is shown in Figure 3.20.

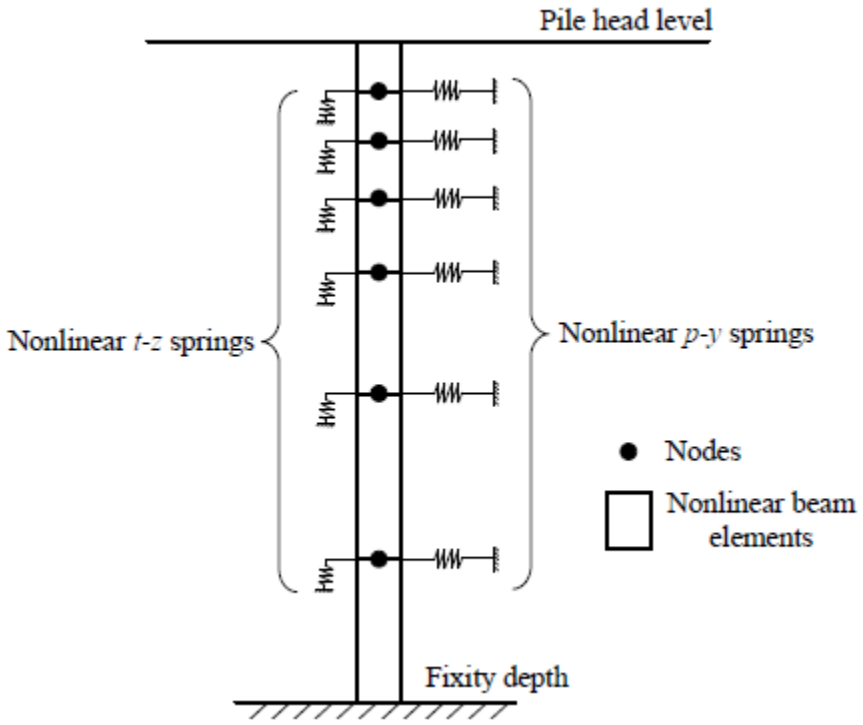

Figure 3.20: Schematic model of pile model with p – y and t – z springs per Luo (2016)

3.5. Bridge Superstructure-Substructure Connection Model

As mentioned in Chapter 1, superstructure-substructure connections, such as elastomeric expansion bearings, transverse bearing retainers and low-profile steel fixed bearings, constitute key elements for developing the concept of an Earthquake Resisting System (ERS) for bridges based on quasi-isolation. During Phase I, numerical models were developed for these components based on experimentally measured response characteristics. The features of these elements are briefly reviewed in this section.

3.5.1. Elastomeric expansion bearings

In order to formulate a numerical model for elastomeric expansion bearings, a zero-length bi-directional model, similar to the one proposed by Constantinou et al. (1990), was specifically created to model the friction stick-slip behavior exhibited by Type I IDOT bearings. The model, schematically shown in Figure 3.21, captures an initial static friction break-off force (μ_{SI}), kinetic friction force (μ_K), and post-slip friction break-off force ($\mu_{SP)}$. Different coefficients of friction were specified for each condition. The formulation of this element also considered variable axial load on the bearing.

Friction properties of the bearing models were defined for the overall bridge models of this study from the results of the report "Experimental Investigation of the Seismic Response of Bridge Bearings" (LaFave et al. 2013a). These properties are summarized in Table 3.10. A sample validation of the bearing model is shown in Figure 3.22. The shear stiffness of the elastomer was estimated as the material shear modulus multiplied by the plan area of the elastomer and then divided by the thickness of the elastomer (Filipov et al., 2013a). A shear modulus of 586 kPa (85 psi) was determined from tests (Steelman et al., 2013).

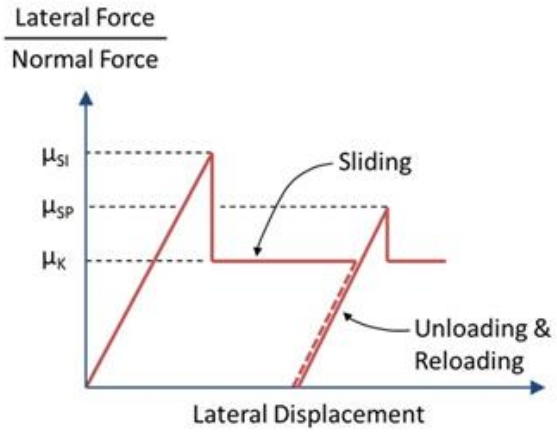

Figure 3.21: Schematic representation of sliding bearing model per LaFave et al. (2013b)

Table 3.10: Friction and shear properties of Type I bearings per LaFave et al. (2013b)

Property		Type I Bearing
G	Shear Modulus	85 psi
μ_{SI}	Initial static coefficient of friction	0.60
μ_{K}	Kinetic coefficient of friction	0.45
μ_{SP}	Stick-slip coefficient of friction	0.50

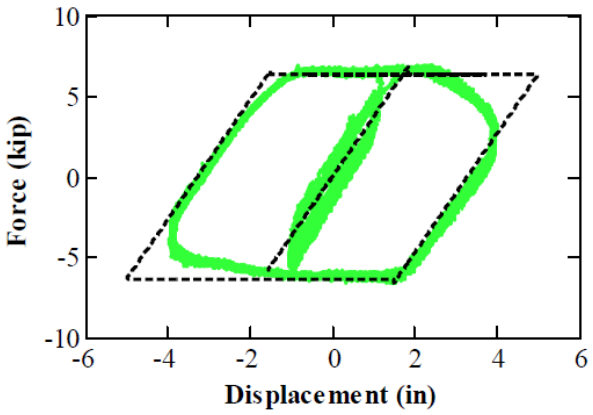

Figure 3.22: Validation of elastomeric bearing model per LaFave et al. (2013b)

3.5.2. Transverse retainers of elastomeric expansion bearings

During laboratory experiments, transverse retainers exhibited roughly elasto-plastic behavior. For these elements, failure was characterized by localized concrete crushing (primarily for larger anchor bolts) followed by anchor bolt tensile-shear failure. For modeling purposes, overall retainer assembly behavior was based only on anchor bolt properties and was calibrated to experimental data from single retainer tests. The nonlinear uniaxial model, schematically represented in Figure 3.23, is characterized by an initial gap followed by elasto-plastic response and failure at a ultimate displacement (LaFave et al., 2013b). Figure 3.24 provides a sample validation of the retainer model.

The properties for the retainer material and gap were based on experimental results. Table 3.11 summarizes the values of these properties that were chosen for the bridge variants to be analyzed in this study. An additional 0.3 in. gap was added to the IDOT specified installation gap of 0.125 in. because testing demonstrated that the oversized bolt hole in the retainer left space for the retainer to slide before actually developing any significant force. In order to represent the bearing systems used in practice, anchor bolt sizes for this bridge model were determined using Section 3.7.3.1 of the IDOT Bridge Manual (IDOT, 2012), with ultimate anchor bolt capacity estimated by Equation 3.1. Testing indicated poor correlation with this equation; therefore, elasto-plastic retainer behavior was defined in the models using Equations 3.2 and 3.3 (LaFave et al., 2013b).

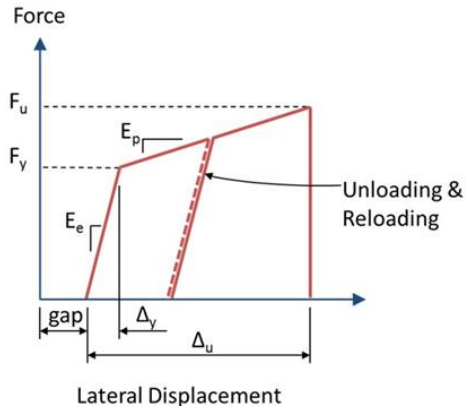

Figure 3.23: Schematic representation of retainer model per LaFave et al. (2013b)

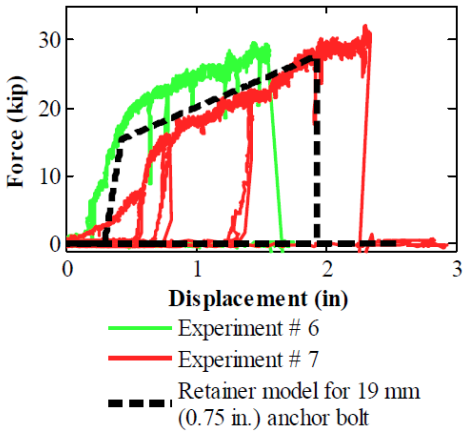

Figure 3.24: Validation of retainer model per LaFave et al. (2013b)

Table 3.11: Retainer properties

Retainer property	Value
Retainer Gap	0.425 in
F_u	60 ksi
$E_{elastic}$	115 kip/in
$E_{plastic}$	8.2 kip/in

$$F_{ult} = \varphi\ 0.48\ A_{bolt} F_u \qquad \varphi = 0.75 \qquad (3.1)$$

$$F_{ult} = \varphi\ 0.80\ A_{bolt} F_u \qquad \varphi = 1.00 \qquad (3.2)$$

$$F_{yield} = \frac{F_{ult}}{1.8} \qquad (3.3)$$

3.5.3. Low-profile steel fixed bearings

On IDOT highway bridges, low-profile fixed steel bearings are often placed at one of the intermediate substructures to prevent any global movements of the bridge deck that could be caused by service-level loads. These bearings are commonly installed on a 0.125-in. thick elastomeric neoprene leveling pad and attached to the substructure using anchor bolts. While in theory either an anchor bolt or pintle failure mode is possible, only the anchor bolt failure mode was modeled. This approach was considered reasonable due to the fact that the minimum pintle diameter of 1.25-in was always larger than the modeled anchor bolt diameter; therefore the anchor bolt was the critical component (LaFave et al., 2013b).

As mentioned in Chapter 1, a bi-directional element was created to model the elasto-plastic yielding and fracture behavior of the anchor bolts. This element was coupled with the sliding bearing element to capture friction between the bearing component and the substructure. A representation of this model in Figure 3.25 shows a peak-oriented model based on a study by Ibarrra et al. (2005) with variable pinching that follows a pre-defined elasto-plastic envelope capable of fracturing at a predefined displacement (LaFave et al., 2013b).

This model was developed based on existing literature of experiments with hysteretic behavior similar to that expected from low-profile fixed bearings (Mander et al., 1996; Klinger et al., 1982; Gomez et al., 2009) and it has been validated against experimental results for the actual fixed bearings as shown in Figure 3.26 (LaFave et al., 2013b). Table 3.12 summarizes the properties used to define low-profile fixed bearings in this study.

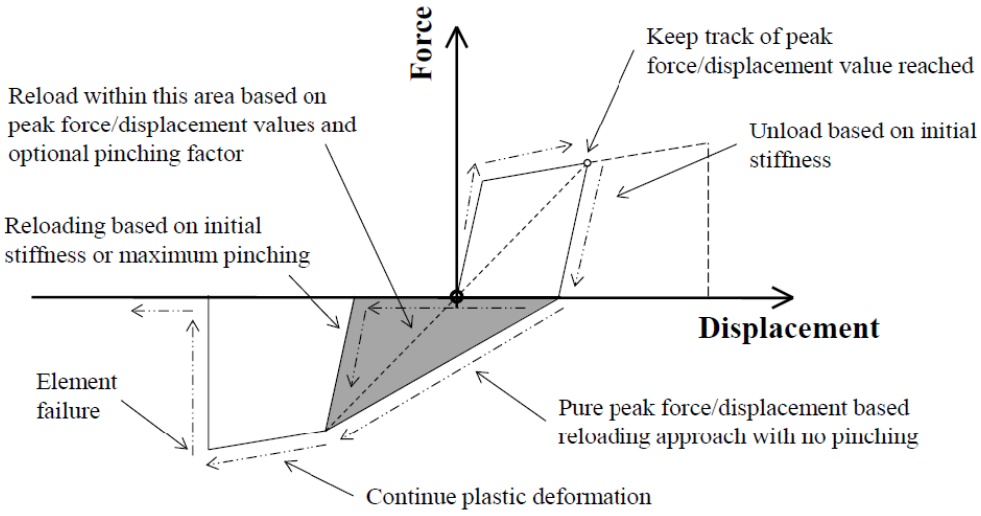

Figure 3.25: Schematic representation of low-profile fixed bearing model per LaFave, et al. (2013b)

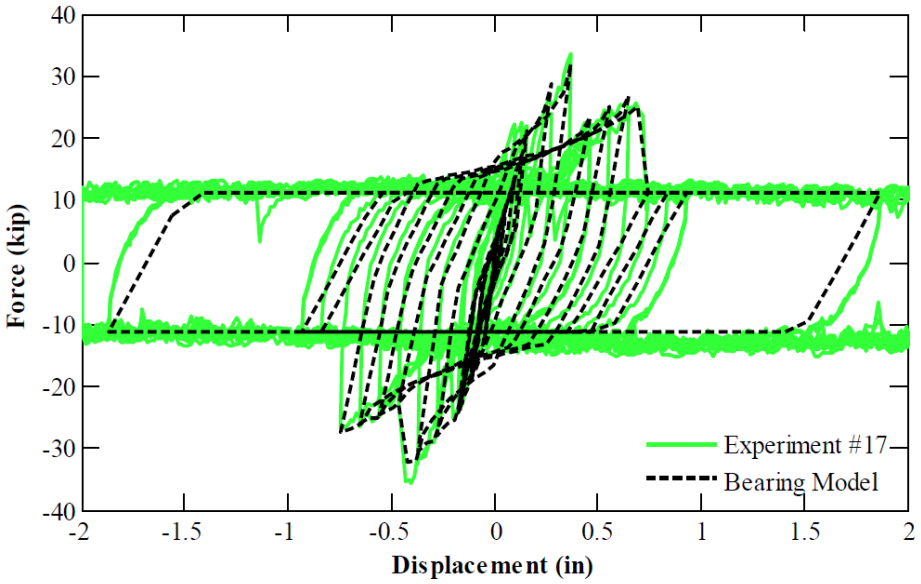

Figure 3.26: Validation of low-profile steel fixed bearing model per LaFave et al. (2013b)

Table 3.12: Low-profile fixed bearing properties

Anchor Bolts	
Fy	36 ksi
Fu	60 ksi
Py	2 x Abolt x 0.48 x Fy
$\triangle_y$	0.1 x Bolt diameter
Pu	2 x Abolt x 0.6 x 0.8 x Fu
$\triangle_u$	1.0 x Bolt diameter
Elastomeric Pad	
E	40 k/in
μ_{SI}	0.31
μ_K	0.31
μ_{SP}	0.31

4. ABUTMENT MODELS FOR QUASI-ISOLATED HIGHWAY BRIDGES

4.1. Overview of Seat-Type Abutment Models

The previous chapter described the modeling techniques used for the formulation of superstructure and intermediate substructures of the selected bridge variants. These elements constitute the principal components of the structural system of the bridge because they transfer a considerable part of gravity and traffic loads to the ground through their foundations. Other elements that withstand these types of loads are abutments. These substructures act as end supports for the bridge superstructure by transferring tributary gravity and traffic loads to embankments and the ground below.

Among the different alternatives for this substructure, seat-type abutments are one of the common options in many regions of the United States. Abutments of this type are often used in quasi-isolated highway bridges in the state of Illinois, in addition to integral abutments and semi-integral abutments (Luo, 2016). Figure 4.1 depicts the typical configuration of a seat-type abutment according to IDOT provisions (IDOT, 2012).

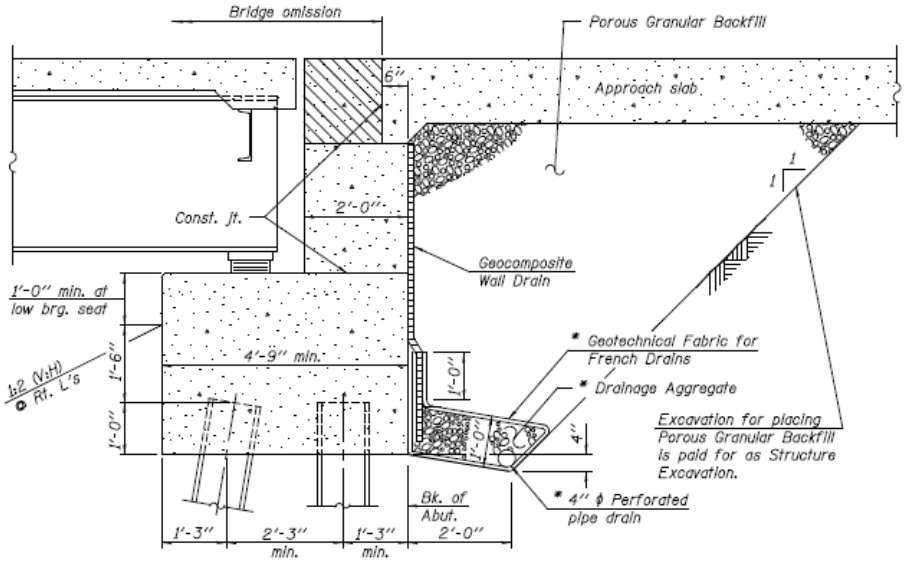

Figure 4.1: Typical seat-type abutment for quasi-isolated highway bridges in Illinois per IDOT (2012)

Abutments play a critical role in overall bridge seismic performance. During major earthquakes, superstructures slide after fusing of sacrificial superstructure-substructure connections. Once these connections fuse, superstructures are weakly restrained by friction forces. In this situation, depending on the incident angle of the seismic excitation, displacements of bridge superstructures are limited by the abutments, whereas these elements are in turn subjected to impact forces from superstructures. The impact of superstructure ends will cause force and deformation demands on the abutment and on its foundation. Therefore, in order to model bridge seismic response, it is required to consider superstructure-abutment-foundation interaction in the computational formulation of the bridge model.

In this chapter, the computational models of abutments of Phase I and Phase II are briefly described in order to analyze their elements, configuration, complexity level, and their capacity to simulate bridge seismic response.

4.2. Phase I Abutment Model

4.2.1. Expansion Joint

For selected bridge variants, abutment backwalls were positioned to provide a 51 mm (2 in) longitudinal expansion joint from the end of the bridge deck. This expansion joint is provided in order to accommodate service level thermal deformations. In the case of seismic excitations, superstructure displacements are large enough to close this expansion joint. When the superstructure contacts the backwall, a nonlinear response is induced on both the backwall and the backfill. The backwall can experience demands from seismic loads in both the longitudinal and transverse directions, since for transverse excitation rotation around the fixed pier can cause corners of the deck and backwall to interact (Filipov, 2012). This response is likely to induce a considerable impact on the overall bridge response (Wilson & Elgamal, 2010). A detail of the expansion joint used in Phase I models is shown in Figure 4.2.

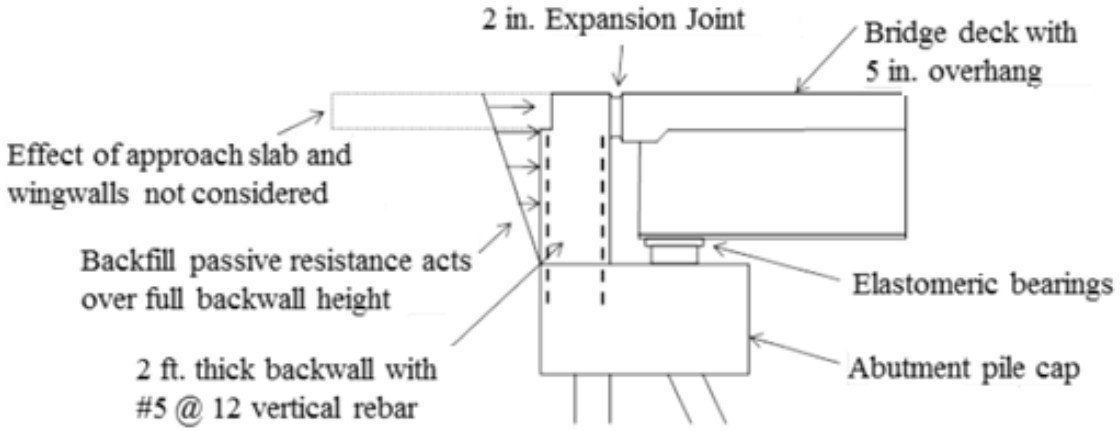

Figure 4.2: Backwall detail per Filipov (2012)

4.2.2. Backwall model

AASHTO Guide Specifications for LRFD Seismic Bridge Design (AASHTO, 2009) consider the backwall to be sacrificial. Therefore, any longitudinal force contribution is only from the soil backfill. For this study, several cases were investigated to verify the potential failure of backwall components. In this case, even though backwalls may be considered sacrificial, it was noticed that these elements are likely to have a substantial force capacity. Although this finding would be beneficial to limit longitudinal superstructure displacements, it could cause large base shears at the abutments which can result in significant damage to the foundation elements (Filipov, 2012).

For the bridge variants selected in this study, the backwall model was based on IDOT provisions (IDOT, 2012). This model consists of two rows of 13 mm (#4 US) vertical reinforcing steel bars spaced at 305 mm (12 in) along the bridge width, and embedded with 51 mm (2 in) clear cover from the backwall faces. Besides, the backwall has contact with the deck at a distance of 138.1 cm (54.4 in) from top of the abutment pile cap. A cold joint is assumed at the interface between the backwall element and the abutment pile cap. Using shear friction calculations, the shear capacity of the backwall is shown to be 2200 kN (495 kips) for the 13.15 m (43.2 ft) long backwall element. Neglecting reinforcement in compression and modeling the backwall as a cantilever

element loaded at the tip (deck interaction location), it is possible to notice that the moment capacity of the wall governs the strength of the element. The backwall has a moment capacity of 1220 kN-m (1370 kip-ft), which corresponds to a deck pounding load of 1340 kN (300 kips), that is considerably lower than the shear capacity. Hence, the contribution of the backwall was captured by using a rotational plastic hinge in the bridge model (Filipov, 2012). This plastic hinge is shown in Figure 4.3.

4.2.3. Backfill model

The nonlinear soil behavior was defined according to the model proposed by Shamsabadi et al. (2007) and implemented using the OpenSees hyperbolic gap material (McKenna, Mazzoni, & Fenves, 2011). This material corresponds to a mathematical model that traces a hyperbolic force-displacement relationship for the backfill, according to a user-defined peak passive resistance. The material model can also be set to reflect an initial gap. Nevertheless, this configuration would preclude backwall modeling, which is an important feature for the bridge model in this study.

Accordingly, this "gap" in the hyperbolic gap material was set to zero, and a separate conventional gap element was defined as shown in Figure 4.3. Input parameters for the hyperbolic material model were based on data from a centrifuge test of a seat-type abutment in dense Nevada sand (Shamsabadi et al., 2007). For the selected bridge variants of this study, backfill stiffness and strength depended on the backwall height. The estimated ultimate passive resistance is 160 kN per meter (10.8 kips per ft) of backwall, and the estimated stiffness is 77,055 kN/m (440 kips/in) (Filipov, 2012).

4.2.4. General abutment formulation

The abutment model consists of several elements. A rigid link represents the backwall. A gap element placed between the top of the backwall and the top deck node located at the end of the superstructure represents the expansion joint. The top of the backwall is also connected to a hyperbolic gap element. This component simulates the interaction between the backwall and the backfill. The bottom of the backwall is connected to springs that model the abutment foundation with a zero length element that represents the

plastic hinge that connects the backwall to the pile cap. Finally, the bottom deck node located at the end of the superstructure is connected to the springs that model the abutment foundation with a zero length element that represents bearing and retainer connectivity.

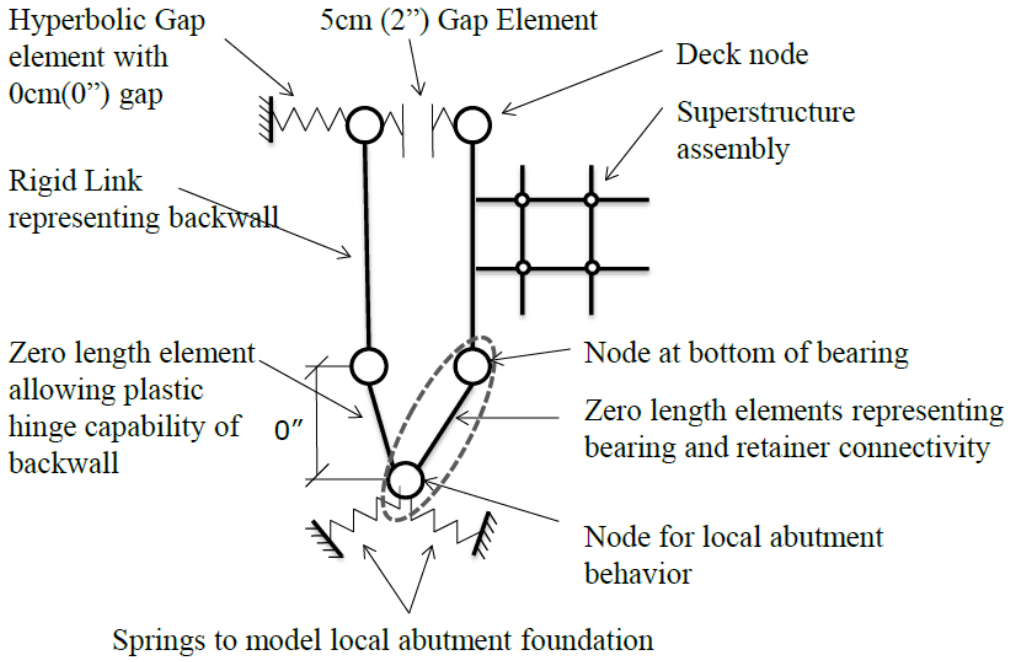

Figure 4.3: Phase I abutment model formulation per Filipov (2012)

4.3. Phase II Abutment Model

The general configuration of the abutment model of Phase II is shown in Figure 4.1. The formulation of each of the elements of this model is presented in the following sections.

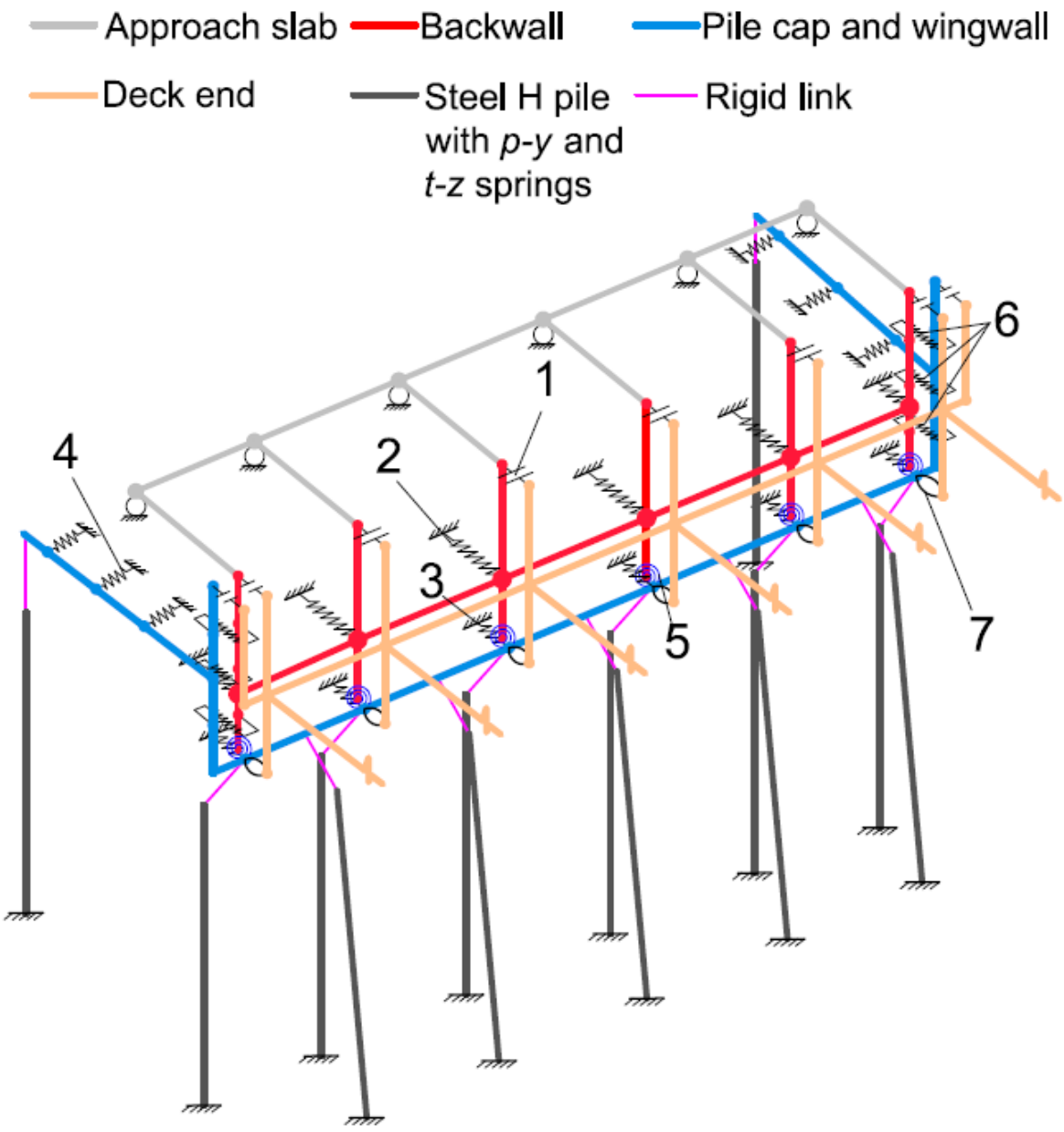

Figure 4.4: Phase II abutment model per Luo (2016)

4.3.1. Abutment pile foundation model

The abutment pile foundation was modeled using the same technique as intermediate pier foundations. Fiber discretized sections and linear elastic elements were employed to model H-piles. These elements were distributed according to IDOT provisions (IDOT, 2012). A detail of the distribution of H-piles for the selected bridge variants is shown in Figure 4.5.

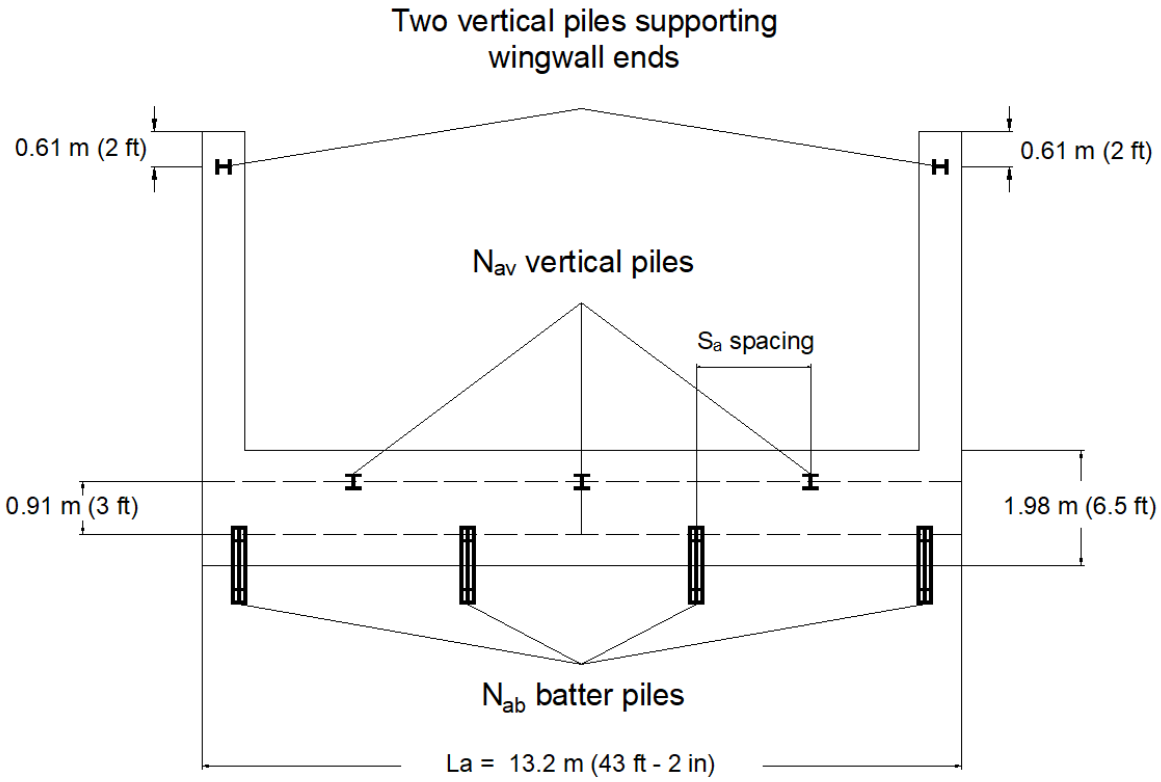

Figure 4.5: Pile layout of abutment foundation for selected bridge variants

The abutment model consists of N_{ab} batter piles with a slope of 152.4 mm (6 in) of vertical rise for every 25.4 mm (1 in) of horizontal run in the front row (the row near the deck end). The angle of batter (the angle made by the batter pile with the vertical) is 9.5°. The direction of batter is to the deck end. N_{av} vertical piles are placed in the back row (the row near the embankment).

Besides these two rows, a single pile supports the end of each piece of wingwall. In addition to Figure 4.5, Table 4.1 indicates details such as the number of piles and spacing for the abutments of the selected bridge variants. In a similar way to the pile distribution at intermediate piers, the abutment piles are also widely spaced (the spacing is greater than four times the pile width). Consequently, pile group effect was not considered for these models. The soil profile and modeling approach for vertical abutment piles is the same as the one employed for pier piles (Luo, 2016).

Table 4.1: Pile number and spacing at abutments per Luo (2016)

Bridge type	Pile member size	No. of batter piles N_{ab}	No. of vertical piles N_{av}	Center-to-center pile spacing S_a [m (ft)]
"Sl"	HP 12x84	3	4	1.98 (6.5)

4.3.2. Expansion joint model

Seat-type abutment bridges include an expansion joint placed between the backwall and the adjacent superstructure end to accommodate thermally-induced bridge deformations by separating superstructure and abutment. This separation allows relative displacements between these structural elements. The joint opening width normal to the joint edge, W, is illustrated in Figure 4.6. IDOT provisions (IDOT, 2012) specify the design value of W at a temperature of 50°F by using the following equation:

$$W(in) = [L(ft.) \times 80(°F) \times 12(in/ft) \times 0.0000065/°F]cos \propto + 0.5(in) \quad (4.1)$$

In this expression, L corresponds to the contributing expansion length of the superstructure and α corresponds to the skew angle.

In the abutment model, gap-spring elements are placed to simulate the instantaneous gap opening/closing, contact, and release at each step of a static pushover analysis or dynamic analysis. These elements are indicated as component No. 1 in Figure 4.4. If these

gap-springs are subjected to a tensile or compressive deformation smaller than the joint opening width W, these elements do not exert any resisting force. If the compressive deformation surpasses the joint opening width W, these gap-springs become very stiff in order to simulate the contact between the deck end and abutment backwall. In the abutment model shown in Figure 4.4., the gap-springs were placed at the girder line and parapet locations. These elements were oriented normal to the edge of the expansion joint (Luo, 2016).

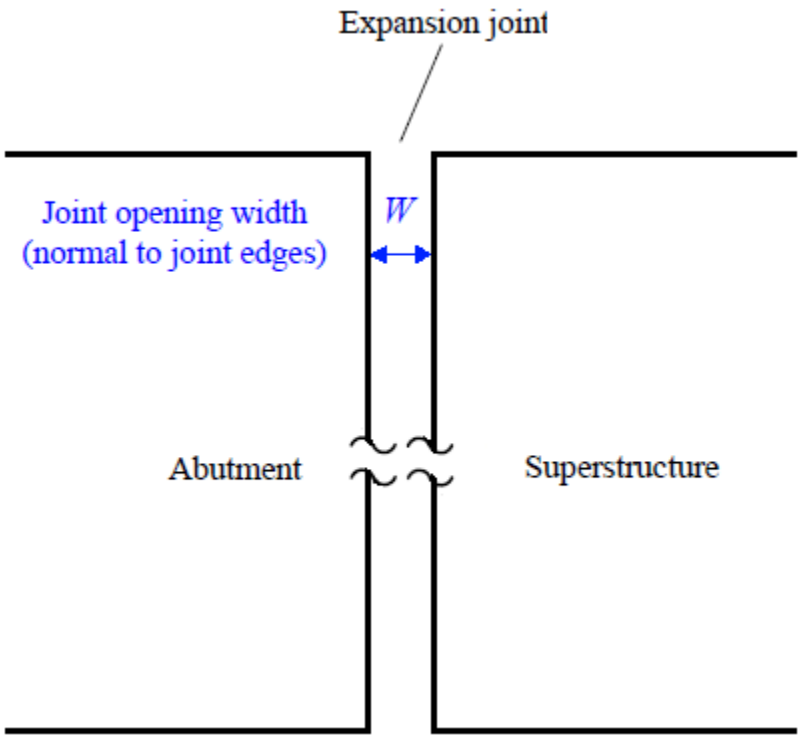

Figure 4.6: Expansion joint opening between abutment and superstructure

4.3.3. Abutment backwall model

The RC backwall is connected to the pile cap by two rows of 15.8 mm (#5 U.S.) reinforcing steel bars with 0.30 m (1 ft) spacing. The reinforcing steel is provided according to the shrinkage and temperature reinforcement in concrete walls specified by (AASHTO, 2010). The thickness of the backwall was defined according to IDOT provisions (IDOT, 2012), which specify a minimum thickness of 0.61 m (2 ft). A detail of the abutment backwall model is shown in Figure 4.7.

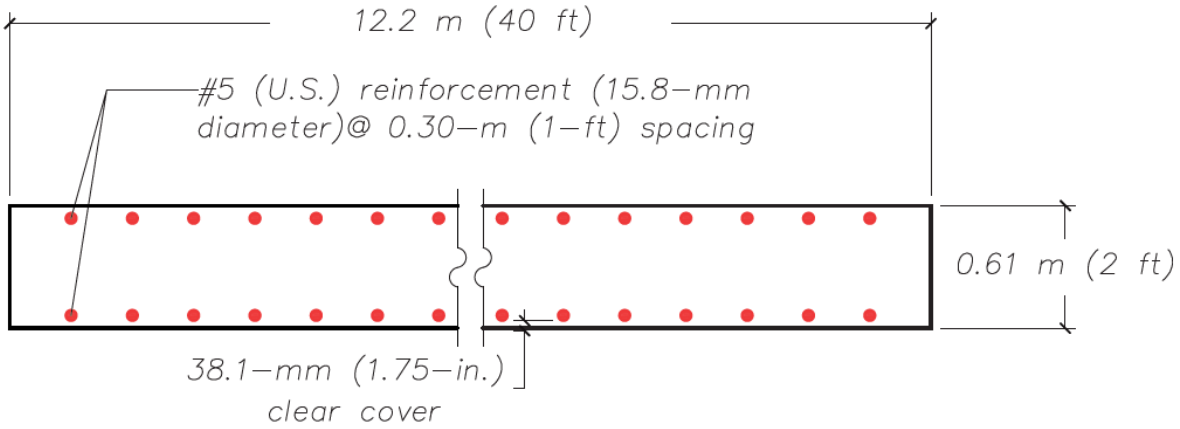

Figure 4.7: Abutment backwall model per Luo (2016)

When the bridge is subjected to longitudinal seismic demands, the backwall that has contact with the bridge superstructure is subjected to out-of-plane forces. The backwall was formulated as a cantilever wall. The bottom of this cantilever is connected to the pile cap through an elasto-plastic hinge (Luo, 2016).

In order to obtain the moment-curvature relation of the backwall section shown in Figure 4.7, a sectional analysis was performed using SAP2000. Based on the moment-curvature relation obtained from this analysis, an equivalent plastic hinge method proposed by Abo-Shadi et al. (2000) for modeling out-of-plane bending behavior of RC walls was used to determine the moment-rotation relation of the backwall bottom. This relation is shown in Figure 4.8. In the formulation of the abutment model, the moment-rotation relation was distributed into a number of rotational nonlinear springs at the backwall bottom based on the tributary wall width of each spring. These springs are indicated as component No. 4 in Figure 4.4. The backwall body was modeled using elastic beam elements. The estimated shear capacity of the concrete backwall is considerably higher than the shear demand required to induce flexural failure of the wall-bottom hinge. Therefore, shear failure of the backwall was not explicitly modeled (Luo, 2016).

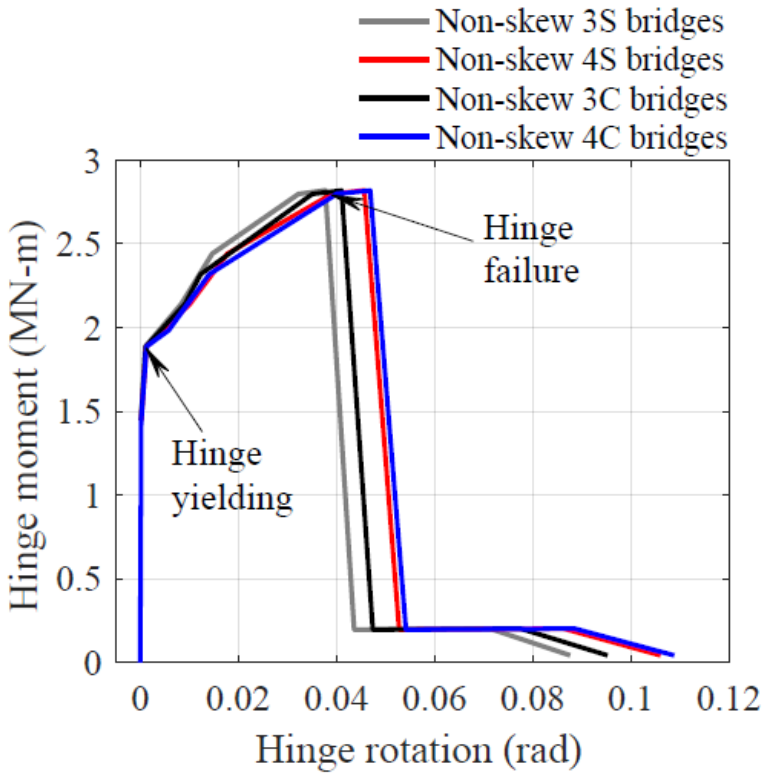

Figure 4.8: Backwall moment-rotation relation per Luo (2016)

4.3.4. Backwall-wingwall connection model

In seat-type abutment bridges, pairs of bent steel dowel bars are typically embedded in the concrete at the junction between a backwall and a wingwall. These dowel bars cross the construction joint between these structural elements. (IDOT, 2012). These connections are provided in order reinforce the construction joints between backwall and wingwall which in turn contributes to preserve abutment overall integrity. During earthquake events the backwall-wingwall connections help to resist the out-of-plane bending response of the abutment backwall, along with the backwall-to-pile-cap connections at the wall bottom. In return, backwall wingwall connections are subjected to shear demands from the superstructure-abutment interactions. The shear force-deformation relation of each pair of steel dowel bars was estimated by using a model proposed by (Vintzeleou & Tassios, 1986). This analytical model was calibrated based on full-scale experimental results in order to predict the shear force-deformation behavior of steel dowel bars embedded in

concrete. This analytical model is shown in Figure 4.9. In the abutment model shown in Figure 4.4, a nonlinear spring was used to simulate each pair of dowel bars that connect the backwall and wingwall (Luo, 2016). These springs are indicated as component No. 6. The shear force-deformation relation shown in Figure 4.9 was assigned to each nonlinear spring.

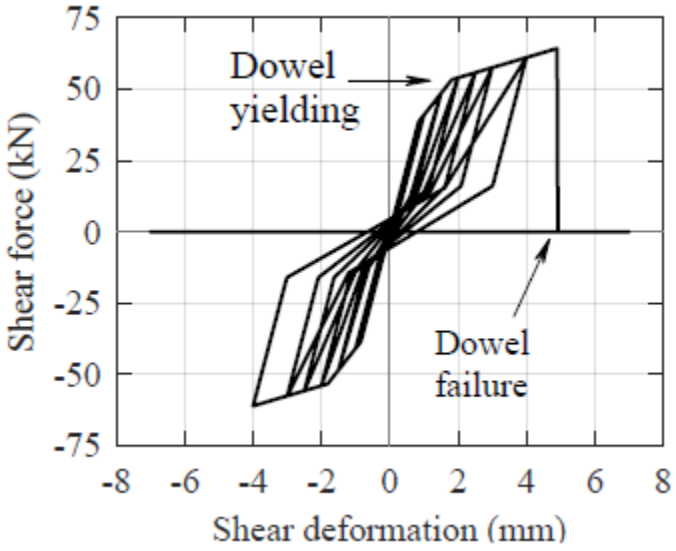

Figure 4.9: Idealized shear force-deformation of one pair of steel dowel bars connecting the abutment backwall and wingwall per Vintzeleou & Tassios, (1986)

4.3.5. Backfill passive resistance model

During seismic excitations, large superstructure displacements in the longitudinal direction may cause the closure of the expansion joint and engagement between the superstructure and abutment backwall. In this situation, the backwall is pushed against the backfill and embankment soil by the superstructure. As a result, the passive resistance from the backfill and embankment soil is mobilized and acts as the principal element to counteract the displacement of the abutment and superstructure, in addition to the resistance of abutment foundation (Luo, 2016).

The force-displacement relation of the passive soil resistance behind the backwall was established using a model proposed by Shamsabadi et al. (2007). The selected model was developed according to the limit-equilibrium logarithmic-spiral surface, method of slices, and hyperbolic stress-strain behavior of soils (Terzaghi et al., 1996). According to

Shamsabadi et al. (2007), the passive force-displacement response of cohesive and cohesionless backfill soils predicted by this model is consistent with small and full-scale experimental test results (Luo, 2016).

For the selected bridge variants, as shown in Figures 4.10, a nearly isosceles right triangular region of porous granular material is placed next to the abutment backwall and pile cap. Figure 4.10 illustrates a logarithmic-spiral soil failure surface in passive conditions (Terzaghi et al., 1996). Stewart (2007) and Bozorgzadeh et al. (2007) performed large-scale experimental tests about the passive response of bridge abutment backfill and found that the length of the passive soil failure wedge, indicated as L_{wedge} in Figure 4.10, was commonly greater than twice the height of the soil wedge, H_{wedge} indicated in Figure 4.10. For abutments, this wedge shape means that the soil failure surface tends to develop in the embankment soil outside the porous granular material, as shown in Figure 4.10. It was assumed that the embankment soil consisted of compacted clean sand. The soil properties included in Table 4.2 were based on the studies of Rollins et al. (2010) and Shamsabadi et al. (2007) for compacted clean sand. These properties were used to determine the backfill passive resistance (Luo, 2016).

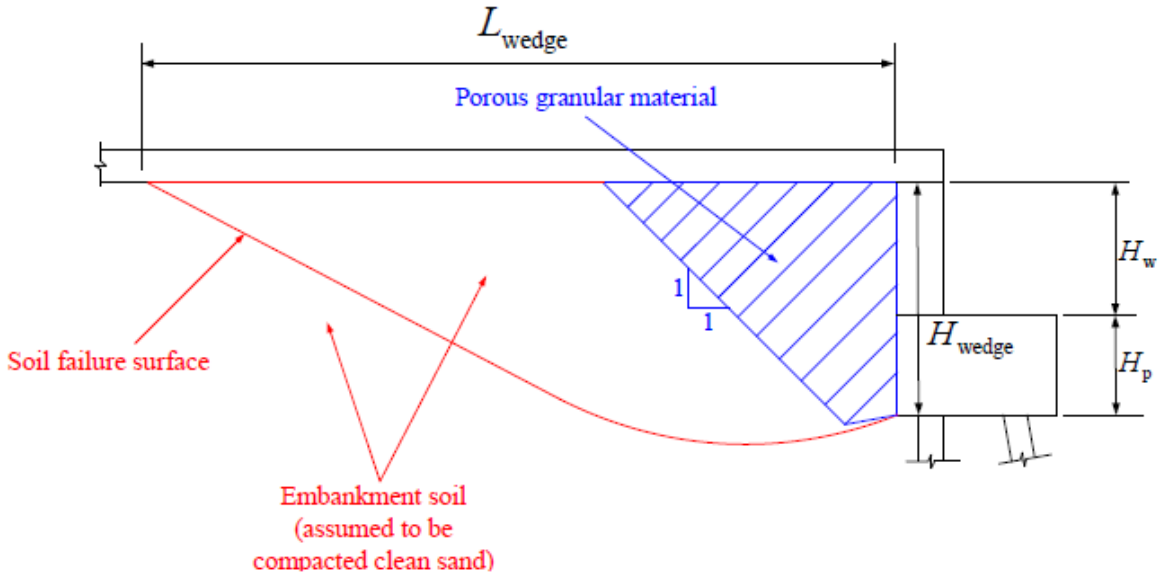

Figure 4.10: Logarithmic-spiral soil failure surface in passive conditions per Terzaghi, et al. (1996)

Table 4.2: Soil properties to determine backfill passive resistance per Rollins et al. (2010) and Shamsabadi et al. (2007)

Backfill soil	Unit weight γ [kN/m^3]	Angle of internal friction ϕ (°)	Cohesion c [kPa]	Angle of wall friction δ (°)	Poisson's ratio ν	Strain at 50% strength ε_{50}	Failure ratio R_f
Compacted clean sand	16.5	37.3	0	25	0.3	0.0035	0.97

Besides soil properties, other critical factor that determines backfill passive resistance is the backwall and pile cap height. The backwall height, indicated as H_w in Figure 4.10, corresponds to the summation of the girder depth and bearing height. The abutment pile cap height is indicated as H_p in Figure 4.10. Table 4.3 includes the value of H_w and H_p for the selected bridge variants.

Table 4.3: Height of abutment backwall and pile cap defined in Figure 4.12 per Luo (2016)

Element	"Sl"
Backwall height H_w [m (ft)]	1.14 (3.75)
Pile cap height H_p [m (ft)]	1.07 (3.5)
Total height $H_w + H_p$ [m (ft)]	2.21 (7.25)

For the non-skew prototype bridges, the computed force *P* versus backwall top displacement *D* of backfill passive resistance is shown in Figure 4.11. The ascending branch of the backbone curves shows a hyperbolic shape and reaches a plateau at the ultimate capacity. The unloading/reloading response was assumed to be linear according to the results obtained in the study of (Stewart, 2007). The force displacement relation, *P*(*D*), indicated in Figure 4.11 was then distributed to the backwall and pile cap based on triangular and trapezoidal soil pressure distributions (Terzaghi et al., 1996), as schematically shown in Figure 4.12. The resistance on the backwall, P_{BW}, and that on the pile cap, P_{PC}, were distributed into a number of nonlinear springs in the abutment model, based on the tributary backwall width of each spring (Luo, 2016). These springs were

located at the centroids of the triangle and trapezoid shown in Figure 4.12. The springs for P_{BW} and P_{PC} are indicated as components No. 2 and 3 in Figure 4.4.

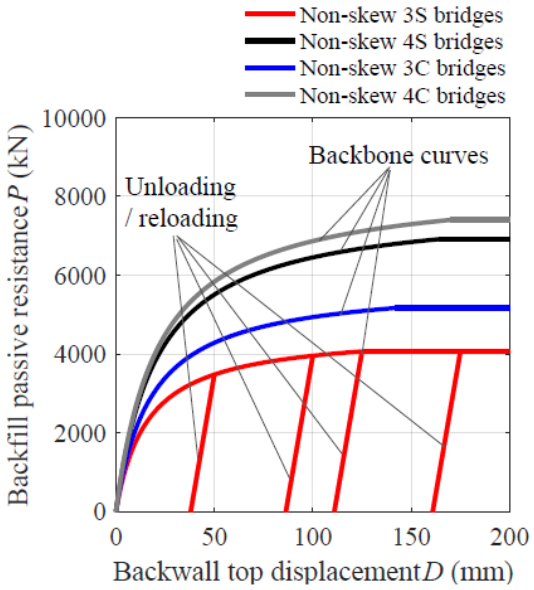

Figure 4.11: Passive resistance of abutment backfill per Luo (2016)

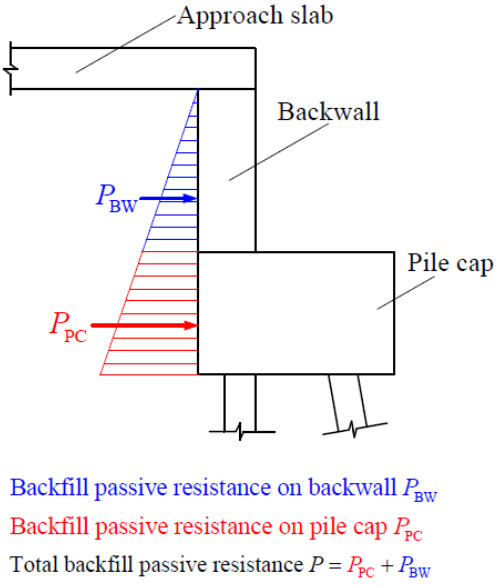

Figure 4.12: Distribution of backfill passive resistance between backwall and pile cap per Luo (2016)

4.3.6. Wingwall model

The backfill passive resistance on abutment wingwalls was modeled by employing the same approach that was considered for the backwall. The nonlinear springs for passive soil resistance on wingwalls are indicated as component No. 4 in the abutment model shown in Figure 4.4. For many bridge embankments in Illinois, the top width of the embankment is close to the abutment width and there is not sufficient soil outside the two wingwall in order to develop a passive soil failure wedge. Hence, the passive resistance from the soil enclosed by the abutment was considered, but that from the soil outside the wingwalls was neglected. For this reason, the nonlinear springs for passive soil resistance to wingwalls, indicated as component No. 4 in Figure 4.4, can only be subjected to compressive forces (Luo, 2016).

4.3.7. Approach slab model

As indicated in Figure 4.1, a concrete approach slab is connected to the top of the abutment backwall. For the selected bridge variants, the length of the approach slab is typically 9.14 m (30 ft), the width is 12.19 m (40 ft), and the thickness is 0.38 m (1.25 ft). The weight of each approach slab is around 1000 kN (225 kips). In order to avoid neglecting this considerable amount of mass for the bridge seismic analysis, the approach slab was included in the abutment model. As indicated in Figure 4.4, the slab is modeled using a grid of elastic beam elements. The total mass was distributed into a number of nodal masses concentrated to the boundary nodes of the beam elements (Luo, 2016).

5. STATIC PUSHOVER ANALYSES OF PROTOTYPE BRIDGE MODELS

A static pushover analysis applies a load pattern, which can vary during the analysis or be constant, in a certain direction to incrementally analyze structural response as increasing levels of load or displacement are imposed on the model. For the case of models of highway bridges, this type of analysis is convenient to investigate structural response characteristics such as force distribution among substructures, sequence of occurrence of limit states, fusing of sacrificial superstructure-substructure connections, and vulnerability of critical components (Luo, 2016).

In this chapter, a comparison of the static pushover analyses of Phase I and Phase II models will be performed in order to study sensitivities and identify differences of structural response characteristics. This comparison considers the differences of the formulations of these structural models, especially regarding the configuration of abutments.

5.1. Identification of Component Limit State Occurrence

For dynamic and pushover analyses, the time series or envelope of the structural response of critical components was recorded. For pushover analyses, the displacement of a controlled location (commonly, a node located near to the geometric center of the bridge model) is considered as the pseudo-time, which is equivalent to time in standard dynamic analyses. The structural response of critical components was analyzed to identify the occurrence of different fusing and damaging limit states, which are indicated in Table 5.1. The limit states defined in this chapter are also considered for the nonlinear dynamic (time history) analyses, which will be discussed in Chapter 6.

Fusing limit states, such as the rupture of steel fixed bearing anchors, rupture of elastomeric bearing retainer anchors and sliding of elastomeric bearings, are preferred according to the principles of the quasi-isolation design methodology of bridges.

Acceptable limit states, such as yielding of reinforcing steel and crushing of concrete cover at pier columns, are permitted as long as the extent of damage is not considerably severe to induce global structural collapse.

Unacceptable limit states, such as unseating of bearings at substructures are prone to cause significant damage to bridge superstructures and even span loss. One of the main objectives of Phase I and Phase II projects is related to minimize the occurrence of this limit state in order to calibrate the quasi-isolation design methodology.

The limit states for this study were established according to the definitions of Phase II (Luo, 2016). These limit states are explained as follows:

Table 5.1: Fusing and damaging limit states of critical bridge components

Substructure	Limit states	Abbreviation	Category
Abutments (A1 and A2)	Closure of expansion joint	CEJ@A1 and/or A2	Preferred
	Mobilization of backfill ultimate capacity	MBU@A1 and/or A2	Damaging, acceptable
	Failure of backwall-to-pile-cap connection	FBP@A1 and/or A2	Fusing, acceptable
	Rupture of retainer anchor	RRA@A1 and/or A2	Fusing, preferred
	Sliding of elastomeric bearing	SEB@A1 and/or A2	Fusing, preferred
	Unseating of elastomeric bearing at acute deck corner	UBA@A1 and/or A2	Damaging, unacceptable
	Unseating of elastomeric bearing at obtuse deck corner	UBO@A1 and/or A2	Damaging, unacceptable
Expansion Pier (P1)	Rupture of retainer anchor	RRA@P1	Fusing, preferred
	Sliding of elastomeric bearing	SEB@P1	Fusing, preferred
	Unseating of elastomeric bearing	UEB@P1	Damaging, unacceptable
	Yielding of vertical reinforcing steel at column base	YRS@P1	Damaging, acceptable
	Crushing of concrete cover at column base	CCC@P1	Damaging, acceptable
Fixed Pier (P2)	Rupture of steel fixed bearing anchor	RFA@P2	Fusing, preferred
	Unseating of steel fixed bearing	USB@P2	Damaging, unacceptable
	Yielding of vertical reinforcing steel at column base	YRS@P2	Damaging, acceptable
	Crushing of concrete cover at column base	CCC@P2	Damaging, acceptable

Closure of expansion joint (CEJ)

The expansion joint was modeled by employing a number of nonlinear springs along the width of the backwall. If any of these springs experiences a compressive deformation that surpasses the joint opening width at a certain time during an analysis, the closure of the expansion joint is identified.

Mobilization of backfill ultimate capacity (MBU)

The passive resistance of the backfill soil was distributed into a number of uniaxial compression-only nonlinear springs along the width of the backwall. If the summation of the spring forces surpasses 95% of the backfill ultimate capacity, the mobilization of the backfill ultimate capacity at this abutment is identified.

Failure of backwall-pile-cap connection (FBP)

The backwall-pile-cap connection at a bridge abutment was modeled as a number of rotational springs along the width of the backwall. If the rotation of all the springs exceeds the ultimate rotational capacity of the connection at any time step, the failure of the backwall-pile-cap connection is identified.

Rupture of retainer anchor (RRA)

The maximum shear deformation of each pair of retainer anchors at an abutment or pier was recorded in each analysis. According to the observations made by (Luo, 2016), in most of the analyses, the maximum deformation and fusing state of retainer anchors are similar to each other at a certain substructure. Hence, the maximum deformations of anchors are averaged into a single deformation value. If this value exceeds the ultimate shear deformation of a retainer anchor, the retainer anchor rupture is identified.

Sliding of elastomeric bearings (SEB)

For this limit state, if the instantaneous shear deformation of an elastomeric bearing surpasses its shear deformation limit in either the longitudinal or transverse bridge axis at any time step, sliding of elastomeric bearings occurs. If any of the several elastomeric bearings at an abutment or pier slides, the limit state of sliding of elastomeric bearings at this substructure is identified.

Unseating of elastomeric bearings at acute or obtuse corner of deck end (UBA @ A1 and/or A2, UBO@A1 and/or A2)

For the case of the selected variants bridges, there are no acute or obtuse corners because these models do not have skew angles. Taking into account this feature, the nomenclature of the limit states defined in Phase II will be considered in this study; nevertheless, considering the plan view of the bridge models, UBA and UBO now refer to unseating of elastomeric bearings at the north and south corners of the superstructure, respectively.

In Phase I and Phase II structural models, bearing unseating was not explicitly simulated; nevertheless, this limit state was identified by comparing the maximum bearing sliding distance with the minimum seat width at substructures. The minimum seat width for a 1000-year seismic event, in inches, is designated as *N* and calculated by using Equation (5.7) (IDOT, 2012).

$$N = 3.94 + 0.0204\,L + 0.084\,H + 1.087\sqrt{H\left[1 + \left(2\frac{B}{L}\right)^2\right]}\frac{1 + 1.25\,F_v S_1}{\cos \propto} \qquad (5.1)$$

In this equation:

L = Typical length between expansion joints (ft.).

H = Height of tallest substructure unit between expansion joints (ft.).

B = Out-to-out width of superstructure (ft.).

α = Skew angle (°).

F_vS_1 = One second period spectral response coefficient modified for site class.

B/L = Not to be taken greater than 3/8.

According to the IDOT Bridge Manual (IDOT, 2012), *N* is measured along the beam from the edges of piers or abutments to the end of the beam in the longitudinal direction. In the transverse direction, *N* is measured from the edges of piers or abutments to the centerline of the edge beams. The calculated minimum seat width *N* at the substructures of the selected bridge variants is indicated in Table 5.2.

Table 5.2: Minimum required seat width N at substructures

Column height [m (ft)]	Minimum seat width (mm)
4.57 (15)	772
12.19 (40)	996

As indicated in Figure 5.1, considering the seat width *N*, as well as the width W_e and length L_e of the bearing elastomer, the sliding limit in the abutment-parallel and abutment-normal directions, designated as d_p and d_n, can be calculated using Equations 5.2 and 5.3.

$$d_p = N - \frac{L_e}{2} \qquad (5.2)$$

$$d_n = N - d_e - \frac{W_e}{2} \qquad (5.3)$$

Finally, d_p and d_n are compared with the maximum bearing sliding distances in the corresponding directions recorded in the analysis. If the maximum sliding distance surpasses d_p or d_n, bearing unseating is identified.

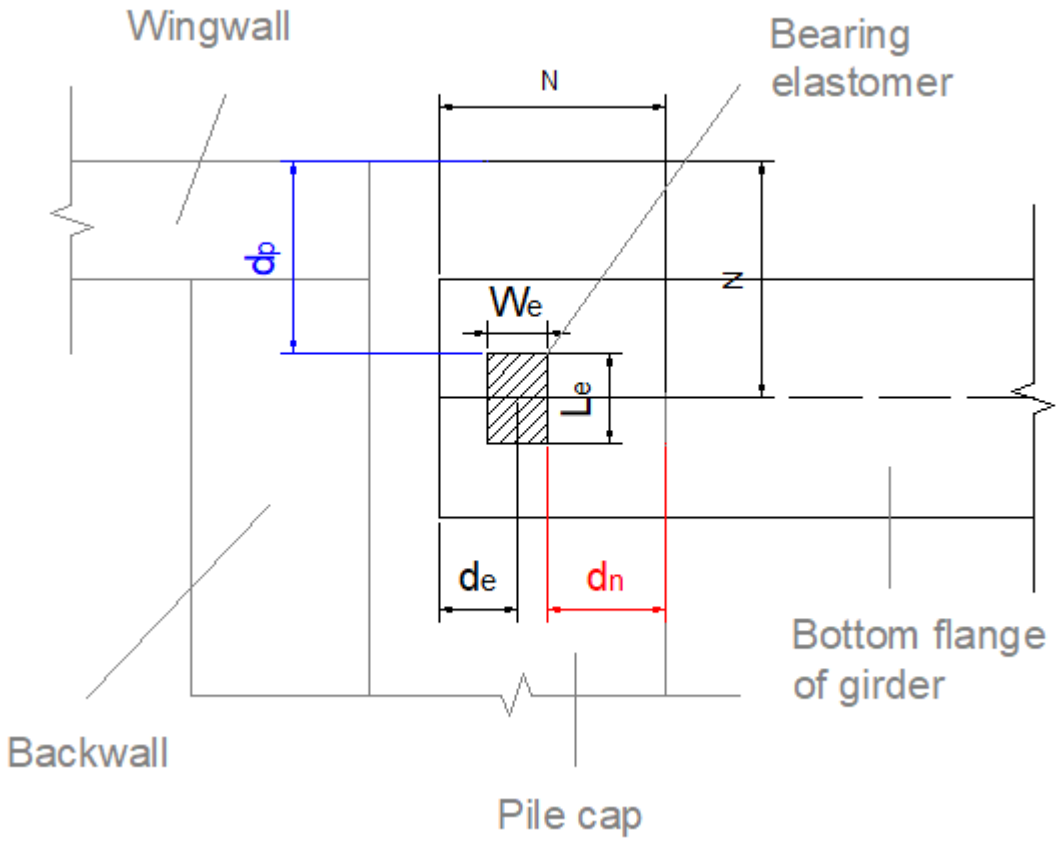

Figure 5.1: Unseating of elastomeric bearings

Unseating of elastomeric bearing (UEB @ P1)

Unseating of the two exterior elastomeric bearings at the expansion pier is identified by using the same definition as that at the abutment, with the minimum required seat width *N* indicated in Table 5.2. The dimensions (length and width) of the elastomeric bearing at the expansion pier are considered instead of those of the elastomeric bearings placed at the abutments.

Yielding of vertical reinforcing steel at column base (YRS)

According to Chapter 4, each pier column in the bridge model was discretized into a number of nonlinear beam-column elements along its length and each element has three integration points. For the element located at the bottom of each column at a pier, the maximum tensile strain of the reinforcing steel was recorded at each of the four locations

along the perimeter of the circular column section at the bottommost integration point (about 1% of the column height measured from the base), as illustrated in Figure 5.2. If the maximum tensile strain of all the monitored locations at the pier exceeds the yield strain of the reinforcing steel, this limit state is identified. The value of the yield strain of the reinforcing steel is 0.0021 (Gr. 60 steel). In addition, a value of strain for reinforcing steel equal to 0.015 was selected to identify moderate structural damage.

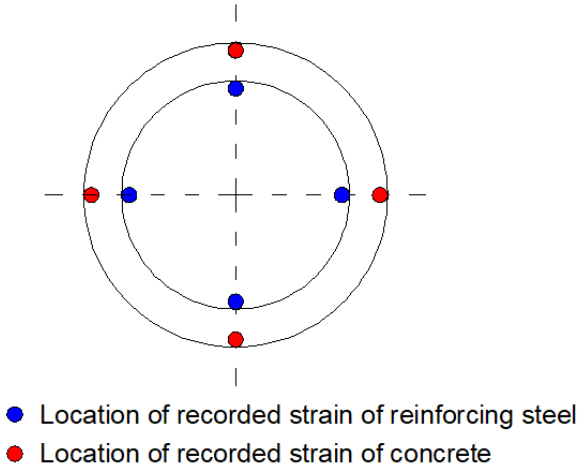

Figure 5.2: Monitored locations for strain of reinforcing steel and concrete cover

Crushing of concrete cover at column base (CCC)

The identification of this limit state is similar to YRS, except that the maximum compressive strain of concrete was recorded at the four locations of a column base indicated in Figure 5.2, instead of the maximum tensile strain of reinforcing steel. The value of the maximum compressive strain of concrete is 0.005 (f'c = 3.5 ksi). In addition, a value of strain for concrete equal to 0.002 was selected to identify moderate structural damage.

Rupture of steel fixed bearing anchor (RFA)

The identification of this limit state is similar to RRA, except that the ultimate shear deformation of the steel fixed anchors is considered.

Unseating of steel fixed bearings (USB @ P2)

Unseating of the two exterior steel fixed bearings at the fixed pier after the failure of their anchors is identified using the same definition as that at the abutment, with the minimum required seat width *N* indicated in Table 5.2. The dimensions (length and width) of the steel fixed bearing at the fixed pier are considered instead of the dimensions of the elastomeric bearings at the abutment.

Additional limit states related to the foundation of abutments and piers were considered in Phase II such as yielding of pile supporting wingwall (YPW), yielding of pile supporting backwall (YPB), and yielding of pile at pier (YPP). These limit states are not considered in this study because the foundation of Phase I models was defined by using uniaxial and rotational springs, instead of modeling foundation H-piles.

5.2. Analysis and Comparison of Pushover Analyses

5.2.1. SlC15T1F

Longitudinal direction

In Phase I and Phase II models, the Fixed Pier (Pier 2) resists a great part of the pushover force before the closure of the expansion joint at Abutment 2 (CEJ @ A2). Once this limit state occurs, Abutment 2 starts to provide a greater resistance. Likewise, for both cases, after pushing the superstructure 200 mm, it was not possible to identify rupture of fixed bearing anchors at the Fixed Pier (RFA @ P2). These unfused connections led to damaging limit states such as yielding of vertical reinforcing steel and concrete crushing at the column base of the Fixed Pier (YRS and CCC @ P2). Even though, these are acceptable limit states, this sequence of damage is not desired for quasi-isolation because the Fixed Pier sustained extensive damage and global yielding before fusing of sacrificial connections. Abutment 1 and the Expansion Pier (Pier 1) did not sustain large forces due to the isolation provided by elastomeric bearings. Details of the longitudinal pushover analyses of Phase I and Phase II models for this bridge variant are shown in Figure 5.3.

Some differences were identified between Phase I and Phase II models. In the Phase I model, after the closure of the expansion joint at Abutment 2 (CEJ @ A2), the force

resisted at this substructure suddenly increases (causing yielding of the backwall-pile-cap connection) whereas the Phase II model presents a much less abrupt increment. This difference can be attributed to the formulation of abutments in each model. In the case of Phase I models, the only element that resists superstructure displacements is the nonlinear spring located at the top of the backwall that represents backfill passive resistance. Conversely, in the case of Phase II models, backfill passive resistance is distributed in two springs located along the height of the backwall and pile cap. Besides these elements, approach slab friction is also modeled. These components and their configuration allow a different distribution of stiffness at this substructure and therefore a continuous and gradual force increment. Moreover, In the Phase I model, the pushover force that Abutment 2 resists is considerably lower than that of Phase II model. In the Phase I model mobilization of the backfill ultimate resistance is reached. After this limit state, Abutment 2 reaches its maximum resistance. In contrast, in the Phase II model, additional conditions, such as friction forces and surcharge effects due to the presence of the approach slab, consistently increase the force that Abutment 2 resists. Limit states such as failure of backwall-pile-cap connection or mobilization of backfill ultimate capacity were not identified.

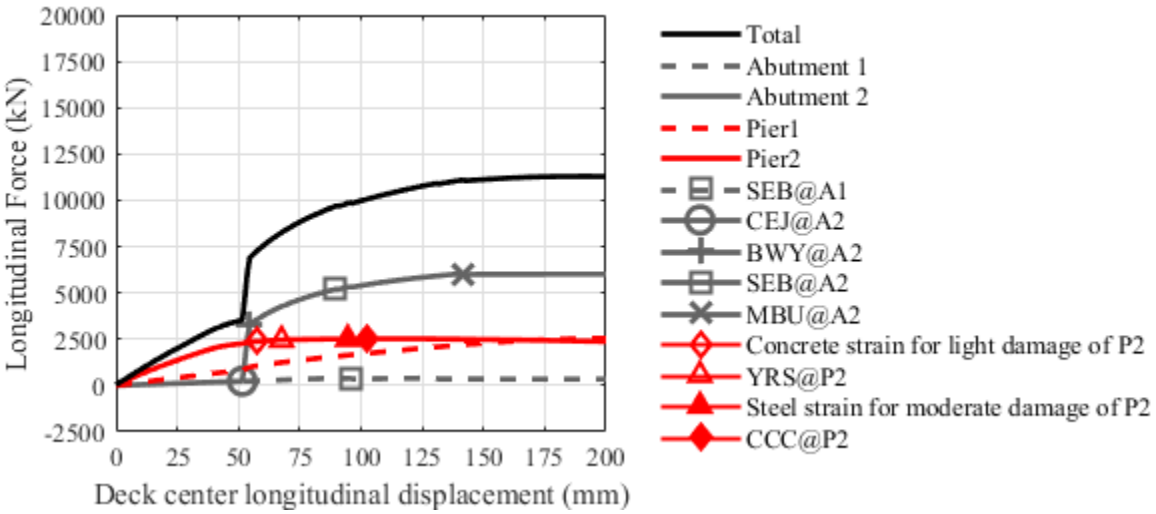

a) Phase I

Figure 5.3: Phase I and Phase II longitudinal pushover analyses of SlC15T1F bridge variant

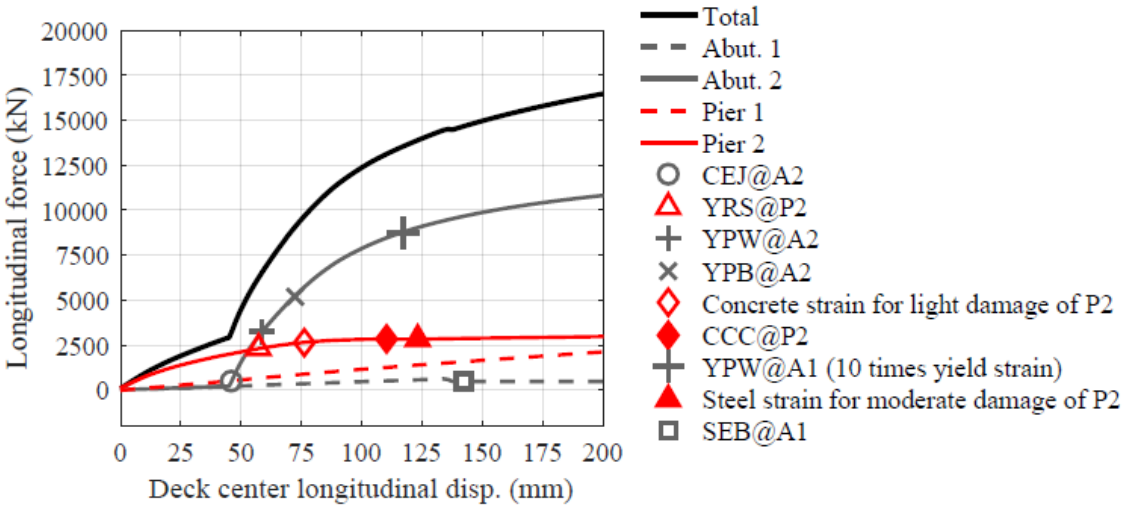

b) Phase II per Luo (2016)

Figure 5.3 continued

Transverse direction

The Expansion Pier (Pier 1) and the Fixed Pier (P2) resist the majority of the pushover force. Both in Phase I and Phase II pushover analyses, the first significant limit state was rupture of fixed bearing anchors (RFA @ P2). Once these connections fail, the Fixed Pier is not able to resist any additional pushover force. The observed sequence of damage in this direction is desired for quasi-isolation because it precludes damaging limit states such as yielding of vertical reinforcing steel or crushing of concrete cover at the column base of the substructures. Details of the transverse pushover analyses of Phase I and Phase II models for this bridge variant are shown in Figure 5.4.

Some similarities and differences were identified between the pushover analyses of Phase I and Phase II models. In both models, Pier 1 and Pier 2 resist the majority of the pushover force. Likewise, the major drops in strength occur when retainers or fixed bearing anchors fail. The magnitude of the pushover force that each substructure resists is similar in Phase I and Phase II models. One of the main differences between these models is the pseudo-time when fixed bearing anchors fail. The rupture of fixed bearing anchors (RFA @ P2) occurs at a greater deck center displacement in the Phase II model in comparison to the Phase I model. In this case, additional effects such as soil passive resistance provided by

wingwalls and the friction forces caused by the presence of the approach slab contribute to reduce the concentration of pushover force in the fixed bearing anchors at early stages of the pushover analysis.

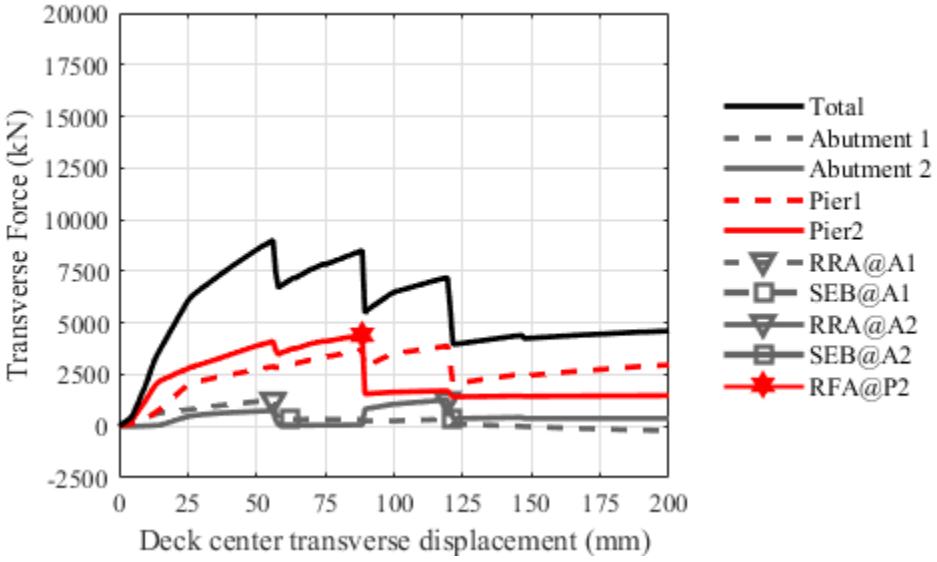

a) Phase I

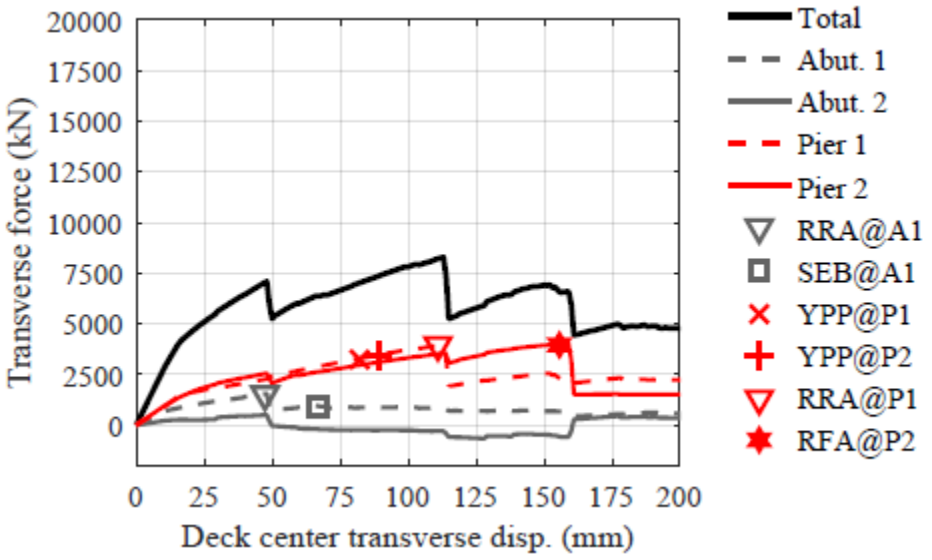

a) Phase II per Luo (2016)

Figure 5.4: Phase I and Phase II transverse pushover analyses of SlC15T1F bridge variant

5.2.2. SlC15T1S

Longitudinal direction

Both Phase I and Phase II models present similar responses to those of the previous bridge variant (SlC15T1F). Since rupture of the fixed bearing anchors (RFA @ P2) did not occur, damaging limit states such as yielding of vertical reinforcing steel and concrete crushing at the column base of the Fixed Pier (YRS and CCC @ P2) developed. This is not a sequence of damage desired for quasi-isolation. Due to the soft soil condition, Abutment 2 of the Phase I and Phase II models sustained lower levels of pushover force in comparison to the previous bridge model, which has a hard (fixed) foundation condition. Details of the longitudinal pushover analyses of Phase I and Phase II models for this bridge variant are shown in Figure 5.5.

Some similarities and differences were identified between the pushover analyses of Phase I and Phase II models. Similar to the previous bridge variant (SlC15T1F), for the case of Phase I model, most of the pushover force is resisted by Abutment 2 after the closure of the expansion joint at this location (CEJ @ A2). This force increases until the backwall reaches its yielding moment (BWY @ A2). After this, the pushover force increases according to the force-displacement relation of the nonlinear spring that represents the backfill. This noticeable increment of the pushover force at Abutment 2 in Phase I (Figure 5.5a), which is not identified in Phase II model (Figure 5.5b), can be attributed to the differences in the abutment configuration that were discussed in the analysis of the previous bridge variant (SlC15T1F). Additionally, in the Phase I model at Abutment 2, a less abrupt increase of the pushover force occurs between the closure of the expansion joint and backwall yielding (Figure 5.5a) compared to the previous hard (fixed) foundation case (Figure 5.3a). This difference can be ascribed to the lower stiffness of the soil condition of this bridge variant.

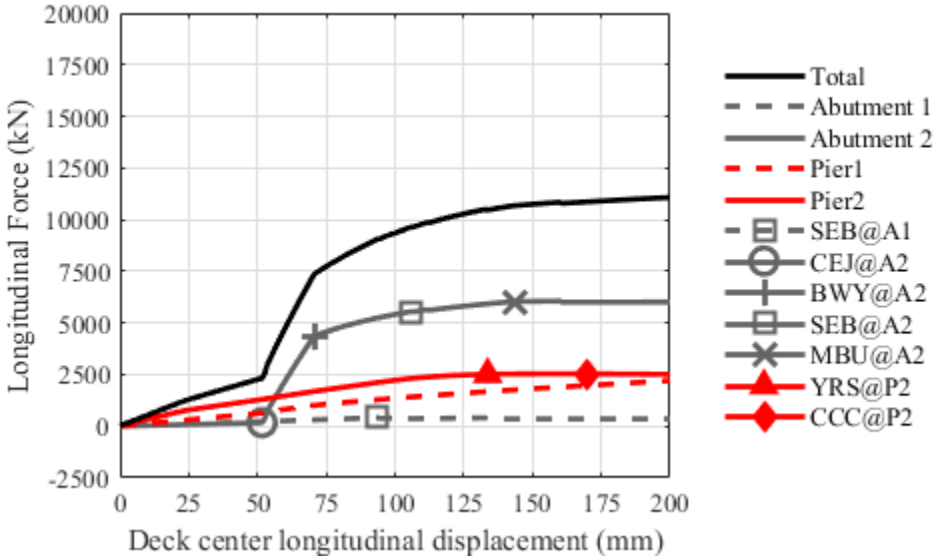

a) Phase I

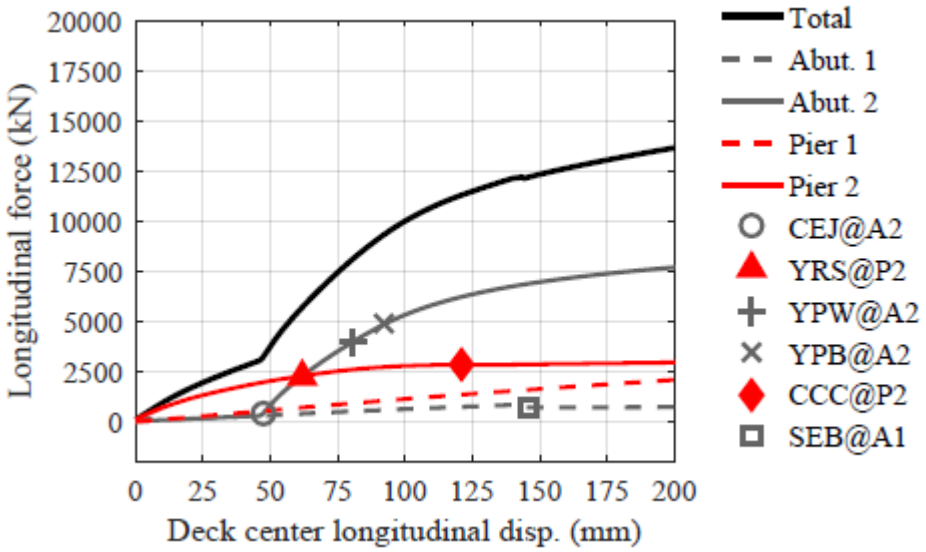

b) Phase II per Luo (2016)

Figure 5.5: Phase I and Phase II longitudinal pushover analyses of SlC15T1S bridge variant

Transverse direction

Phase I and Phase II models present a similar structural response for the applied pushover force. Like the previous case, both for Phase I and Phase II models, the Expansion Pier (Pier 1) and the Fixed Pier (Pier 2) sustain the majority of the pushover force. Fusing limit states such as rupture of retainer anchors at Abutment 1 (RRA @ A1) and sliding of elastomeric bearings at Abutment 1 were identified; nevertheless, rupture of fixed bearing anchors (RFA @ A2) and damaging limit states such as yielding of vertical reinforcing steel (YRS) and concrete cover crushing (CCC) did not occur. These findings indicate that a larger superstructure displacement is required in order to induce additional limit states for this type of soil foundation. Details of the transverse pushover analyses of Phase I and Phase II models for this bridge variant are shown in Figure 5.6.

Some similarities and similarities were identified between the pushover analyses of Phase I and Phase II models. Fusing of sacrificial connections such as rupture of retainer anchors at Abutment 1 (RRA @ A1) and sliding of elastomeric bearings at Abutment 1 (SEB @1) were identified approximately at the same deck center displacement. Abutment 1 and Abutment 2 of the Phase II model (Figure 5.6b) resist greater forces in comparison to the Phase I model (Figure 5.6a). This difference can be attributed to additional elements such as wingwalls and approach slab that increase resistance due to frictional forces.

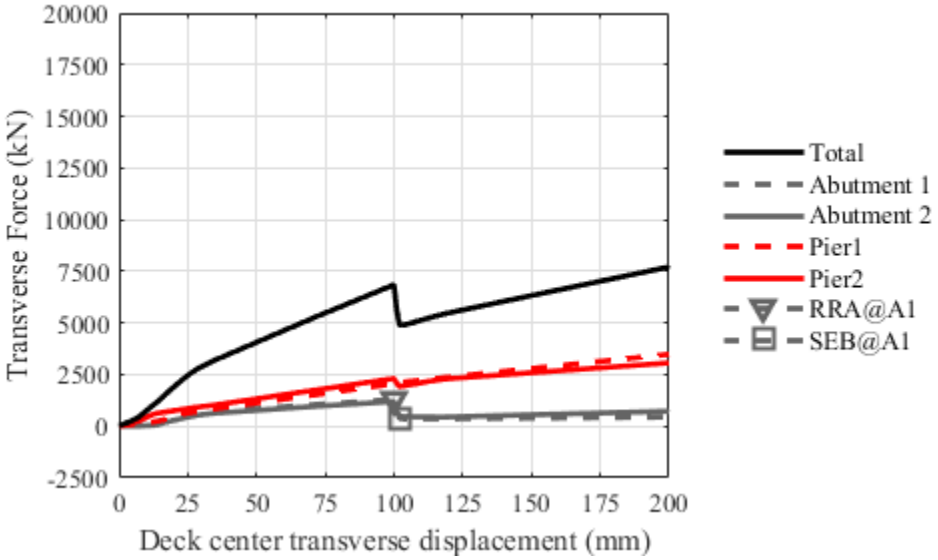

a) Phase I

Figure 5.6: Phase I and Phase II transverse pushover analyses of SlC15T1S bridge variant

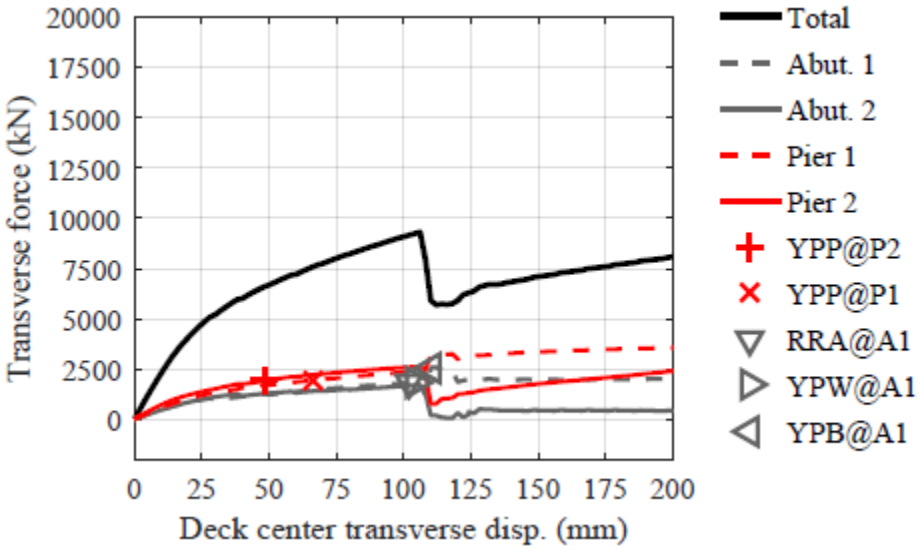

b) Phase II per Luo (2016)

Figure 5.6 continued

5.2.3. SlC40T1F

Longitudinal direction

In the Phase I and Phase II models, the overall structural response of this bridge variant is similar to the short-pier equivalent bridge (SlC15T1F), especially regarding the response of Abutment 1 and Abutment 2. The main difference between these bridge variants is the pushover force resisted by the Expansion Pier (P1) and the Fixed Pier (P2), which is considerably lower on these substructures for SlC40T1F. This difference can be ascribed to the lower lateral stiffness of 12.2. m (40-ft) column piers in comparison to 4.6 m (15-ft) column piers. Even though 12.2 m (40-ft) piers have columns with slightly larger diameter, the column height difference between these bridge variants is the predominant factor that determines a lower stiffness for the substructures of SlC40T1F. In addition, as previously mentioned for the case of the short-pier equivalent bridge (SlC15T1F), the pushover force resisted by the Fixed Pier (Pier 2) was greater than that of the Expansion Pier (P1). In contrast, for the SlC40T1F bridge variant, the forces resisted by the Expansion Pier or the Fixed Pier are almost equal. Likewise, this difference can be attributed to the lower stiffness of 12.2 m (40-ft) column piers. In this case the larger stiffness of the

sacrificial connections at each substructure dominates the overall structural response, which results in little difference between the pushover force resisted by the Expansion Pier or the Fixed Pier. Details of the longitudinal pushover analyses of Phase I and Phase II models for this bridge variant are shown in Figure 5.7.

Some similarities and differences were identified between the pushover analyses of Phase I and Phase II models. Likewise to the short-pier equivalent bridge (SlC15T1F) (Figure 5.3a), for the Phase I model, it the pushover force resisted by Abutment 2 increases rapidly after the closure of the expansion joint at this location (CEJ @ A2) (Figure 5.7a). This sudden increase causes yielding of the backwall-pile-cap connection (BWY @ A2), which is followed by a gradual increase of the pushover force that follows the trend determined by the force-displacement relation of the nonlinear spring that represents the backfill. In contrast, for the Phase II model, the pushover force increases more gradually without sudden increments or breaks (Figure 5.7b). Similar to the short-pier equivalent bridge (SlC15T1F), this difference can be ascribed to the differences in the abutment configuration that were previously discussed. Additionally, in the Phase I model, yielding of the vertical reinforcing steel at the Fixed Pier (YRS @ P2) occurs after mobilization of the backfill ultimate capacity at Abutment 2 (MBU @ A2). These limit states were not identified in the Phase II model. This difference can be attributed to the lower stiffness of abutments of Phase I models that allow greater displacements of the superstructure. These displacements induce forces on the Fixed Pier (P2) that lead to damaging limit states since fusing of the sacrificial connections at this location (RFA @ P2) cannot.

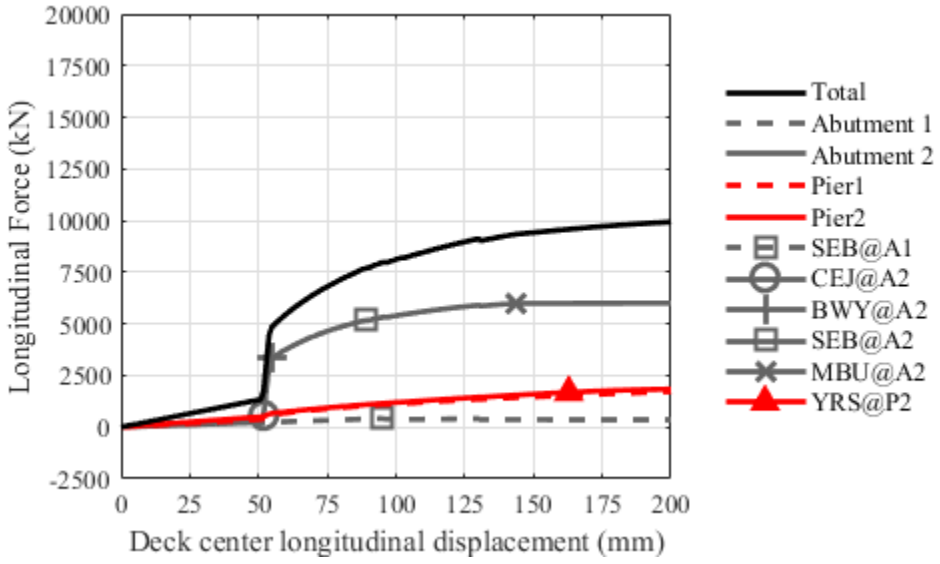

a) Phase I

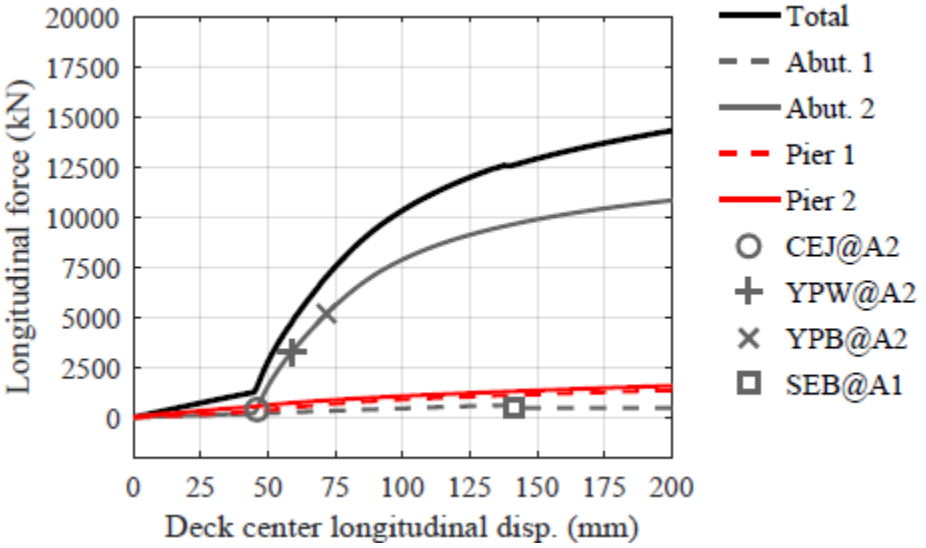

b) Phase II per Luo (2016)

Figure 5.7: Phase I and Phase II longitudinal pushover analyses of SlC40T1F bridge variant

Transverse direction

Phase I and Phase II models present a similar structural response for the applied pushover force. Unlike the short-pier equivalent bridge (SlC15T1F), the rupture of fixed bearing anchors (RFA @ P2) did not occur, which allowed damaging limit states such as the yielding of the vertical reinforcing steel at the Expansion Pier (YRS @ P1) and at the Fixed Pier (YRS @ P2). The lower stiffness of column piers of SlC40T1F precludes the

concentration of forces at sacrificial connections which is required to induce fusing in these components and consequently avoid substructure-related damaging limit states. Details of the transverse pushover analyses of Phase I and Phase II models for this bridge variant are shown in Figure 5.8.

Some similarities were identified between Phase I and Phase II models. Fusing of sacrificial connections such as rupture of retainer anchors at Abutment 1 (RRA @ A1) and sliding of elastomeric bearings at Abutment 1 (SEB @1) were identified approximately at the same deck center displacement. Likewise, in the Phase I and Phase II models, rupture of retainer anchors at the Expansion Pier (RRA @ P1) and rupture of fixed bearing anchors at the Fixed Pier (RFA @ P2) did not occur. Therefore, yielding of the vertical reinforcing steel occurred at these locations (YRS @ P1 and P2).

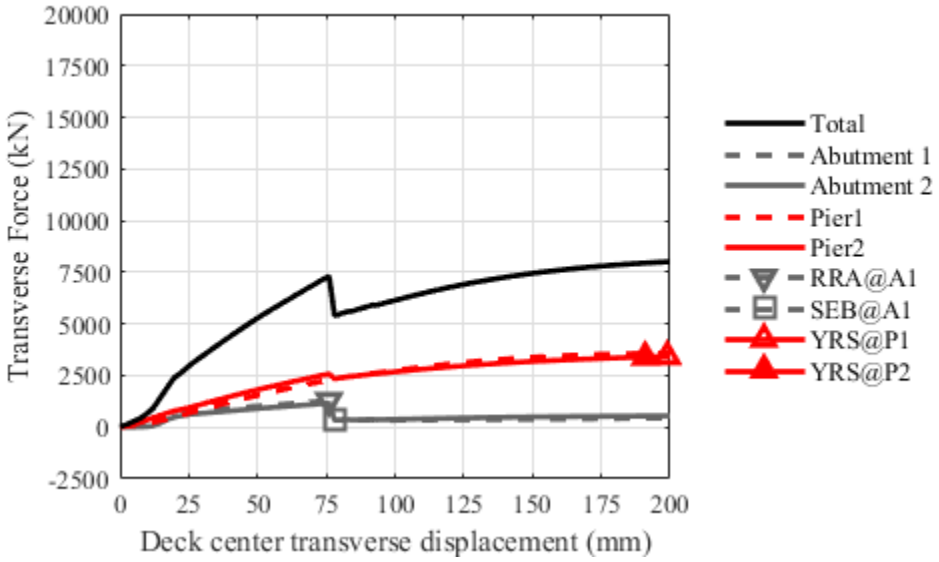

a) Phase I

Figure 5.8: Phase I and Phase II transverse pushover analyses of SlC40T1F bridge variant

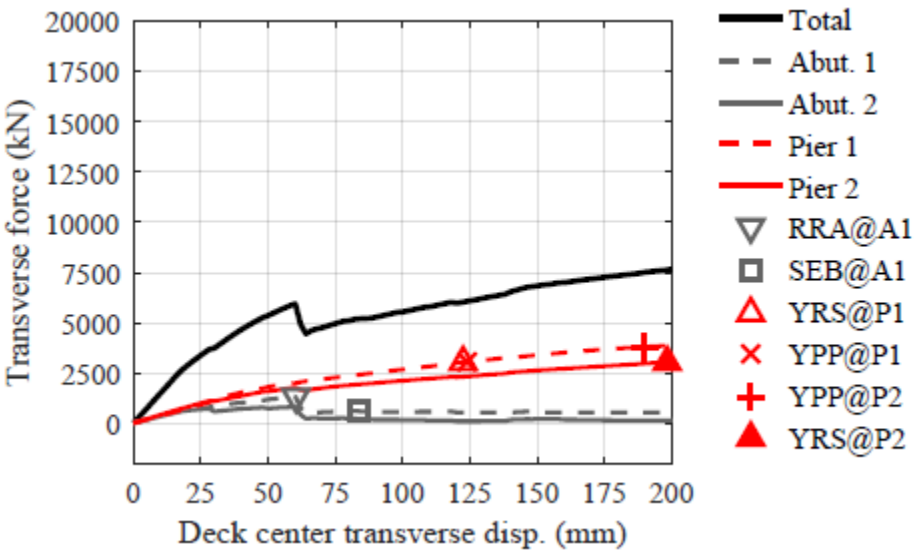

b) Phase II per Luo (2016)

Figure 5.8 continued

6. DYNAMIC ANALYSES OF PROTOTYPE HIGHWAY BRIDGES

Seismic performance of the Phase I bridges was analyzed by employing a suite of 20 synthetic ground motions that were formulated based on the Uniform Hazard Spectrum (UHS). These ground motions were developed for Paducah, Kentucky and Cape Girardeau, Missouri which are locations close to Cairo, the geographic site with the highest seismic hazard in Illinois (Fernandez & Rix, 2008).

For Phase II, seismic performance of bridges was analyzed by using a new suite of 20 synthetic ground motions which were formulated based on the Conditional Mean Spectrum (CMS). These ground motions were specifically designed for Cairo, Illinois considering the seismic hazard and geotechnical conditions of this location (Kozak et al., 2017).

A summary of the definition of these concepts will be included in this chapter in order to analyze the development of the techniques that were considered for the formulation of synthetic ground motions throughout Phase I and Phase II.

As mentioned in Chapter I, the bridge variants selected for this study can be found both in Phase I and Phase II parametric studies. In order to make an accurate comparison of the structural response of these bridge variants, Phase I models were analyzed by employing the ground motions and limit states defined in Phase II

In order to complement this analysis, a detailed assessment of the dynamic response of the selected bridge variants, was performed by implementing an incremental dynamic analysis (IDA), using Phase I models, and considering linear scale factors of 0.50, 0.75, 1.00, 1.25, 1.50, 1.75. The purpose of this IDA is to investigate when fusing and damaging limit states start to occur according to an increasing seismic force pattern.

6.1. Phase I Ground Motions

6.1.1. Definition of Uniform Hazard Spectra

According to Chin-Hsiung et al. (1994), before the development of Probabilistic Risk Assessment (PRA) methodologies and development of the concept of Uniform Hazard Spectrum (UHS), it was a common practice to establish sets of spectra normalized to a Peak Ground Acceleration (PGA) equal to 1 g. After this procedure, these sets were scaled down to specified PGA levels according to the requirements of design applications.

The shape of a set of normalized spectra was usually determined by obtaining the average spectra generated from a family of real recorded accelerograms scaled to 1 g PGA level. The essential feature of a family of accelerograms is that they should represent a common site condition and that all their members should represent ground motions produced by critical large-magnitude (M) and short-distance (R) seismic events.

The introduction into Earthquake Engineering of PRA methodologies made possible to use a consistent probabilistic approach. The results of these new methodologies were seismic hazard curves which are plots that express annual mean frequency of exceedance as a function of the PGA for the particular site to be analyzed.

One of the deficiencies of the procedure that was used before the development of PRA methodologies was the fact that the resulting spectra did not represent the same probability of exceedance over the full period of interest. For this reason the Uniform Hazard Spectra (UHS) concept was developed. The UHS generates sets of seismic hazard curves, each of which express annual mean frequency of exceedance as a function of an acceleration response spectral value for a specified discrete value of frequency (or period) and a specified discrete value of damping.

6.1.2. Development of synthetic ground motions using UHS

Based on studies of the New Madrid Seismic Zone (NMSZ), (Fernandez & Rix, 2008) developed various synthetic ground motions using the concept of UHS that are suitable for modeling different soil characteristics in the Upper Mississippi embayment.

Figure 6.1 indicates locations with available ground motions that consider the effects of inelastic soil response for deep soil conditions. Suites of surface ground acceleration records were generated at each one of the locations indicated on the map, with ten records produced for 475, 975 and 2475 return period events. From these ground motions, two sets of 10 synthetic ground motion records were formulated to provide accurate hazard approximations for an event with probability of exceedance of 7% in 75 years (1000 year return period) for southern Illinois locations with rock (Cape Girardeau, Missouri) and stiff soils (Paducah, Kentucky).

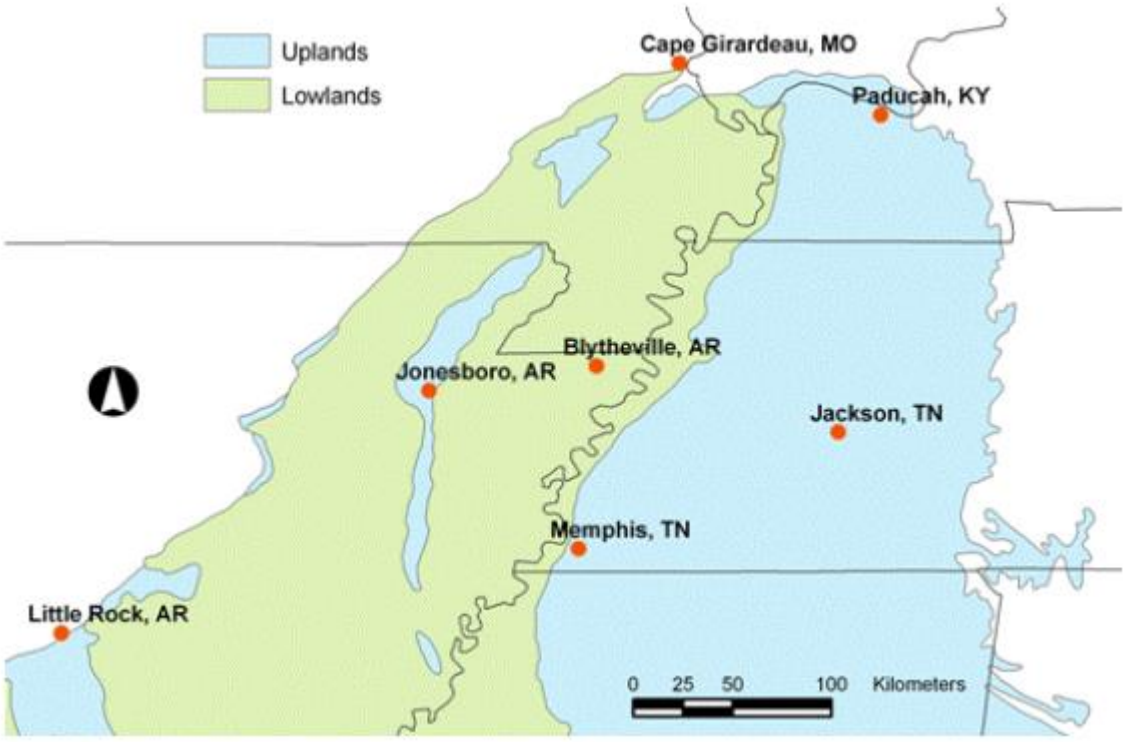

Figure 6.1: Locations considered for the development of synthetic ground motions per Fernandez & Rix (2008)

6.2. Phase II Ground Motions

6.2.1. Definition of Conditional Mean Spectrum

In general, UHS can be defined as an envelope of maximum spectral accelerations which has to be matched by a group of ground motions in order to be used for dynamic analyses Conversely, the Conditional Mean Spectrum (CMS) is a target spectrum that focuses on a certain period (commonly the fundamental period of a structure) (Baker, 2011). The CMS is able to better reflect the magnitude, distance, and epsilon parameter (ground motion parameter that indicates the number of standard deviations at a specific period that the mean spectral acceleration is form the corresponding acceleration of the design earthquake). The fundamental motivation for the development of the CMS is that the UHS generally produces unrealistically large spectral acceleration values across all periods. The fact that the UHS integrates multiple seismic sources means that no single earthquake will have the large spectral accelerations present in the UHS at all periods (Kozak et al., 2017).

A deaggregation process for ground motions based on features such as magnitude and distance for a specific site and particular period of interest, allow for creation of an appropriate CMS. For the case of southern Illinois sites, such as Cairo, these locations have similar CMS and UHS due to the predominant influence of a single seismic hazard source (the NMSZ). In contrast, other sites such as East St. Louis, Illinois, are located sufficiently far from the NMSZ to be significantly influenced by additional hazard sources, leading to CMS being considerably different from the UHS and more beneficial for ground motion creation (Kozak et al., 2017).

6.2.2. Development of ground motions using CMS

In order to develop synthetic ground motions for Phase II, 138 historical earthquake ground motions recorded at bedrock were obtained from the NUREG/CR-6728 report (McGuire et al., 2001) and used as base ground motions for subsequent modification. After this, five CMS (Baker, 2011) with different conditional periods (0.2, 0.3, 0.5, 1.0 and 2.0

seconds) were developed for Cairo, Illinois considering a seismic hazard level of 5% probability of exceedance in 50 years (1000 year return period).

This hazard level is consistent with the 1000 year return period established by AASHTO (2008b) since 2008. Four of the 138 source motions that had the most similar spectral shapes to the CMS were selected and each of the four source motions was spectrally matched to the five CMS using a time-domain spectral matching program RspMatch09 (Al Atik & Abrahamson, 2010), therefore generating 20 modified ground motions. To account for the site condition, a shear wave velocity profile was developed from the boring logs of the completed bridge construction projects at Cairo. Finally, one-dimensional ground motion response analyses were performed on the 20 modified ground motions using the nonlinear site response analysis platform DEEPSOIL (Hashash et al., 2015).

6.3. Comparison of Nonlinear Dynamic Analyses of Phase I and Phase II Models

Tables 6.1, 6.2, 6.3, and 6.4 summarize the limit state occurrences for each of the four bridge variants selected for this study, when subjected to the suite of 20 synthetic ground motions developed for Cairo, Illinois, applied in the longitudinal and transverse directions. Each percentage in the table indicates the number of analyses with occurrences of a limit state out of the 20 analyses with the 20 ground motions applied to a bridge variant in one incident direction.

For instance, the percentage of occurrence of CEJ (closure of expansion joint) at Abutment 1 of the SlC15T1F bridge variant when subjected to longitudinal ground motions is 100% , as shown in Table 6.1. This percentage implies that closure of the expansion joint at Abutment 1 was observed in all of the 20 analyses performed on the SlC15T1F bridge variant with longitudinal ground motions. Three gradient color scales, blue, yellow and red were used along with the percentages of Table 6.1 to highlight the occurrences of the preferred, acceptable and unacceptable limit states that were defined in Table 5.1. This color scale is shown in Figure 6.2.

Figure 6.2: Color scale for identification of limit states

The data listed in Tables 6.1, 6.2, 6.3, and 6.4 was grouped by bridge substructures, namely the two abutments, expansion pier and fixed pier. For the substructure groups, the data of the following tables was further analyzed and their statistical summaries are presented in Tables 6.5, 6.6, 6.7, and 6.8

Table 6.1: Limit state occurrences of SlC15T1F bridge variant under longitudinal and transverse ground motions

	Abutment 1 (A1)							Pier 1 (P1)					Pier 2 (P2)				Abutment (A2)						
	CEJ	**FBP**	**MBU**	**RRA**	**SEB**	**UBA**	**UBO**	**RRA**	**SEB**	**UEB**	**YRS**	**CCC**	**RFA**	**USB**	**YRS**	**CCC**	**CEJ**	**FBP**	**MBU**	**RRA**	**SEB**	**UBA**	**UBO**
Ph. I	100%	0%	0%	0%	0%	0%	0%	0%	0%	0%	0%	0%	0%	0%	100%	0%	100%	0%	0%	0%	5%	0%	0%
Ph. II	100%	0%	0%	0%	0%	0%	0%	0%	0%	0%	0%	0%	0%	0%	100%	0%	100%	0%	0%	0%	0%	0%	0%

a) Longitudinal Ground Motions

	Abutment 1 (A1)							Pier 1 (P1)					Pier 2 (P2)				Abutment (A2)						
	CEJ	**FBP**	**MBU**	**RRA**	**SEB**	**UBA**	**UBO**	**RRA**	**SEB**	**UEB**	**YRS**	**CCC**	**RFA**	**USB**	**YRS**	**CCC**	**CEJ**	**FBP**	**MBU**	**RRA**	**SEB**	**UBA**	**UBO**
Ph. I	0%	0%	0%	90%	80%	0%	0%	0%	0%	0%	0%	0%	0%	0%	0%	0%	0%	0%	0%	10%	5%	0%	0%
Ph. II	0%	0%	0%	50%	5%	0%	0%	0%	0%	0%	0%	0%	0%	0%	0%	0%	0%	0%	0%	0%	0%	0%	0%

b) Transverse Ground Motions

Table 6.2: Limit state occurrences of SlC15T1S bridge variant under longitudinal and transverse ground motions

	Abutment 1 (A1)							Pier 1 (P1)					Pier 2 (P2)				Abutment (A2)						
	CEJ	**FBP**	**MBU**	**RRA**	**SEB**	**UBA**	**UBO**	**RRA**	**SEB**	**UEB**	**YRS**	**CCC**	**RFA**	**USB**	**YRS**	**CCC**	**CEJ**	**FBP**	**MBU**	**RRA**	**SEB**	**UBA**	**UBO**
Ph. I	100%	0%	5%	0%	35%	0%	0%	0%	0%	0%	0%	0%	0%	0%	75%	0%	100%	0%	10%	0%	35%	0%	0%
Ph. II	100%	0%	0%	0%	0%	0%	0%	0%	0%	0%	0%	0%	0%	0%	100%	0%	100%	0%	0%	0%	0%	0%	0%

a) Longitudinal Ground Motions

	Abutment 1 (A1)							Pier 1 (P1)					Pier 2 (P2)				Abutment (A2)						
	CEJ	**FBP**	**MBU**	**RRA**	**SEB**	**UBA**	**UBO**	**RRA**	**SEB**	**UEB**	**YRS**	**CCC**	**RFA**	**USB**	**YRS**	**CCC**	**CEJ**	**FBP**	**MBU**	**RRA**	**SEB**	**UBA**	**UBO**
Ph. I	0%	0%	0%	80%	80%	0%	0%	0%	0%	0%	0%	0%	0%	0%	0%	0%	0%	0%	0%	50%	45%	0%	0%
Ph. II	0%	0%	0%	25%	5%	0%	0%	0%	0%	0%	0%	0%	0%	0%	0%	0%	0%	0%	0%	0%	0%	0%	0%

b) Transverse Ground Motions

Table 6.3: Limit state occurrences of SlC40T1F bridge variant under longitudinal and transverse ground motions

	Abutment 1 (A1)						
	CEJ	**FBP**	**MBU**	**RRA**	**SEB**	**UBA**	**UBO**
Ph. I	100%	0%	0%	0%	90%	0%	0%
Ph. II	100%	0%	0%	0%	35%	0%	0%

	Pier 1 (P1)				
	RRA	**SEB**	**UEB**	**YRS**	**CCC**
Ph. I	0%	0%	0%	45%	0%
Ph. II	0%	0%	0%	5%	0%

	Pier 2 (P2)			
	RFA	**USB**	**YRS**	**CCC**
Ph. I	0%	0%	55%	0%
Ph. II	0%	0%	0%	0%

	Abutment (A2)						
	CEJ	**FBP**	**MBU**	**RRA**	**SEB**	**UBA**	**UBO**
Ph. I	100%	0%	0%	0%	90%	0%	0%
Ph. II	100%	0%	0%	0%	30%	0%	0%

a) Longitudinal Ground Motions

	Abutment 1 (A1)						
	CEJ	**FBP**	**MBU**	**RRA**	**SEB**	**UBA**	**UBO**
Ph. I	0%	0%	0%	100%	100%	0%	0%
Ph. II	0%	0%	0%	100%	85%	0%	0%

	Pier 1 (P1)				
	RRA	**SEB**	**UEB**	**YRS**	**CCC**
Ph. I	0%	0%	0%	10%	0%
Ph. II	0%	0%	0%	65%	0%

	Pier 2 (P2)			
	RFA	**USB**	**YRS**	**CCC**
Ph. I	0%	0%	55%	0%
Ph. II	0%	0%	15%	0%

	Abutment (A2)						
	CEJ	**FBP**	**MBU**	**RRA**	**SEB**	**UBA**	**UBO**
Ph. I	0%	0%	0%	100%	100%	0%	0%
Ph. II	0%	0%	0%	55%	10%	0%	0%

b) Transverse Ground Motions

Table 6.4: Limit state occurrences of SlC40T1S bridge variant under longitudinal and transverse ground motions

	Abutment 1 (A1)							Pier 1 (P1)					Pier 2 (P2)				Abutment (A2)						
	CEJ	**FBP**	**MBU**	**RRA**	**SEB**	**UBA**	**UBO**	**RRA**	**SEB**	**UEB**	**YRS**	**CCC**	**RFA**	**USB**	**YRS**	**CCC**	**CEJ**	**FBP**	**MBU**	**RRA**	**SEB**	**UBA**	**UBO**
Ph. I	100%	0%	5%	0%	65%	0%	0%	0%	0%	0%	40%	0%	0%	0%	40%	0%	100%	0%	10%	0%	65%	0%	0%
Ph. II	100%	0%	25%	0%	70%	0%	0%	0%	0%	0%	25%	0%	0%	0%	35%	0%	100%	0%	15%	0%	75%	0%	0%

a) Longitudinal Ground Motions

	Abutment 1 (A1)							Pier 1 (P1)					Pier 2 (P2)				Abutment (A2)						
	CEJ	**FBP**	**MBU**	**RRA**	**SEB**	**UBA**	**UBO**	**RRA**	**SEB**	**UEB**	**YRS**	**CCC**	**RFA**	**USB**	**YRS**	**CCC**	**CEJ**	**FBP**	**MBU**	**RRA**	**SEB**	**UBA**	**UBO**
Ph. I	0%	0%	0%	100%	100%	0%	0%	0%	0%	0%	10%	0%	0%	0%	30%	0%	0%	0%	0%	100%	100%	0%	0%
Ph. II	0%	0%	0%	90%	65%	0%	0%	0%	0%	0%	35%	0%	0%	0%	10%	0%	0%	0%	0%	30%	10%	0%	0%

b) Transverse Ground Motions

Abutments (A1 and A2)

Longitudinal ground motions

Closure of expansion joint (CEJ)

- This limit state was identified on each abutment (CEJ @ A1 and A2) in all the analyses in both Phase I and Phase II models.

Mobilization of backfill ultimate capacity (MBU)

- This limit state occurred more frequently in bridge variants with soft soil foundation. The occurrence of this limit state could be attributed to the fact that soft soil foundations have lower stiffness. Therefore, this condition requires backfills to resist a greater part of the forces induced by the superstructure, which in certain cases could exceed their ultimate capacity.
- Phase I models had a greater percentage of occurrences of this limit state compared to Phase II models. This difference can be ascribed to the fact that Phase I models have a lower backfill resistance due to the absence of elements such as approach slabs which induce surcharge effects (Luo et al., 2017).

Sliding of elastomeric bearings (SEB)

- Bridge variants with 40-ft column piers were more likely to experience this limit state. For these bridge variants, seismic forces are concentrated at abutments because these locations have greater stiffness compared to intermediate piers. The stiffness of these elements determines the magnitude of superstructure displacements in the longitudinal direction and therefore the probability of inducing forces that trigger the sliding of elastomeric bearings.
- Like mobilization of backfill ultimate capacity, Phase I models experienced SEB more often than Phase II models. In these models, additional stiffness –due to elements such as approach slabs that generate surcharge effects and friction forces–

reduces the magnitude of superstructure displacements and therefore sliding of elastomeric bearings does not occur as frequently.

Transverse ground motions

Rupture of retainer anchors (RRA) and sliding of elastomeric bearings (SEB)

- Limit states such as rupture of retainer anchors and sliding of elastomeric bearings at Abutment 1 (RRA @ A1 and SEB @ A1) were consistently identified in all bridge variants. These limit states were not identified at the Expansion Pier (RRA @ P1 and SEB @ P1) neither the rupture of fixed bearing anchors at the Fixed Pier (RFA @ P2). These results indicate that the superstructure rotates around the Fixed Pier in a considerable number of seismic analyses.
- The rupture of retainer anchors and sliding of elastomeric bearings at Abutment 1 (RRA @ A1 and SEB @ A1) occurred more frequently in Phase I models. This difference can be ascribed to the fact that Phase I models only depend on these elements to transmit forces from the superstructure to the substructure. On the other hand, Phase II models were formulated including wingwalls (which are connected to backwalls by bent dowel bars) (Luo et al., 2017). These elements have capacity to resist seismic demands, which allows force redistribution at abutments. Consequently, this redistribution reduces the magnitude of the forces in retainers and bearings.

Table 6.5: Abutment 1 limit states occurrences summary

Limit state	Phase	Occurrence[1]	Foundation Soil[2]		Column height[2]		Ground motion incident angle[2]	
			Fixed	Soft	4.57 m (15 ft)	12.19 m (40 ft)	0° (Long.)	90° (Tran.)
Closure of expansion joint (CEJ@A1)	Ph. I	80	40	40	40	40	80	0
		50%	50%	50%	50%	50%	100%	0%
	Ph. II	80	40	40	40	40	80	0
		50%	50%	50%	50%	50%	100%	0%
Failure of backwall-to-pile-cap connection (FBP@A1)	Ph. I	0	0	0	0	0	0	0
		0%	0%	0%	0%	0%	0%	0%
	Ph. II	0	0	0	0	0	0	0
		0%	0%	0%	0%	0%	0%	0%
Mobilization of backfill ultimate capacity (MBU@A1)	Ph. I	2	0	2	1	1	2	0
		1%	0%	100%	50%	50%	100%	0%
	Ph. II	5	0	5	0	5	5	0
		3%	0%	100%	0%	100%	100%	0%
Rupture of retainer anchor bolts (RRA@A1)	Ph. I	74	38	36	34	40	0	74
		46%	51%	49%	46%	54%	0%	100%
	Ph. II	53	30	23	15	38	0	53
		33%	57%	43%	28%	72%	0%	100%
Sliding of elastomeric bearings (SEB@A1)	Ph. I	110	54	56	39	71	38	72
		69%	49%	51%	35%	65%	35%	65%
	Ph. II	53	25	28	2	51	21	32
		33%	47%	53%	4%	96%	40%	60%
Unseating of bearing at acute corner (UBA@A1)	Ph. I	0	0	0	0	0	0	0
		0%	0%	0%	0%	0%	0%	0%
	Ph. II	0	0	0	0	0	0	0
		0%	0%	0%	0%	0%	0%	0%
Unseating of bearing at obtuse corner (UBO@A1)	Ph. I	0	0	0	0	0	0	0
		0%	0%	0%	0%	0%	0%	0%
	Ph. II	0	0	0	0	0	0	0
		0%	0%	0%	0%	0%	0%	0%

[1] The number above the percentage indicates the number of analyses with occurrences of a limit state.
The percentage indicates the ratio between the number above to all the 160 analyses.
[2] The number above the percentage indicates the number of analyses with occurrences of a limit state contributed by a parametric variation.
The percentage indicates the relative contribution of a parametric variation to the total occurrences of a limit state.

Table 6.6: Abutment 2 limit states occurrences summary

Limit state	Phase	Occurrence[1]	Foundation Soil[2]		Column height[2]		Ground motion incident angle[2]	
			Fixed	Soft	4.57 m (15 ft)	12.19 m (40 ft)	0° (Long.)	90° (Tran.)
Closure of expansion joint (CEJ@A2)	Ph. I	80	40	40	40	40	80	0
		50%	50%	50%	50%	50%	100%	0%
	Ph. II	80	40	40	40	40	80	0
		50%	50%	50%	50%	50%	100%	0%
Failure of backwall-to-pile-cap connection (FBP@A2)	Ph. I	0	0	0	0	0	0	0
		0%	0%	0%	0%	0%	0%	0%
	Ph. II	0	0	0	0	0	0	0
		0%	0%	0%	0%	0%	0%	0%
Mobilization of backfill ultimate capacity (MBU@A2)	Ph. I	4	0	4	2	2	4	0
		3%	0%	100%	50%	50%	100%	0%
	Ph. II	3	0	3	0	3	3	0
		2%	0%	100%	0%	100%	100%	0%
Rupture of retainer anchor bolts (RRA@A2)	Ph. I	52	22	30	12	40	0	52
		33%	42%	58%	23%	77%	0%	100%
	Ph. II	17	11	6	0	17	0	17
		11%	65%	35%	0%	100%	0%	100%
Sliding of elastomeric bearings (SEB@A2)	Ph. I	89	40	49	18	71	39	50
		56%	45%	55%	20%	80%	44%	56%
	Ph. II	25	8	17	0	25	21	4
		16%	32%	68%	0%	100%	84%	16%
Unseating of bearing at acute corner (UBA@A2)	Ph. I	0	0	0	0	0	0	0
		0%	0%	0%	0%	0%	0%	0%
	Ph. II	0	0	0	0	0	0	0
		0%	0%	0%	0%	0%	0%	0%
Unseating of bearing at obtuse corner (UBO@A2)	Ph. I	0	0	0	0	0	0	0
		0%	0%	0%	0%	0%	0%	0%
	Ph. II	0	0	0	0	0	0	0
		0%	0%	0%	0%	0%	0%	0%

[1] The number above the percentage indicates the number of analyses with occurrences of a limit state.
The percentage indicates the ratio between the number above to all the 160 analyses.
[2] The number above the percentage indicates the number of analyses with occurrences of a limit state contributed by a parametric variation.
The percentage indicates the relative contribution of a parametric variation to the total occurrences of a limit state.

Expansion Pier (P1)

Longitudinal ground motions

Yielding of vertical reinforcing steel (YRS)

- This limit state was only identified for bridge variants with 40-ft column piers. As mentioned before, for these bridge variants, seismic forces are concentrated at abutments because these locations have greater stiffness compared to intermediate piers. The stiffness of these elements determines the magnitude of superstructure displacements in the longitudinal direction and therefore the probability of inducing forces that trigger limit states at these locations and at intermediate piers. The magnitude of these forces was enough to cause sliding of elastomeric bearings at abutments (SEB @ A1 and A2); nevertheless, it did not reach the required level to induce this limit state at the Expansion Pier (SEB @ P1) nor the rupture of fixed bearing anchors (RFA @ P2). For this reason, the Expansion Pier was likely to experience yielding of the vertical reinforcing steel (YRS @ P1)
- Among these bridge variants, yielding of the vertical reinforcing steel at Expansion Pier (YRS @ P1) occurred more frequently in Phase I models. This difference can be attributed to the lower stiffness of abutments due to the absence of approach slabs in the formulation of these models. As previously mentioned, these elements induce surcharge effects and friction forces that increase overall abutment resistance.

Transverse ground motions

Yielding of vertical reinforcing steel (YRS)

- This limit state was only identified on bridge variants with 40-ft column piers. As previously stated, seismic forces are concentrated at abutments due to the reduced stiffness of column piers. For this reason, abutments' stiffness governs the magnitude of superstructure displacements and induced forces at each substructure.

Similar to the previous analysis direction, the magnitude of these forces was usually enough to cause rupture of retainer anchors and sliding of elastomeric bearings at abutments (RRA @ A1 and A2; SEB @ A1 and A2); however, they did not reach the required level to induce these limit states at the Expansion Pier (SEB @ P1; RRA @ P1) nor the rupture of fixed bearing anchors (RFA @ P2). For this reason, the Expansion Pier was likely to experience yielding of the vertical reinforcing steel (YRS @ P1)

- No significant differences were found between the number of occurrences of this limit state in Phase I and Phase II models.

Table 6.7: Expansion pier limit states occurrences summary

Limit state	Phase	Occurrence[1]	Foundation Soil[2]		Column height[2]		Ground motion incident angle[2]	
			Fixed	Soft	4.57 m (15 ft)	12.19 m (40 ft)	0° (Long.)	90° (Tran.)
Rupture of retainer anchor bolts (RRA@P1)	Ph. I	0	0	0	0	0	0	0
		0%	0%	0%	0%	0%	0%	0%
	Ph. II	0	0	0	0	0	0	0
		0%	0%	0%	0%	0%	0%	0%
Sliding of elastomeric bearings (SEB@P1)	Ph. I	0	0	0	0	0	0	0
		0%	0%	0%	0%	0%	0%	0%
	Ph. II	0	0	0	0	0	0	0
		0%	0%	0%	0%	0%	0%	0%
Unseating of elastomeric bearing (UEB@P1)	Ph. I	0	0	0	0	0	0	0
		0%	0%	0%	0%	0%	0%	0%
	Ph. II	0	0	0	0	0	0	0
		0%	0%	0%	0%	0%	0%	0%
Yielding of vertical reinforcing steel (YRS@P1)	Ph. I	21	11	10	0	21	17	4
		13%	52%	48%	0%	100%	81%	19%
	Ph. II	26	14	12	0	26	6	20
		16%	54%	46%	0%	100%	23%	77%
Crushing of concrete cover (CCC@P1)	Ph. I	0	0	0	0	0	0	0
		0%	0%	0%	0%	0%	0%	0%
	Ph. II	0	0	0	0	0	0	0
		0%	0%	0%	0%	0%	0%	0%

[1] The number above the percentage indicates the number of analyses with occurrences of a limit state.
The percentage indicates the ratio between the number above to all the 160 analyses.
[2] The number above the percentage indicates the number of analyses with occurrences of a limit state contributed by a parametric variation.
The percentage indicates the relative contribution of a parametric variation to the total occurrences of a limit state.

Fixed Pier (P2)

Longitudinal ground motions

Yielding of vertical reinforcing steel (YRS)

- Unlike the previous substructure, for this direction, yielding of vertical reinforcing steel (YRS @ P2) was also identified on bridge variants with 15-ft column piers. Limit states such as sliding of elastomeric bearings at abutments and Expansion Pier (SEB @ A1, A2 and P1) and rupture of fixed bearing anchors (RFA @ P2) did not occur. Therefore, due to the fact that these structural fuses did not reach their limit state, seismic demands could be fully transmitted from the superstructure to the substructure causing yielding of the vertical reinforcing steel of columns at the Fixed Pier (YRS @ P2).
- Generally, no substantial differences were found between the number of occurrences of this limit state in Phase I and Phase II models.

Transverse ground motions

Yielding of vertical reinforcing steel (YRS)

- Like the Expansion Pier, for this direction, this limit state was only identified on bridge variants with 40-ft column piers. Seismic forces are concentrated at abutments due to the reduced stiffness of column piers. Hence, the stiffness of abutments determines the magnitude of superstructure displacements and induced forces at each substructure. The magnitude of these forces was frequently enough to cause rupture of retainer anchors and sliding of elastomeric bearings at abutments (RRA @ A1 and A2; SEB @ A1 and A2); however, they did not reach the required level to induce these limit states at the Expansion Pier (SEB @ P1; RRA @ P1) nor the rupture of fixed bearing anchors (RFA @ P2). For this reason, the Fixed Pier was likely to experience yielding of the vertical reinforcing steel (YRS @ P2)

- For the case of bridge variants with 40-ft column piers, yielding of the vertical reinforcing steel at Fixed Pier (YRS @ P2) occurred more frequently in Phase I models. This difference can be attributed to the lower stiffness of abutments due to the absence of wingwalls and approach slabs in the formulation of these models. As previously mentioned, these elements increase overall abutment resistance which reduces superstructure displacements. This reduction limits the magnitude of forces transmitted to the Fixed Pier that cause yielding of the vertical reinforcing steel.

Table 6.8: Fixed pier limit states occurrences summary

Limit state	Phase	Occurrence[1]	Foundation Soil[2]		Column height[2]		Ground motion incident angle[2]	
			Fixed	Soft	4.57 m (15 ft)	12.19 m (40 ft)	0° (Long.)	90° (Tran.)
Rupture of steel fixed bearing anchor bolts (RFA@P2)	Ph. I	0	0	0	0	0	0	0
		0%	0%	0%	0%	0%	0%	0%
	Ph. II	0	0	0	0	0	0	0
		0%	0%	0%	0%	0%	0%	0%
Unseating of steel fixed bearing (USB@P2)	Ph. I	0	0	0	0	0	0	0
		0%	0%	0%	0%	0%	0%	0%
	Ph. II	0	0	0	0	0	0	0
		0%	0%	0%	0%	0%	0%	0%
Yielding of vertical reinforcing steel (YRS@P2)	Ph. I	71	42	29	35	36	54	17
		44%	59%	41%	49%	51%	76%	24%
	Ph. II	52	23	29	40	12	47	5
		33%	44%	56%	77%	23%	90%	10%
Crushing of concrete cover (CCC@P2)	Ph. I	0	0	0	0	0	0	0
		0%	0%	0%	0%	0%	0%	0%
	Ph. II	0	0	0	0	0	0	0
		0%	0%	0%	0%	0%	0%	0%

[1] The number above the percentage indicates the number of analyses with occurrences of a limit state.
The percentage indicates the ratio between the number above to all the 160 analyses.
[2] The number above the percentage indicates the number of analyses with occurrences of a limit state contributed by a parametric variation.
The percentage indicates the relative contribution of a parametric variation to the total occurrences of a limit state.

6.4. Incremental Dynamic Analysis

6.4.1. Ground motion scaling

Figure 6.3 shows the acceleration motion spectra for the selected suite of synthetic ground motions. The ground motions as shown are considered to be at a scale factor (SF) of 1.0 and represent the reference hazard for this study. The ground motions response spectra were obtained using SeismoSignal (Seismosoft, 2016). For this study, six different scale factors were used (0.50; 0.75; 1.00 (design level); 1.25; 1.50; 1.75) in order to analyze different hazard levels and generate a coarse incremental dynamic analysis (IDA) (Vamvatsikos & Cornell, 2002). The ground motions with a SF = 1.0 were linearly scaled up and down to provide relative estimates of structural performance for different hazard levels.

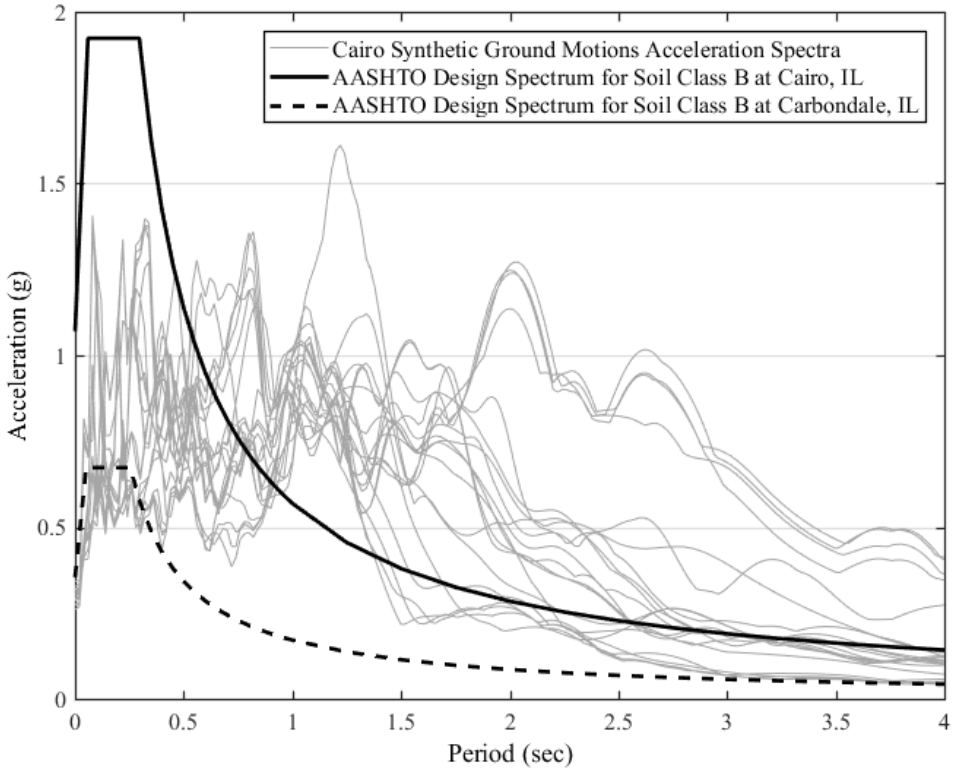

Figure 6.3: Cairo synthetic ground motions spectra and AASHTO design spectra

Cairo, Illinois, has one of the highest hazards of the state and a considerable high hazard within the New Madrid Seismic Zone (NMSZ). Other locations in Illinois usually have lower hazards. This is the case of Carbondale, whose design hazard can be approximately obtained by scaling the reference ground motions with a factor of 0.5. The spectral acceleration for actual earthquake events increases logarithmically for higher magnitude hazards. For this reason, the linear scaling procedure used in this study does not correspond directly to particular higher hazard levels. Nevertheless, the maximum considered earthquake (MCE) hazard (an event with probability of exceedance of 2% in 50 years) for Cairo can be approximated to be between the 1.5 and 1.75 linearly scaled ground motion levels.

6.4.2. Incremental dynamic analysis discussion

Tables 6.9 and 6.10 summarize the limit state occurrences for each of the four bridge variants selected for this study, when subjected to the suite of 20 synthetic ground motions developed for Cairo, Illinois, applied in the longitudinal and transverse directions, for scale factors of 0.5, 0.75, 1.00, 1.25, 1.50, 1.75. Each percentage in the table indicates the number of analyses with occurrences of a limit state out of the 20 analyses with the 20 ground motions applied to a bridge variant in one incident direction for a certain scale factor.

These tables were organized according to the direction of the applied ground motions, namely longitudinal and transverse ground motions, in order to simplify the analysis and comparison among the responses of each of the bridge variants.

Table 6.9: Incremental dynamic analysis for longitudinal ground motions

	Abutment 1 (A1)							Pier 1 (P1)					Pier 2 (P2)				Abutment (A2)						
S.F.	**CEJ**	**FBP**	**MBU**	**RRA**	**SEB**	**UBA**	**UBO**	**RRA**	**SEB**	**UEB**	**YRS**	**CCC**	**RFA**	**USB**	**YRS**	**CCC**	**CEJ**	**FBP**	**MBU**	**RRA**	**SEB**	**UBA**	**UBO**
SF0.50	100%	0%	0%	0%	0%	0%	0%	0%	0%	0%	0%	0%	0%	0%	65%	0%	100%	0%	0%	0%	0%	0%	0%
SF0.75	100%	0%	0%	0%	0%	0%	0%	0%	0%	0%	0%	0%	0%	0%	100%	0%	100%	0%	0%	0%	0%	0%	0%
SF1.00	100%	0%	0%	0%	0%	0%	0%	0%	0%	0%	0%	0%	0%	0%	100%	0%	100%	0%	0%	0%	5%	0%	0%
SF1.25	100%	0%	0%	0%	20%	0%	0%	0%	0%	0%	0%	0%	0%	0%	100%	0%	100%	0%	0%	0%	30%	0%	0%
SF1.50	100%	0%	0%	0%	65%	0%	0%	0%	15%	0%	15%	0%	0%	0%	100%	0%	100%	0%	0%	0%	70%	0%	0%
SF1.75	100%	0%	0%	0%	75%	0%	0%	0%	70%	0%	60%	0%	0%	0%	100%	0%	100%	0%	0%	0%	85%	0%	0%

a) SlC15T1F Incremental Dynamic Analysis for longitudinal ground motions

	Abutment 1 (A1)							Pier 1 (P1)					Pier 2 (P2)				Abutment (A2)						
S.F.	**CEJ**	**FBP**	**MBU**	**RRA**	**SEB**	**UBA**	**UBO**	**RRA**	**SEB**	**UEB**	**YRS**	**CCC**	**RFA**	**USB**	**YRS**	**CCC**	**CEJ**	**FBP**	**MBU**	**RRA**	**SEB**	**UBA**	**UBO**
SF0.50	100%	0%	0%	0%	0%	0%	0%	0%	0%	0%	0%	0%	0%	0%	0%	0%	100%	0%	0%	0%	0%	0%	0%
SF0.75	100%	0%	5%	0%	0%	0%	0%	0%	0%	0%	0%	0%	0%	0%	10%	0%	100%	0%	5%	0%	10%	0%	0%
SF1.00	100%	0%	5%	0%	35%	0%	0%	0%	0%	0%	0%	0%	0%	0%	75%	0%	100%	0%	10%	0%	35%	0%	0%
SF1.25	100%	0%	10%	0%	35%	0%	0%	0%	0%	0%	0%	0%	0%	0%	100%	0%	100%	0%	15%	0%	50%	0%	0%
SF1.50	100%	0%	10%	0%	75%	0%	0%	0%	20%	0%	45%	0%	0%	0%	100%	0%	100%	0%	15%	0%	70%	0%	0%
SF1.75	100%	0%	10%	0%	80%	0%	0%	0%	40%	5%	70%	0%	0%	0%	100%	0%	100%	0%	15%	0%	80%	0%	0%

b) SlC15T1S Incremental Dynamic Analysis for longitudinal ground motions

Table 6.9 continued

	Abutment 1 (A1)							Pier 1 (P1)					Pier 2 (P2)				Abutment (A2)						
S.F.	**CEJ**	**FBP**	**MBU**	**RRA**	**SEB**	**UBA**	**UBO**	**RRA**	**SEB**	**UEB**	**YRS**	**CCC**	**RFA**	**USB**	**YRS**	**CCC**	**CEJ**	**FBP**	**MBU**	**RRA**	**SEB**	**UBA**	**UBO**
SF0.50	100%	0%	0%	0%	60%	0%	0%	0%	0%	0%	0%	0%	0%	0%	0%	0%	100%	0%	0%	0%	45%	0%	0%
SF0.75	100%	0%	5%	0%	80%	0%	0%	0%	0%	0%	5%	0%	0%	0%	5%	0%	100%	0%	0%	0%	90%	0%	0%
SF1.00	100%	0%	5%	0%	90%	0%	0%	0%	0%	0%	45%	0%	0%	0%	55%	0%	100%	0%	0%	0%	90%	0%	0%
SF1.25	100%	0%	5%	0%	85%	0%	0%	0%	0%	0%	80%	0%	0%	0%	80%	0%	100%	0%	15%	0%	85%	0%	0%
SF1.50	100%	0%	5%	0%	100%	0%	0%	0%	0%	0%	85%	0%	0%	0%	95%	0%	100%	0%	15%	0%	90%	0%	0%
SF1.75	100%	0%	20%	0%	95%	10%	10%	0%	0%	0%	85%	0%	0%	0%	100%	0%	100%	0%	40%	0%	95%	10%	10%

c) SlC40T1F Incremental Dynamic Analysis for longitudinal ground motions

	Abutment 1 (A1)							Pier 1 (P1)					Pier 2 (P2)				Abutment (A2)						
S.F.	**CEJ**	**FBP**	**MBU**	**RRA**	**SEB**	**UBA**	**UBO**	**RRA**	**SEB**	**UEB**	**YRS**	**CCC**	**RFA**	**USB**	**YRS**	**CCC**	**CEJ**	**FBP**	**MBU**	**RRA**	**SEB**	**UBA**	**UBO**
SF0.50	100%	0%	0%	0%	50%	0%	0%	0%	0%	0%	0%	0%	0%	0%	0%	0%	100%	0%	0%	0%	45%	0%	0%
SF0.75	100%	0%	5%	0%	70%	0%	0%	0%	0%	0%	0%	0%	0%	0%	5%	0%	100%	0%	5%	0%	65%	0%	0%
SF1.00	100%	0%	5%	0%	65%	0%	0%	0%	0%	0%	40%	0%	0%	0%	40%	0%	100%	0%	10%	0%	65%	0%	0%
SF1.25	100%	0%	10%	0%	70%	0%	0%	0%	0%	0%	75%	0%	0%	0%	75%	0%	100%	0%	10%	0%	65%	0%	0%
SF1.50	100%	0%	10%	0%	80%	10%	10%	0%	0%	0%	85%	0%	0%	0%	85%	0%	100%	0%	10%	0%	70%	10%	10%
SF1.75	100%	0%	10%	0%	85%	20%	20%	0%	0%	0%	85%	0%	0%	0%	90%	0%	100%	0%	10%	0%	60%	20%	20%

d) SlC40T1F Incremental Dynamic Analysis for longitudinal ground motions

Table 6.10: Incremental dynamic analysis for transverse ground motions

	Abutment 1 (A1)							Pier 1 (P1)					Pier 2 (P2)				Abutment (A2)						
S.F.	**CEJ**	**FBP**	**MBU**	**RRA**	**SEB**	**UBA**	**UBO**	**RRA**	**SEB**	**UEB**	**YRS**	**CCC**	**RFA**	**USB**	**YRS**	**CCC**	**CEJ**	**FBP**	**MBU**	**RRA**	**SEB**	**UBA**	**UBO**
SF0.50	0%	0%	0%	0%	0%	0%	0%	0%	0%	0%	0%	0%	0%	0%	0%	0%	0%	0%	0%	0%	0%	0%	0%
SF0.75	0%	0%	0%	60%	45%	0%	0%	0%	0%	0%	0%	0%	0%	0%	0%	0%	0%	0%	0%	0%	0%	0%	0%
SF1.00	0%	0%	0%	90%	80%	0%	0%	0%	0%	0%	0%	0%	0%	0%	0%	0%	0%	0%	0%	10%	5%	0%	0%
SF1.25	0%	0%	0%	95%	90%	0%	0%	15%	0%	0%	0%	0%	5%	0%	0%	0%	0%	0%	0%	45%	35%	0%	0%
SF1.50	0%	0%	0%	100%	100%	0%	0%	80%	20%	0%	0%	0%	65%	0%	0%	0%	0%	0%	0%	80%	80%	0%	0%
SF1.75	30%	0%	0%	100%	100%	20%	20%	85%	75%	25%	0%	0%	85%	15%	0%	0%	35%	0%	0%	90%	85%	5%	5%

a) SlC15T1F Incremental Dynamic Analysis for transverse ground motions

	Abutment 1 (A1)							Pier 1 (P1)					Pier 2 (P2)				Abutment (A2)						
S.F.	**CEJ**	**FBP**	**MBU**	**RRA**	**SEB**	**UBA**	**UBO**	**RRA**	**SEB**	**UEB**	**YRS**	**CCC**	**RFA**	**USB**	**YRS**	**CCC**	**CEJ**	**FBP**	**MBU**	**RRA**	**SEB**	**UBA**	**UBO**
SF0.50	0%	0%	0%	0%	0%	0%	0%	0%	0%	0%	0%	0%	0%	0%	0%	0%	0%	0%	0%	0%	0%	0%	0%
SF0.75	0%	0%	0%	55%	45%	0%	0%	0%	0%	0%	0%	0%	0%	0%	0%	0%	0%	0%	0%	15%	15%	0%	0%
SF1.00	0%	0%	0%	80%	80%	0%	0%	0%	0%	0%	0%	0%	0%	0%	0%	0%	0%	0%	0%	50%	45%	0%	0%
SF1.25	10%	0%	0%	100%	100%	0%	0%	5%	0%	0%	0%	0%	40%	0%	0%	0%	10%	0%	0%	80%	80%	0%	0%
SF1.50	30%	0%	0%	100%	100%	5%	10%	65%	5%	5%	0%	0%	75%	5%	0%	0%	45%	0%	0%	100%	100%	10%	10%
SF1.75	55%	0%	0%	100%	100%	60%	60%	90%	60%	60%	0%	0%	100%	55%	0%	0%	55%	0%	0%	100%	100%	45%	45%

b) SlC15T1S Incremental Dynamic Analysis for transverse ground motions

Table 6.10 continued

	Abutment 1 (A1)							Pier 1 (P1)					Pier 2 (P2)				Abutment (A2)						
S.F.	**CEJ**	**FBP**	**MBU**	**RRA**	**SEB**	**UBA**	**UBO**	**RRA**	**SEB**	**UEB**	**YRS**	**CCC**	**RFA**	**USB**	**YRS**	**CCC**	**CEJ**	**FBP**	**MBU**	**RRA**	**SEB**	**UBA**	**UBO**
SF0.50	0%	0%	0%	80%	55%	0%	0%	0%	0%	0%	0%	0%	0%	0%	0%	0%	0%	0%	0%	5%	0%	0%	0%
SF0.75	0%	0%	0%	100%	100%	0%	0%	0%	0%	0%	0%	0%	0%	0%	0%	0%	0%	0%	0%	85%	80%	0%	0%
SF1.00	0%	0%	0%	100%	100%	0%	0%	0%	0%	0%	10%	0%	0%	0%	55%	0%	0%	0%	0%	100%	100%	0%	0%
SF1.25	0%	0%	0%	100%	100%	0%	0%	0%	0%	0%	80%	0%	0%	0%	100%	0%	0%	0%	0%	100%	100%	0%	0%
SF1.50	10%	0%	0%	100%	100%	5%	5%	0%	0%	0%	100%	0%	0%	0%	100%	0%	15%	0%	0%	100%	100%	0%	0%
SF1.75	25%	0%	0%	100%	100%	25%	25%	0%	0%	0%	100%	0%	0%	0%	100%	0%	25%	0%	0%	100%	100%	0%	0%

c) SlC40T1F Incremental Dynamic Analysis for transverse ground motions

	Abutment 1 (A1)							Pier 1 (P1)					Pier 2 (P2)				Abutment (A2)						
S.F.	**CEJ**	**FBP**	**MBU**	**RRA**	**SEB**	**UBA**	**UBO**	**RRA**	**SEB**	**UEB**	**YRS**	**CCC**	**RFA**	**USB**	**YRS**	**CCC**	**CEJ**	**FBP**	**MBU**	**RRA**	**SEB**	**UBA**	**UBO**
SF0.50	0%	0%	0%	50%	35%	0%	0%	0%	0%	0%	0%	0%	0%	0%	0%	0%	0%	0%	0%	0%	0%	0%	0%
SF0.75	0%	0%	0%	100%	100%	0%	0%	0%	0%	0%	0%	0%	0%	0%	0%	0%	0%	0%	0%	65%	75%	0%	0%
SF1.00	0%	0%	0%	100%	100%	0%	0%	0%	0%	0%	10%	0%	0%	0%	30%	0%	0%	0%	0%	100%	100%	0%	0%
SF1.25	5%	0%	0%	100%	100%	0%	0%	0%	0%	0%	75%	0%	0%	0%	85%	0%	5%	0%	0%	100%	100%	0%	0%
SF1.50	10%	0%	0%	100%	100%	15%	15%	0%	0%	0%	80%	0%	0%	0%	95%	0%	10%	0%	0%	100%	100%	0%	0%
SF1.75	20%	0%	0%	100%	100%	40%	40%	0%	0%	0%	85%	0%	0%	0%	100%	0%	25%	0%	0%	100%	100%	20%	20%

d) SlC40T1S Incremental Dynamic Analysis for transverse ground motions

Abutments (A1 and A2)

Longitudinal ground motions

Closure of expansion joint (CEJ)

- This limit state was identified on each abutment (CEJ @ A1 and A2), in all the bridge variants, for all the scale factors of this analysis (SF=0.50 to SF=1.75)

Mobilization of backfill ultimate capacity (MBU)

- This limit state occurred on each abutment (MBU @ A1 and A2), in a limited number of ground motions (5% - 15% of the 20 ground motions), in scale factors that range from SF=0.75 to SF=1.75, especially in bridge variants with soft soil foundation or 40-ft column piers.
- In the case of soft soil, abutment foundations present lower stiffness, which requires other components of the abutment to resist greater seismic forces. For this reason, in certain cases, the forces induced on the abutment backfill exceed its ultimate capacity.
- In the case of 40-ft pier columns, seismic forces are concentrated at abutments because intermediate piers have lower stiffness. Abutments induce displacements on the superstructure, which in turn exerts forces on the abutment elements, especially on the backwall and backfill.

Sliding of elastomeric bearings (SEB)

- This limit state occurred on each abutment (SEB @ A1 and A2). For the case of 15-ft column piers, sliding of elastomeric bearings starts to occur in scale factors close to the design level (SF=1.00 or SF= 1.25). Conversely, for the case of 40-ft column piers, this limit state was observed more frequently at all the scale factors.
- As mentioned before, superstructures of bridge variants with 40-ft pier columns are likely to experience greater displacements. These displacements induce forces on elastomeric bearings whose magnitude is sufficient to exceed static friction and cause sliding.

Unseating of elastomeric bearings (UBA and UBO)

- For bridge variants with 40-ft column piers, the magnitude of seismic forces was sufficient to induce unseating of bearings (UBA and UBO @ A1 and A2) for high scale factors (SF=1.50 and SF=1.75)

Transverse ground motions

Closure of expansion joint (CEJ)

- This limit state was identified at each abutment (CEJ @ A1 and A2), in all the bridge variants, especially at high scale factors (SF=1.5 and SF=1.75).
- For high scale factors, seismic forces induce large rotations that close the gap between the backwall and the superstructure, especially at the corners of this structural component.

Rupture of retainer anchors (RRA) and sliding of elastomeric bearings (SEB)

- These limit states were identified at each abutment (RRA @ A1 and A2; SEB @ A1 and A2). Rupture of retainer anchors and sliding of elastomeric bearings was more likely to occur in bridge variants with 40-ft column piers than in 15-ft column piers.
- In the case of 40-ft pier columns, seismic forces are concentrated at abutments because intermediate piers have lower stiffness. Therefore, retainer anchors and elastomeric bearings are subjected to greater forces that exceed their strength or static friction, respectively.

Unseating of elastomeric bearings (UBA and UBO)

- The magnitude of seismic forces was sufficient to induce unseating of bearings (UBA and UBO @ A1 and A2) in all bridge variants, at high scale factors (SF=1.50 or SF=1.75)

Expansion Pier (P1)

Longitudinal ground motions

Sliding of elastomeric bearings (SEB)

- This limit state (SEB @ P1) was only identified in bridge variants with 15-ft column piers at high scale factors (SF=1.50 and SF=1.75).
- For 15-ft column piers, at high scale factors, elastomeric bearings located at this substructure start contributing to resist longitudinal seismic demands because elastomeric bearings located at abutments have already reached their limit state.

Yielding of vertical reinforcing steel (YRS)

- For the case of 15-ft column piers, yielding of vertical reinforcing steel (YRS @ P1) starts to occur at high scale factors (SF=1.5 and SF=1.75). In contrast, for the case of 40-ft column piers, this limit state starts to occur at scale factors close to the design level (SF=0.75 and SF=1.00).
- The lower stiffness of 40-ft pier columns reduces the concentration of forces at superstructure-substructure connections which precludes fusing limit states such as sliding of elastomeric bearings. If this structural fuse does not fail, damaging limit states such as yielding of the vertical reinforcing steel are likely to occur.

Transverse ground motions

Rupture of retainer anchors (RRA) and sliding of elastomeric bearings (SEB)

- These limit states (RRA @ P1; SEB @ P1) were mostly identified in bridge variants with 15-ft column piers at high scale factors (SF=1.50 and SF=1.75).
- For these bridge variants, pier columns have sufficient stiffness to concentrate seismic forces and induce fusing limit states on retainer anchors and elastomeric bearings.

Unseating of elastomeric bearings (UEB)

- The magnitude of seismic forces was sufficient to induce unseating of elastomeric bearings (UEB @ P1) in bridge variants with 15-ft column piers, at high scale factors (SF=1.50 or SF=1.75)

Yielding of vertical reinforcing steel (YRS)

- This limit state (YRS @ P1) was only identified for bridge variants with 40-ft column piers, at scale factors greater than the design level (SF=1.00 to SF=1.75).
- Like previous cases, the lower stiffness of 40-ft column piers reduces the concentration of seismic forces at superstructure-substructure connections which precludes fusing limit states such as rupture of retainer anchors and sliding of elastomeric bearings. If these structural fuses do not fail, damaging limit states such as yielding of the vertical reinforcing steel have a greater probability to occur.

Fixed Pier (P2)

Longitudinal ground motions

Yielding of longitudinal reinforcing steel (YRS)

- This limit state (YRS @ P2) was observed in all the bridge variants. Yielding of the vertical reinforcing steel occurred more frequently on bridge variants with 15-ft column piers.
- Failure of sacrificial connections such as rupture of fixed bearing anchors did not occur in any bridge variant. For this reason damaging limit states like yielding of vertical reinforcing steel were observed in most scale factors.

Transverse ground motions

Rupture of fixed bearing anchors (RFA)

- This limit state (RFA @ P2) was only observed in bridge variants with 15-ft column piers.
- Likewise Expansion Pier (Pier 1), column pier stiffness allowed the concentration of forces at this sacrificial connection, which caused its failure.

Unseating of steel fixed bearings (USB)

- The magnitude of seismic forces was sufficient to induce unseating of steel fixed bearings (USB @ P2) in bridge variants with 15-ft column piers, at high scale factors (SF=1.50 or SF=1.75)

Yielding of vertical reinforcing steel (YRS)

- This limit state (YRS @ P2) was only observed in bridge variants with 40-ft column piers.
- Likewise Expansion Pier (Pier 1), the lower stiffness of 40-ft column piers reduces the concentration of seismic forces at superstructure-substructure connections. This

prevents fusing limit states such as rupture of fixed bearing anchors, allowing damaging limit states such yielding of vertical reinforcing steel.

7. SUMMARY AND CONCLUSIONS

7.1. Objectives and Scope of Research

The research presented in this thesis focused on the comparison of structural models of seat-type abutment bridges developed for the studies "Seismic Performance of Quasi-Isolated Highway Bridges in Illinois: Phase I" (Report ICT-R27-070) (LaFave et al., 2013a) and "Calibration and Refinement of Illinois' Earthquake Resisting System Bridge Design Methodology: Phase II) (Report ICT-R27-133) (LaFave et al., 2018).

Parametric variations of bridge models that can be found both in Phase I and Phase II were chosen for a sensitivity study, primarily related to abutment modeling. This selection of bridges consists of three-span bridges with steel-plate girders that have sequential span lengths of 24.4, 36.6, and 24.4 m (80, 120 and 80 ft). These bridges are supported by non-skew seat-type abutments and RC multi-column intermediate piers. Superstructure girders are supported by IDOT Type I bearings at the abutments and at Pier 1, and by low-profile fixed bearings at Pier 2. The RC multi-column intermediate piers are 4.57 or 12.19 m high (15 or 40 ft). Soft or hard foundation soil conditions are considered. The combination of these parameters results in 4 bridge variants in total.

The sensitivity study of these structural models was related to the complexity and the number of elements considered for modeling abutment substructures. The Phase I abutment formulation was based on a simplified model that primarily considers the interaction between superstructure and backfill by employing a single hyperbolic gap element as well as the behavior of the backwall-pile-cap connection using an elastoplastic rotational spring. Additional elements such as wingwalls and approach slabs were not included. The formulation of Phase II abutments was improved by using two hyperbolic gap elements placed along the height of backwall and pile cap to better represent backfill response. A nonlinear spring calibrated according to the moment-curvature relation of the backwall was used to model the behavior of the backwall-pile connection. Wingwalls and approach slabs were included in order to account for soil passive resistance in the transverse direction and surcharge effects, respectively.

Pushover analyses were performed to compare the sensitivity of structural response in the Phase I and Phase II models when subjected to a uniform force pattern and monotonically increasing global displacement increments. This comparison includes the identification of sequences of damage as well as the distribution of forces on each substructure of the selected bridge variants.

Likewise, nonlinear dynamic analyses were performed using a supercomputer to compare the sensitivity of structural response for Phase I and Phase II models when subjected to input ground acceleration records. A suite of 20 synthetic ground motions, with a 1,000-year return period, developed according to the site condition and regional seismicity of Cairo, Illinois, the geographic location with the highest seismic hazard in the state, was applied to each bridge variant in the longitudinal and transverse direction. Fusing and damaging limit states were identified and statistically summarized to perform comparisons. For this purpose, 160 nonlinear dynamic analyses were performed

An assessment of the dynamic response of the selected bridge variants was performed by implementing an incremental dynamic analysis (IDA), using the synthetic ground motions of Phase II and considering linear scale factors of 0.50, 0.75, 1.00, 1.25, 1.50, 1.75. These analyses were performed using Phase I models. For this case, 800 additional nonlinear dynamic analysis were performed. In total, 960 nonlinear dynamic analyses were performed.

7.2. Comparison of Nonlinear Static Analyses

7.2.1. Longitudinal pushover analyses

The following similarities and differeces were found between Phase I and Phase II models by performing longitudinal pushover analyses:

- In Phase I models, a rapid increase in the force resisted by Abutment 2 occurred after closure of the expansion joint. This increase is related to the simplified abutment model used in this phase which basically consists of a rigid link that represents the backwall connected to a hyperbolic gap element that represents

backfill passive resistance, and an elastoplastic rotational spring that represents the backwall-pile-cap connection, at each end, respectively. These elements can be compared to a spring arrangement in series. In this case, after closure of the expansion joint, both elements contribute to resisting the applied pushover force, which generates an abrupt change in stiffness. Then, when the applied force on the superstructure causes yielding of the backwall-pile-cap connection, a break in the trend of the pushover force occurs, indicating that the backfill resistance has become the only component that resists additional forces. In contrast, in the case of Phase II models, backfill passive resistance is distributed in two springs located along the height of the backwall and pile cap. Besides these elements, additional effects such as approach slab friction are considered. These components and their configuration distribute stiffness at the abutment and therefore a continuous and gradually softening force-deformation behavior is observed.

- The pushover force resisted by Abutment 2 was greater in Phase II models for all the analyzed bridge variants. The greater magnitude of the pushover force at this substructure is related to the additional stiffness provided by surcharge effects and friction forces and due to the presence of the approach slab. For these reasons, unlike Phase I models, limit states such as failure of the backwall-pile-cap connection or mobilization of backfill ultimate capacity were not identified.

- For the case of bridge variants with tall piers (40-ft piers), the greater stiffness of abutments of Phase II models reduces the displacement of the superstructure. This reduction diminishes the magnitude of forces transmitted to the substructure (this transmission of forces is possible due to the lower lateral stiffness of 40-ft column piers that precludes fusing of sacrificial connections such as elastomeric bearings and fixed bearing anchors), which in turn prevents damaging limit states such as yielding of the vertical reinforcing steel.

7.2.2. Transverse pushover analyses

The following similarities and differences were found between Phase I and Phase II models by performing transverse pushover analyses:

- In Phase II models, the inclusion of additional effects such as soil passive resistance provided by wingwalls and the friction forces originated by presence of the approach slab contribute to reducing the concentration of pushover force in sacrificial connections at early stages of the pushover analysis, in comparison to Phase I models. This contribution is especially notable for the case of bridge variants with considerable structural stiffness (such as variants with short piers (15-ft piers) and a hard foundation).

- Abutments of Phase II models resist greater forces in comparison to Phase I models. This resistance is related to additional elements such as wingwalls and approach slabs, which induce passive soil resistance and friction effects that increase abutment stiffness. Even though it is possible to notice this difference between Phase I and Phase II models, the magnitude of the additional resistance provided by these elements in the transverse direction is much less remarkable compared to that provided by the elements that increase abutment stiffness in the longitudinal direction.

- In Phase II models, additional elements such as wingwalls and approach slabs may contribute to increase abutment stiffness and reduce superstructure displacements in the transverse direction. Nevertheless, in comparison to the longitudinal direction, especially for the case of bridge variants with tall piers (40-ft piers), these elements do not provide the same additional stiffness in order to prevent the transmission of forces to the substructures that cause damaging limit states such as yielding of the vertical reinforcing steel.

7.3. Comparison of Dynamic Analyses for Design Level Ground Motions

7.3.1. Fusing of sacrificial connections

For longitudinal ground motions, in the case of Phase I models the sliding of elastomeric bearings at abutments occurred more often in comparison to Phase II models, especially in bridge variants with tall piers (40-ft piers). As mentioned in the previous section dedicated to nonlinear static analyses, in Phase II models, additional stiffness due to elements, such as approach slabs that generate surcharge effects and friction forces, reduces the magnitude of superstructure displacements and therefore the forces that induce sliding of elastomeric bearings.

For transverse ground motions, fusing limit states such as rupture of retainer anchors and sliding of elastomeric bearings occurred more frequently in Phase I models, in all the analyzed bridge variants. This difference can be ascribed to the fact that Phase I models only depend on these elements to transmit forces from the superstructure to the substructure. On the other hand, Phase II models were formulated including wingwalls and approach slabs. These components are able to resist seismic demands, which allows a redistribution of forces at abutments. Consequently, this redistribution reduces the magnitude of the forces in retainers and bearings.

7.3.2. Mobilization of backfill ultimate capacity

For the selected bridge variants, this limit state only occurred in the longitudinal direction. Phase I models had a greater number of occurrences of this limit state compared to Phase II models, especially for the case of bridge variants with the soft soil foundation condition and tall piers (40-ft piers). This difference can be attributed to the fact that Phase I models have a lower backfill resistance due to the absence of elements such as approach slabs which induce surcharge effects and friction forces.

7.3.3. Damage of pier columns

For longitudinal ground motions, in the case of tall piers (40-ft piers), a greater number of occurrences of yielding of the vertical reinforcing steel were observed, especially at the Expansion Pier for the case of Phase I models. As mentioned in the previous section related to nonlinear static analyses, additional elements such as approach slabs increase abutment stiffness, which reduces superstructure displacements. In turn, this reduction decreases the magnitude of the forces transmitted to the intermediate substructure that cause yielding of the vertical reinforcing steel.

Similarly, for transverse ground motions, in the case of tall piers (40-ft piers), a greater number of occurrences of yielding of the vertical reinforcing steel were observed, particularly at the Fixed Pier for the case of Phase I models. This difference can be attributed to the lower stiffness of abutments due to the absence of wingwalls and approach slabs in the formulation of these models. As previously mentioned, these elements increase overall abutment stiffness which reduces superstructure displacements. This reduction limits the magnitude of forces transmitted to the Fixed Pier that cause yielding of the vertical reinforcing steel.

7.3.4. Unseating of elastomeric bearings

For the selected bridge variants and design level ground motions, unseating of elastomeric bearings was not identified in any longitudinal or transverse dynamic analysis.

7.4. Incremental Dynamic Analysis

In this section, an assessment of the dynamic response of the selected bridge variants is performed by implementing an incremental dynamic analysis (IDA), using Phase I models, the ground motions developed in Phase II, and considering linear scale factors of 0.50, 0.75, 1.00, 1.25, 1.50, 1.75.

7.4.1. Longitudinal ground motions

At abutments, fusing limit states such as sliding of elastomeric bearings (SEB @ A1 and A2) were identified, especially in bridge variants with tall piers (40-ft piers). At this location, undesired limit states such as unseating of elastomeric bearings (UBA and UBO @ A1 and A2) were identified at high scale factors (SF=1.50 and SF=1.75), only in bridge variants with tall piers (40-ft piers), in a small number of ground motions (10% – 20%).

At the Expansion Pier and Fixed Pier, fusing limit states such as sliding of elastomeric bearings (SEB @ P1) and rupture of fixed bearing anchors (RFA @ P2) did not occur in almost all the analyses. For this reason, damaging limit states such as yielding of the vertical reinforcing steel were identified (YRS @ P1 and P2) beyond the design level (SF=1.00 – SF=1.75), especially for the case of bridge variants with tall piers (40-ft piers).

In summary, bridge variants with tall piers (40-ft piers) were more likely to experience damaging limit states and undesired limit states due to the lower stiffness of column piers and the fact that fusing of sacrificial superstructure-substructure connections did not occur. The sequence of occurrence of these limit states is not desirable for quasi-isolation.

7.4.2. Transverse ground motions

At abutments, fusing limit states such as rupture of retainer anchors and sliding of elastomeric bearings (RRA and SEB @ A1 and A2) were identified, especially in bridge variants with tall piers (40-ft piers). Subsequently, at this location, undesired limit states such as unseating of elastomeric bearings (UBA and UBO @ A1 and A2) were identified at high scale factors (SF=1.50 and SF=1.75), in all the bridge variants. For certain bridge variants, especially for the case SlC15T1S), the percentage of occurrence reached values of 60%.

At the Expansion Pier and Fixed Pier, fusing limit states such as rupture of retainer anchors (RRA @ P1), sliding of elastomeric bearings (SEB @ P1), and rupture of fixed bearing anchors (RFA @ P2) occurred in bridge variants with short piers (15-ft piers) at high scale factors (SF=1.25 – SF=1.75). In this case, the fusing of these sacrificial

connections precluded damaging limit states; nevertheless, unacceptable limit states such as unseating of elastomeric bearings at the Expansion Pier (UEB @ P1) and unseating of fixed bearings (USB @ P2) did occur, especially at high scale factors (SF=1.50 – SF=1.75).

In contrast, for the case of 40-ft column piers, fusing of sacrificial connections at the Expansion Pier and Fixed Pier were not identified. Therefore, damaging limit states such as yielding of the vertical reinforcing steel occurred in both substructures (YRS @ P1 and P2) beyond the design level (SF=1.00 – SF=1.75).

In summary, bridge variants with short piers (15-ft piers) experienced fusing limit states which prevented damaging limit states due to the higher lateral stiffness of column piers. For certain scale factors, this sequence of damage is desired for quasi-isolation. Conversely, in the case of bridge variants with tall piers (40-ft piers), fusing limit states did not occur, which caused damaging limit states because of the lower lateral stiffness of column piers. This sequence of damage is not appropriate for quasi-isolation.

7.5. General Observations and Recommendations

7.5.1. Comparison of Phase I and Phase II model sensitivity

- In the longitudinal direction, additional elements included in Phase II models such as approach slabs, which induce surcharge effects and friction forces, as well as the inclusion of additional spring elements to represent backfill passive resistance, increased abutment stiffness and allowed a redistribution of forces at this location. This redistribution precluded the concentration of forces in sacrificial connections and reduced superstructure displacements. In general, these conditions diminished the occurrence of fusing limit states at abutments and damaging limit states at intermediate substructures in comparison to Phase I models.

- Similarly, in the transverse direction, additional elements included in Phase II models, especially wingwalls, which induce passive soil resistance effects, increased abutment stiffness that allowed a redistribution of forces that essentially reduced the concentration of demands on sacrificial connections at this location.

Generally, for the case of nonlinear static analyses and nonlinear dynamic analyses, the stiffness increment in the transverse direction provided by these elements is lower compared to the longitudinal direction.

- In nonlinear static analyses and nonlinear dynamic analyses, it was not possible to identify significant differences in the occurrence of limit states between Phase I and Phase II models, especially regarding damaging limit states. Even though the formulation of Phase II models resembled more closely the structural configuration of seat-type abutment bridges, Phase I models require less computational resources to be analyzed. For this reason, it is possible to employ Phase I models as a preliminary assessment tool, before using more complex formulations for definitive structural analysis of seat-type abutment bridges.

- According to the study "Seismic analysis incorporating detailed structure-abutment foundation interaction for quasi-isolated highway bridges" (Luo et al., 2017), which defined the detailed abutment model for Phase II models, there are noticeable differences between the response of commonly used abutment models (which usually exclude elements such as RC backwalls, wingwalls and approach slabs) and the proposed abutment model. In contrast, for the case of Phase I models, which include RC backwalls, fewer differences were observed when comparing this model to the detailed formulation of Phase II models. For this reason, as previously mentioned, it is feasible to use Phase I models to perform preliminary analyses.

- The analyses of Phase II models consistently demand more computational resources due to the formulation of a detailed abutment model which is based on the discretization of the backfill passive resistance, wingwalls, and other components into a number of nonlinear springs. In order to reduce the computational resources required for the analysis of these models while keeping its reliability, it may be possible to use fewer springs, lump these elements or try new configurations for the formulation of these structural models.

7.5.2. Incremental dynamic analysis

- For the structural configuration of the bridge variants with tall piers (40-ft piers), the size of the sacrificial superstructure-substructure connections does not permit these elements to reach fusing limit states, even for high scale factors. Therefore damaging limit states, especially yielding of the vertical reinforcing steel, were frequently identified.

- For the structural configuration of bridge variants with short piers (15-ft piers), the greater stiffness of pier columns makes possible to concentrate forces on sacrificial connections and induce fusing limit states. For this reason, unlike tall piers (40-ft piers), damaging limit states were prevented. Even though these conditions are avoided due to fusing of sacrificial connections, high scale factors induce large superstructure displacements that cause unseating of bearings.

- The study “Seismic performance assessment of quasi-isolated highway bridges with seat-type abutments” (Luo, 2016) suggested several modifications focused on the size of sacrificial connections in order to improve the performance of quasi-isolated highway bridges. Nevertheless, considering the scenarios mentioned above, a parametric study is recommended to determine an appropriate size of sacrificial connections as well as structural elements in order to minimize the occurrence of damaging limit sates (yielding of the vertical reinforcing steel) and unacceptable limit states (unseating of bearings). A detailed parametric study based on the elements of the overall structural model may allow for further improvement and optimization the quasi-isolation strategy for Illinois highway bridges.

REFERENCES

AASHTO. (2008a). *LRFD Bridge Design Specifications and Interim Specifications.* Washington D.C: AASHTO.

AASHTO. (2008b). *Guide Specifications for LRFD Seismic Bridge Design.* Washington D.C.: AASHTO.

AASHTO. (2009). *AASHTO Guide Specifications for LRFD Seismic Bridge Design.* Washington D.C.: AASHTO.

AASHTO. (2010). *AASHTO LRFD Bridge Design Specifications.* Washington D.C.: AASHTO.

Abo-Shadi, N., Saiidi, M., & Sanders, D. (2000). *"Seismic response of reinforced concrete bridge pier walls in the weak direction".* Reno, NV.: Rep. No. MCEER-00-0006, University of Nevada.

Al Atik, L., & Abrahamson, N. (2010). "An improved method for nonstationary spectral matching". *Earthq. Spectra*, 26(3), 601-617.

American Concrete Institute (ACI). (2008). *Building Code Requirements for Structural Concrete (ACI 318-08).* Farmington Hills, MI: American Concrete Institute (ACI).

Argyroudis, S., Mitoulis, S., & Pitilakis, K. (2013). "Seismic response of bridge abutments on surface foundation subjected to collision forces". *4th ECCOMAS Thematic Conference on Computational Methods in Structural Dynamics and Earthquake Engineering*.

Baker, J. (2011). "Conditional Mean Spectrum: Tool for Ground Motion Selection". *Journal of Structural Engineering 137(3)*, 322-331.

Barth, K., & H. Wu. (2006). "Efficient Nonlinear Finite Element Modeling of Slab on Steel Stringer Bridges". *Finite Elements in Analysis and Design 42(14-15)*, 1304-1313.

Bignell, J., LaFave, J., & Hawkins, N. (2005). "Seismic Vulnerability Assessment of Wall Pier Supported Highway Bridges Using Nonlinear Pushover Analyses". *Engineering Structures*, 2044-2063.

Boulanger, R., Curras, C., Kutter, B., Wilson, D., & Abghari, A. (1999). "Seismic soil-pile-structure interaction experiments and analyses". *J. Geotech. Geoenviron. Eng.*, 10.1061/(ASCE)1090-0241(1999)125:9(750),750-759.

Bozorgzadeh, A., Ashford, S., Restrepo, J., & Nimityongskul, N. (2007). *"Experimental and analytical investigation of stiffness and ultimate capacity of bridge abutments".* La Jolla, CA: Rep. No. UCSD/SSRP-07/12, University of California, San Diego.

Buckle, I., Constantinou, M., Dicleli, M., & Ghasemi, H. (2006). *Seismic Isolation of Highway Bridges. Special Report MCEER06-SP07.* Buffalo, NY: Multidisciplinary Center for Earthquake Engineering Research.

Building Seismic Safety Council. (2000). *Prestandard and Commentary for the Seismic Rehabilitation of Buildings, FEMA-356.* Washington, DC.: Federal Emergency Management Agency.

Caltrans. (2006). *"Seismic Design Criteria" Section 5.* Sacramento, CA: California Department of Transportation.

Chang, C., & White, D. (2008). "An Assessment of Modeling Strategies for Composite Curved Steel I-Girder Bridges". *Engineering Structures 30(11)*, 2991-3002.

Chin-Hsiung, L., Wen-Yu, J., & Penzien, J. (1994). "Uniform-Hazard Response Spectra-An Alternative Approach". *Earthquake Engineering and Structural Dynamics (23)*, 433-445.

Constantinou, M., Mokha, A., & Reinhorn, A. (1990). "Teflon Bearings in Base Isolation II: Modeling". *Journal of Structural Engineering 116(2)*, 455-474.

Fernandez, J., & Rix, G. (2008). "Seismic Hazard Analysis and Probabilistic Ground Motions in the Upper Mississippi Embayment.". *Geotechnical Earthquake Engineering and Soil Dynamics Special Publication n181. ASCE.*

Filipov, E. (2012). *"Nonlinear seismic analysis of quasi-isolation systems for earthquake protection of bridges".* Urbana, IL: M.Sc. Thesis, University of Illinois at Urbana-Champaign.

Filipov, E., Fahnestock, L., Steelman, J., Hajjar, J., & LaFave, J. (2013a). "Evaluation of quasi-isolated seismic bridge behavior using nonlinear bearing models". *Eng. Struct. 49(0)*, 168-181.

Filipov, E., Revell, J., Fahnestock, L., LaFave, J., Hajjar, J., & Foutch, D. (2013b). "Seismic performance of highway bridges with fusing bearing components for quasi-isolation". *Earthq. Eng. Struct*, 42(9), 1375-1394.

Gomez, I., Kavinde, A., Smith, C., & Deierlein, G. (2009). *"Shear Transfer in Exposed Column Base Plates".* Report to the American Institute of Steel Construction. National Science Foundation Grant Number NSF-CMMI 0421492.

Hashash, Y., Musgrove, M., Harmon, J., Groholski, D., Phillips, C., & Park, D. (2015). *DEEPSOIL 6.1, User Manual.* Urbana, IL: Board of Trustees of Univ. of Illinois at Urbana-Champaign.

Ibarrra, I., Medina, R., & Krawinkler, H. (2005). "Hysteretic Models that Incorporate Strength and Stiffness Deterioration". *Earthquake Engineering & Structural Dynamics 34(12)*, 1489-1511.

IDOT. (2012). *Bridge Manual.* Springfield, IL.: IDOT.

Klinger, R., Mendonca, J., & Malik, J. (1982). "Effect of Reinforcing Details on the Shear Resistance of Anchor Bolts Under Reversed Cyclic Loading.". *Journal of the American Concrete Institute (79)1*, 3-12.

Kornkasem, W., Foutch, D., & Long, J. (2001). *"Seismic behavior of pile-supported bridges" Rep. No. 03-05.* Champaign, IL: Mid-America Earthquake Center, University of Illinois at Urbana-Champaign.

Kozak, D., Luo, J., Olson, S., LaFave, J., & Fahnestock, L. (2017). "Modification of ground motions for use in Central North America". *Department of Civil and Environmental Engineering, University of Illinois at Urbana-Champaign*, 1-29.

Kunde, M., & Jangid, R. (2003). "Seismic behavior of isolated bridges: A-state-of-the-art review". *Electronic Journal of Structural Engineering*, 140-170.

LaFave, J., Fahnestock, L., Foutch, D., Steelman, J., Revell, J., Filipov, E., & Hajjar, J. (2013a). *"Experimental investigation of the seismic response of bridge bearings"*. Springfield, IL: Rep. No FHW-ICT-13-002 Illinois Center for Transportation.

LaFave, J., Fahnestock, L., Foutch, D., Steelman, J., Revell, J., Filipov, E., & Hajjar, J. (2013b). *"Seismic Performance of Quasi-Isolated Highway Bridges in Illinois"*. Springfield, IL: Rep. No. FHWA -ICT-13-015. Illinois Center for Transportation.

LaFave, J., Fahnestock, L., Kozak, D., & Luo, J. (2018). *"Calibration and Refinement of Illinois Earthquake Resisting System Bridge Design Methodology"*. Springfield, IL: Illinois Center for Transportation.

Luo, J. (2016). *"Seismic performance assessment of quasi-isolated highway bridges with seat-type abutments"*. Urbana, IL: University of Illinois at Urbana-Champaign.

Luo, J., Fahnestock, L., Kozak, D., & LaFave, J. (2017). "Seismic analysis incorporating detailed structure-abutment-foundation interaction for quasi-isolated highway bridges". *Structure and Infrastructure Engineering, 13:5*, 581-603.

Mander, J., Kim, D., Chen, S., & Premus, G. (1996). *"Response of Steel Bridge Bearings to Reversed Cyclic Loading"*. Buffalo, NY: Technical Report NCEER-96-0014, State University of New York at Buffalo.

Mander, J., Priestley, M., & Park, R. (1988). "Theoretical stress-strain model for confined concrete". *J. Struct Eng.*, 10.1061/(ASCE)0733-9445(1988)114:8(1804), 1804-1826.

Matlock, H., Foo, S., & Bryant, L. (1978). "Simulation of lateral pile behavior". *Proc., Earthq. Eng. and Soil Dyn.*, 600-619.

McGuire, R., Silva, W., & Constantino, C. (2001). *"Technical basis for revision of regulatoria guidance on design ground motions: Hazard and risk consistent ground motion spectra guidelines"*. Washington, D.C.: Rep. No. NUREG/CR-6728. U.S. Nuclear Regulatory Commission.

McKenna, F., Mazzoni, S., & Fenves, G. (2011). *Open System for Earthquake Engineering Simulation (OpenSees) Software Version 2.2.0 University of California.* Berkeley, CA: Available from http://opensees.berkeley.edu/.

Menegotto, M., & Pinto, P. (1973). "Method of analysis for cyclically loaded reinforced concrete plane frames including changes in geometry and non-elastic behavior of elements under combined normal force and bending". *Proc., IABSE Symp. of Resistance an Ultimate Deformability of Structures Acted on by Well-Defined Repeated Loads, Vol. 13, Lisbon, Portugal*, 15-22.

Mitoulis, S. (2012). *"Seismic design of bridges with seat-type abutments considering the participation of the abutments during earthquake excitation"*. Lisbon: 15 WCEE.

Mohd Yassin, M. (1994). "Nonlinear analysis of prestressed concrete structures under monotonic and cyclic loading". Ph.D. Dissertation, Univ. of California, Berkeley, CA.

Neuenhofer, A., & Filippou, F. (1997). "Evaluation of nonlinear frame finite-element models.". *J. Struct. Eng.*, 10.1061/(ASCE)0733-9445(1997)123:7(958).

Nogami, T., Otani, J., Konagai, K., & Chen, H. (1992). "Nonlinear soil-pile interaction model for dynamic lateral motion". *J. Geotech. Engr.*, 10.1061/(ASCE)0733-9410(1992)118:1(89), 89-106.

Novak, M., & Sheta, M. (1980). "Approximate approach to contact problems of piles". *Proc., ASCE Nat. Convention, Dyn. Response of Pile Found: Analytical Aspects.*, 55-79.

Roeder, C., & Stanton, J. (1991). "State of the Art Elastomeric Bridge Bearing Design". *ACI Structural Journal 88*, 31-41.

Rollins, K., Gerber, T., Cummings, C., & Pruett, J. (2010). *"Dynamic passive pressure on abutments and pile caps"* . Provo, UT: Rep. No. UT-10.18, Brigham Young University.

Scott, M., & Fenves, G. (2006). "Plastic Hinge Integration Methods for Force-Based Beam-Column Elements". *Journal of Structural Engineering 132(2)*, 244-252.

Seismosoft. (2016). SeismoSignal.

Shamsabadi, A., Rollins, K., & Kapuskar, M. (2007). "Nonlinear Soil-Abutment-Bridge Structure Interaction for Seismic Performance-Based Design.". *Journal of Geotechnical and Geoenvironmental Engineering 133(6)*, 707-720.

Steelman, J. (2013). *"Sacrificial bearing components for quasi-isolated response of bridges subjected to high-magnitude, low probability seismic hazard."*. Champaign, IL: Ph.D Dissertation, Univesity of Illinois at Urbana-Champaign.

Steelman, J., Fahnestock, L., Hajjar, J., & LaFave, J. (2016). "Performance or nonseismic PTFE sliding bearings when subjected to seismic demands". *J. Bridge Eng.* , 10.1061/(ASCE)BE. 1943-5592.0000777,04015028.

Steelman, J., Filipov, E., Fahnestock, L., Revell, J., LaFave, J., Hajjar, J., & Foutch, D. (2014). "Experimental behavior of steel fixed bearings and implications for seismic bridge response". *J. Bridge Eng. 19(8)*, A4014007.

Stewart, J. (2007). *"Full scale cyclic testing of foundation support systems for highway bridges. Part II: Abutment backwalls"*. University of California, Los Angeles: Rep. No. UCLA-SGEL-2007/02, Structural and Geotechnical Engineering Laboratory.

Terzaghi, K., Peck, R., & Mesri, G. (1996). *"Soil mechanics in engineering practice, 3rd Ed"*. U.K: Wiley.

Tobias, D., Anderson, R., Hodel, C., Kramer, W., Wahab, R., & Chaput, R. (2008). "Overview of earthquake resisting system design and retrofit strategy for bridges in Illinois". *Pract. Period. Struct. Des. and Constr.*, 10.1061/(ASCE)1084-0680(2008)13:3(147), 147-158.

Vamvatsikos, D., & Cornell, C. (2002). "Incremental Dynamic Analysis". *Earthquake Engineering & Structural Dynamics 31(3)*, 491-514.

Vintzeleou, E., & Tassios, T. (1986). "Mathematical models for dowel action under monotonic and cyclic conditions". *Mag. Concrete res.*, 38(134), 13-22.

Wilson, P., & Elgamal, A. (2010). "Bridge-Abutment-Backfill Dynamic Interaction Modeling Based on Full Scale Tests". *In proceedings of the 9th U.S. National and 10th Canadian Conference on Earthquake Engineering.* Toronto, ON.

Zandieh, A., & Pezeshk, S. (2011). "A study of Horizontal-to-Vertical Component Spectral Ration in the New Madrid Seismic Zone". *Bulletin of the Seismological Society of America 101(1)*, 287-296.